ADDIS ABABA UNIVERSITY

SCHOOL OF GRADUATE STUDIES

SCHOOL OF EARTH SCIENCES

THE GEOLOGY AND GEOCHEMISTRY OF NEOPROTEROZOIC ROCK UNITS IN MAI KINETAL AREA, NORTHERN ETHIOPIA: IMPLICATION FOR PETROGENETIC AND TECTONIC SETTING.

BY

MISGAN MOLLA TAMINEW

ADVISOR: Dr. MULUGETA ALENE ARAYA

28/6/ 2016/17

ADDIS ABABA, ETHIOPIA

ADDIS ABABA UNIVERSITY
COLLEGE OF NATURAL SCIENCES
SCHOOL OF EARTH SCIENCES

THE GEOLOGY AND GEOCHEMISTRY OF NEOPROTEROZOIC ROCK UNITS IN MAI KINETAL AREA, NORTHERN ETHIOPIA: IMPLICATION FOR PETROGENETIC AND TECTONIC SETTING.

BY
MISGAN MOLLA TAMINEW
ADVISOR: Dr. MULUGETA ALENE ARAYA

A Thesis Submitted to School of Graduate Studies of Addis Ababa University, in Partial Fulfillment of the Requirements for the Degree of Masters of Earth Sciences in Petrology.

28/6/ 2016/17
ADDIS ABABA, ETHIOPIA

ADDIS ABABA UNIVERSITY

COLLEGE OF NATURAL SCIENCES

SCHOOL OF EARTH SCIENCES

THE GEOLOGY AND GEOCHEMISTRY OF NEOPROTEROZOIC ROCK UNITS IN MAI KINETAL AREA, NORTHERN ETHIOPIA: IMPLICATION FOR PETROGENETIC AND TECTONIC SETTING.

BY

MISGAN MOLLA TAMINEW

Approved by the Examining Committee

Dr. BALEMWAL ATNAFU	____________________	____________________
Department Chairman and Graduate committee	Signature	Date
Dr. MULUGETA ALENE ARAYA	____________________	____________________
Advisor	Signature	Date
____________________	____________________	____________________
Examiner	Signature	Date
____________________	____________________	____________________
Examiner	Signature	Date

28/6/ 2016/17

ADDIS ABABA, ETHIOPIA

ADDIS ABABA UNIVERSITY

COLLEGE OF NATURAL SCIENCES

SCHOOL OF EARTH SCIENCES

This is to certify that the thesis prepared by Misgan Molla, entitled: “The geology and geochemistry of Neoproterozoic rock units in Mai Kinetal area, Northern Ethiopia: implication for petrogenetic and tectonic setting” and submitted in partial fulfillment of the requirement for the Degree of Master of Science in Petrology compiles with the regulations of the University and meets the accepted standards with respect to originality and quality.

Approved by the Examining Committee

Dr. Balemwal Atnafu ________________ ______________________
Head, School of Earth Science Signature Date

Dr. Mulugeta Alene __________________ _____________________
Advisor Signature Date

Prof. Asfawossen Asrat __________________ _____________________
Examiner Signature Date

Prof. Dereje Ayalew ___________________ ___________________
Examiner Signature Date

28/6/ 2016/17

ADDIS ABABA, ETHIOPIA

Declaration of Originality

I hereby declare that the thesis entitled “The geology and geochemistry of Neoproterozoic rock units in Mai Kinetal area, Northern Ethiopia: Implication for petrogenetic and tectonic setting” has been carried out by me under the supervision of Dr .Mulugeta Alene Araya, School of Earth Science, Addis Ababa University, during the year 2017-2018 as part of Masters of Science program in Petrology. I further declare that this work has not been submitted to any university or institution in the past for the award of any degree or diploma at any other university.

Misgan Molla

Addis Ababa University

Addis Ababa

Date: 28/ 6/ 2017

Sign: --

Acknowledgment

I would like to thank very much to Adigrat University for giving me an opportunity to start my postgraduate program in Addis Ababa University.

I would like also thank very much to Addis Ababa University, school of Earth Science for its complete support from the beginning to the end of this work.

My deepest gratitude goes to my advisor Dr. Mulugeta Alene Araya for his follow up, invaluable advices, constructive comment and suggestion, encouragement, discussion and limitless support at various times, extensive knowledge has kept me on-track and was able to find amazing opportunities for me and continuous support throughout the entire thesis and his friendly approach throughout my research . I feel I have really been lucky to be working with him.

During the research work I got a lot of support from my friends, and colleagues Mr. Angesom Resom, Mr. Hayelom Mengesha, Mr. Hagos Hiluf, Mr. Wendwossen Sisay, Mr. Daneil Alemayoh, Mr. Hailu G/Kidan, Mr. Alemu Tesfalem, Mr. Samuel Getachew, Mr. Yemane Kelemework, Mr. Earmiyas Filfilu, Mss. Trhas Hadush and Mss. Selamawit Abdissa.

My greatest appreciation goes to my family for giving me courage and unforgettable support.

Last but not least, the community of Mai Kinetal town have great place in my heart. I thank them all, for their kind and memorable help during the field work.

Table of Contents **Page**

List of Figures

List of Tables

List of Appendix

List of Acronyms

- a.s.l — above mean sea level
- A-CN-K — Al_2O_3- CaO*+Na_2O-K_2O
- ALS — Australian Laboratory Science
- ANS — Arabian Nubian Shield
- Bt — Biotite
- CAB — Calc-alkali basalts
- Cal — Calcite
- Chl — Chlorite
- CIA — Chemical index of alteration
- CIPW — Cross, Iddings, Pirsson and Washington
- CIW — Chemical index weathering
- D1 — Deformational event 1
- D2 — Deformational event 2
- D3 — Deformational event 3
- E.G — East Gondwana
- E-MORB — Enriched mid-ocean ridge basalts
- EAO — East African Orogeny
- Ep — Epidote
- ES — European Shale
- Fig. — Figure
- GCD Kit tool — Geochemical data kit tool
- GPS — Global Positioning System
- Hem — Hematite
- HREEs — Heavy rare earth elements
- LILEs — Large ion lithophile elements
- LOI — Loss on Ignition
- MB — Mozambique Belt
- ME- ICP06 — Multi element Inductively Coupled Plasma 06
- ME-MS81 — Multi Element Mass Sepectrometry 81
- mm — Millimeter

– MORB	Mid-ocean ridge basalts
– Ms	Muscovite
– MV	Meta volcanic
– MVC	Metavolcanoclastic
– NASC	North American Shale Composite
– N-MORB	Normal mid-ocean ridge basalt
– Opa	Opaque
– Or	Orthoclase
– Pyro	Pyroxene
– PAAS	Post Archean Australian Sedimentary
– PAO	Pan African Orogen
– PIA	Plagioclase Index of Alteration
– Pl	Plagioclase
– PPL	Plane Polarized Light
– ppm	part per million
– Qtz	Quartz
– REE	Rare Earth Element
– S0	Primary bedding
– S1	Secondary foliation
– S2	Crenulation cleavage
– Ser	Sericite
– UCC	Average Upper Continental Crust
– W.G	West Gondwana
– WPB	Within plate basalt
– XPL	Cross polarized light

Abstract

Mai Kinetal area is one of the four exposed Neoproterozoic inliers in northern Ethiopia that consists of both Tsaliet and Tambien Group. The metavolcanic rock consists of metabasic and meta-acidic rocks, whereas metavolcanoclastic unit consists of metagreywacke, welded tuff, and metabreccia that belong to Tsaliet Group. Tambien Group consists of lower slate, lower limestone, upper slate and upper limestone. The integration of structural, petrological and geochemical studies has been carried out to understand the petrogenic evolution and tectonic setting of the area. The field and microscopic structural data analysis shows that there are at least three phases of deformation: The first phase of deformation (D1) is associated with the formation of pervasive regional foliation and minor tight folds; the second phase of deformation (D2) is responsible for the formation of crenulation cleavages; the third phase of deformation (D3) was followed by latter brittle deformation. The presence of relict texture, preserved primary structures (bedding and cross bedding) and certain mineral assemblages such as chlorite, epidote, muscovite, sericite and albite indicates that the rocks in the study area experienced very low to low grade of metamorphism that belong to green schist facies. The overall geochemical characteristics of the metavolcanic rocks display calcalkaline affinity. The discrimination diagram of Th-Hf-Ta suggested that the metavolcanics were developed in volcanic arc tectonic setting. The micrograntic intrusions display high potassium calcalkaline and peraluminous affinity and the discrimination diagrams of Ta - Yb, Rb – Yb + Ta, and Rb – Y + Nb of suggested that the micrograntic intrusions were developed in volcanic arcs . This is consistent with tectonic environment of metavolcanic rocks. The various chemical indices such as CIA, CIW, PIA, K_2O/Al_2O_3, Th/U and ACNK diagram suggested that the metasediments have been subjected to intermediate degree of chemical weathering. The analyzed metasediments are most likely derived from intermediate igneous rock source and the discrimination diagram of Th - Co - Zr/10 suggested that the sediments were deposited in the oceanic island arc tectonic setting.

Key words: Deformation, Foliation, Metamorphism, Metasediment, Metavolcanic Neoproterozoic and Petrography.

CHAPTER ONE

1. INTRODUCTION

1.1. BACKGROUND AND JUSTIFICATION

The concept of Pan African Orogen (PAO) was formerly introduced by Kennedy (1964) to designate the peak of a wide spread orogenic thermo-tectonic episode characterized by intense period of reactivation and crustal formation. The term Pan African Orogen was used to describe the structural differentiation of Africa into cratons and mobile belts during the Neoproterozoic to earliest Paleozoic time (Kennedy, 1964). However, Kröner (1984) reformulate the term Pan-African to describe the tectonic, magmatic, and metamorphic activity of Neoproterozoic to earliest Paleozoic age throughout the Gondwanaland and in many parts of Laurasia. East Africa orogen (EAO) was formed by the closuring of Mozambique Ocean during the collision of East and West Gondwana (Stern, 1994; Kröner and Stern, 2005; Fritz et al., 2013). It represents the greatest collision zone which extends from southern Israel in the north to Madagascar to the south. The Neoproterozoic basement of Ethiopia is found at the transition between the northern and southern sectors of the East African Orogen (EAO) namely the Arabian-Nubian Shield and the Mozambique Belt respectively (Kazmin et al., 1978; Tarekegn Tadesse et al., 1999; Asfawossen Asrat et al., 2001; Miller et al., 2003). Kroner and Stern (2005) identify two broad types of tectonic domains within the Pan-African/East African Orogen. The first one consists of Neoproterozoic supracrustal and magmatic assemblages many of juvenile (mantle derived) origin, with structural and metamorphic histories that are similar to those in Phanerozoic collision and accretion belts. These belts are exposing rocks of the upper to middle crustal levels and contain diagnostic features such as ophiolite, subduction- or collision-related granitoid, island-arc or passive continental margin assemblages. Such belts include the Arabian-Nubian shield and north-east Africa. The other type of mobile belt generally contains polydeformed high-grade metamorphic assemblages, exposing middle to lower crustal levels. The protoliths of these assemblages consist predominantly of much older Mesoproterozoic to Archaean continental crust that was strongly reworked during the Neoproterozoic. Such belts include the Mozambique

Belt. The formation and evolution of the Shield is related to Neoproterozoic supercontinent cycle notably: the breakup of the supercontinent Rodinia in the first half of the era, formation and closure of major ocean basin, and there by the formation of the new supercontinent, Gondwana, near the era end (Stern, 1994). The process is not a single event rather it consists of the collision and coalescence of numerous juvenile island arcs terranes in between 870-630 Ma. The island arcs were created in association with subduction to close the major ocean basin i.e. Mozambique Ocean (Stern, 1994; Kroner and Stern, 2005). The Northern metamorphic terrains of Ethiopia are mainly composed of low grade metavolcano-sedimentary assemblages that belong to the Arabian---Nubian Shield of the Pan-African orogen (Beyth, 1972; Kazmin, 1973; Kazmin et al., 1978; Garland, 1980; Tarekegn Tadesse, 1996; Tarekegn Tadesse et al., 1999; Asfawossen Asrat et al., 2001 and Mulugeta Alene et al., 2006). Geochemical studies of metasedimentary rock units are used to understand their provenance, weathering condition of the source area and the tectonic setting in which the ancient sediments were deposited (Kibret Sifeta et al., 2005). In similar way, the geochemistry of metavolcanic and micrograntic intrusion are also used to understand the tectonic setting of the volcanic suite and to evaluate their magma type (Mulugeta Alene et al., 2000). The methods and approaches that will be followed / conducted to achieve the general and specific objectives are fieldwork, petrographic analysis, geochemical and structural data analysis.

1.2. General description of the study area

1.2.1. Location

The study area is located around Mai Kinetal in Tigray Region, Northern Ethiopia. Geographically, the study area is bounded between 1530000 m and 1538000 m N latitude and 497000 m and 505000m E longitude (Fig.1.1). The area coverage of study area is approximately 64 Km^2. The average elevation of the area is approximately 1650 m a.s.l.

1.2.2. Accessibility

The study area is accessed by asphalt road which is running from Addis Ababa through Mekelle, Hagere Selam, Abi Adi, Werki Amba, Mai Kinetal and Adwa. The mappable area is accessed by foot path and trails stretching to different locations of the study area.

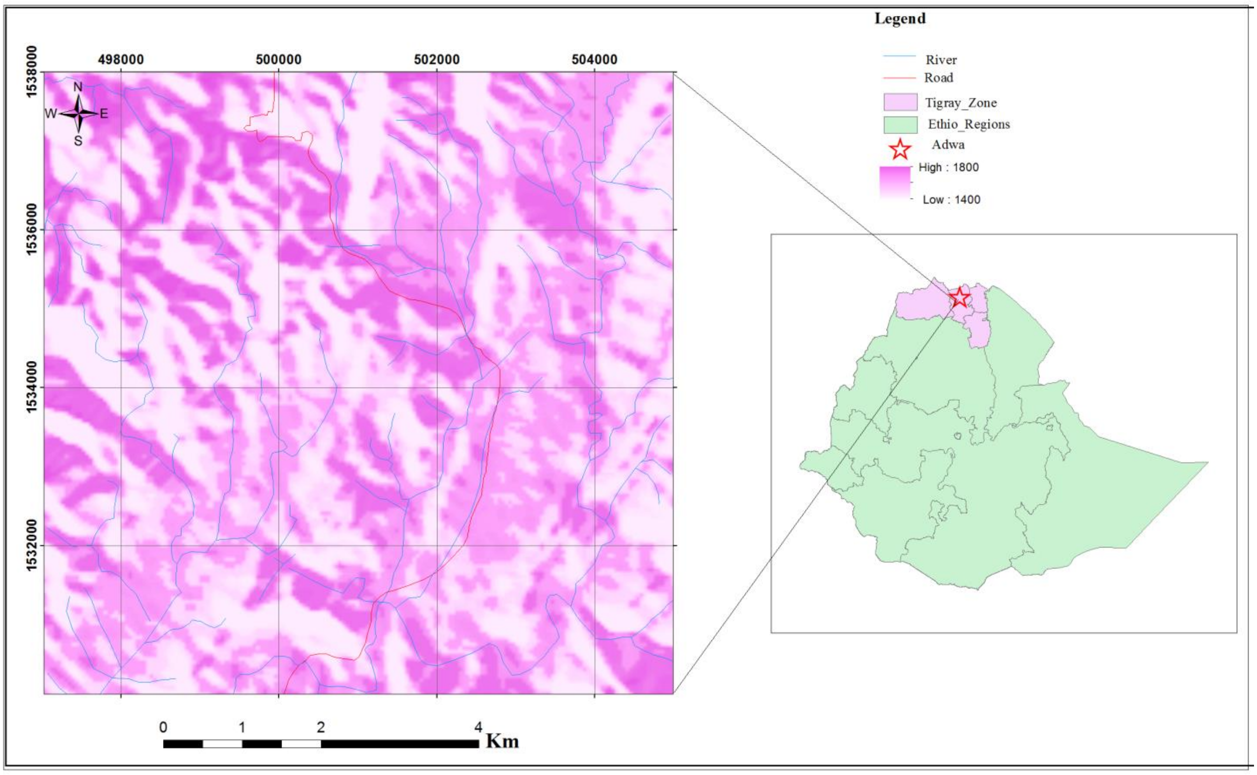

Fig.1.1: Location map and digital elevation model (DEM) of the study area.

1.2.3. Physiography

The study area is characterized by different topographic features such as ridges, hills and flat surface. Hill topography is found in the northern, northeastern and northwestern parts, but the central part is flat and commonly forms a basin type nature. The hills or plateaus of the area are constituted by metavolcanics, metalimestone & some metasedimentary unit, whereas the flat surfaces are mainly constituted by metasediment rock units. Generally, the ridges have N-S trending with a series of saddle and steep slopes (Fig.1.2).

1.2.4. Drainage pattern

The study area is drained with the Werii main river and other small tributaries. Most of the streams flow seasonally and joining with the main Werii river flowing together towards the south western direction of the study area. The drainage pattern of the stream shows variation of density of water flow because of the seasonal variation. Overall, the study area is characterized by trellis drainage pattern.

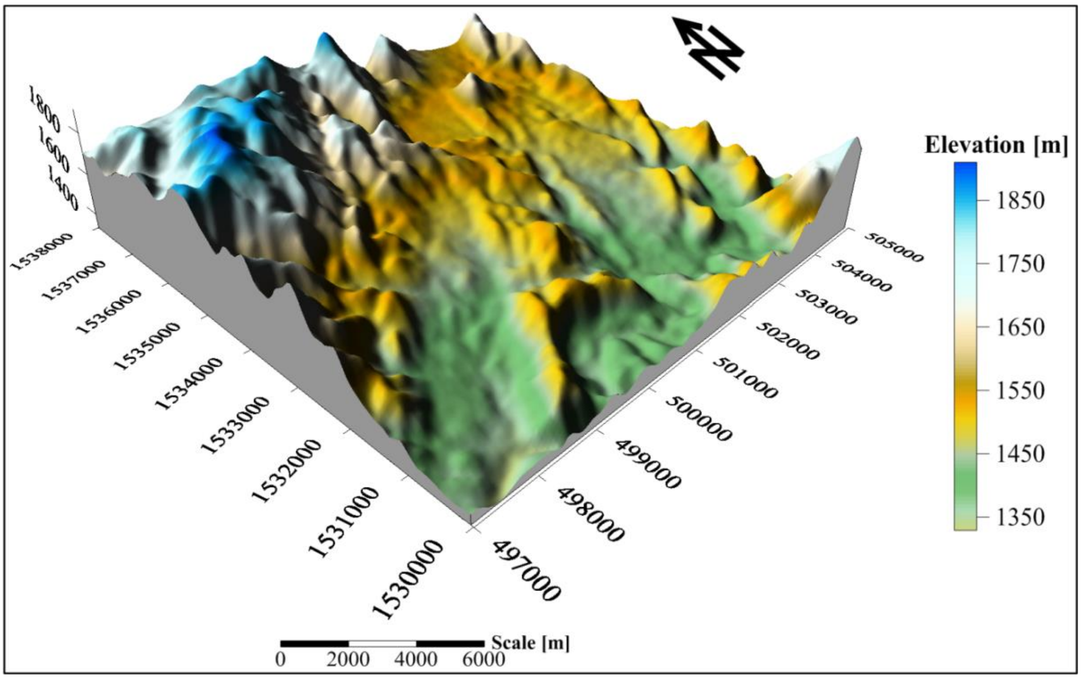

Fig.1.2: Physiographic map of the Mai Kinetal area.

1.2.5. Climatic condition

The climate condition of the area is mainly characterized by warm climatic condition. Besides, this region is known to have arid to semiarid climatic condition with the average rainfall of 610mm and average annual average temperature of 18.2^{0}c (http://en.climate-data.org/location/2108/).

1.2.6. Soil

The study area is categorized among the regions that have poor soil fertility and it is covered by thin soil. This is due to weathering and erosion process. It is not suitable for growth of vegetation; because, the soil of the rock unit is not fertilized. However, the soil at the flat area is little bit fertile than the hill top soils.

1.2.7. Vegetation

The study area is generally characterized by sparsely distributed vegetation coverage. However, the vegetation on the north eastern & north western parts of the study area is slightly denser than the other parts. The vegetation types found in the study are Mekere, shrubs and bushes.

1.3. Research problem

Previous researchers studied the geology and geochemistry of Neoproterozoic rocks in the northern Ethiopia. For instance, granitiods from Negash and Axum area shows geochemical characteristics typical of volcanic arc and the plutonism is subduction related (Asfawossen Asrat, 1997; Tadesse Alemu, 1998; Tarekegn Tadesse et al., 1999). Metavolcanic rocks from Mai Kenetal-Negash and Werii area display geochemical characteristics of depleted magma source and volcanic arc setting (Mulugeta Alene et al., 2000; Kibret Sifeta et al., 2005). However, the metavolcanic rocks of the Axum area display geochemical characteristics typical of intra oceanic island arc systems (Tarekegn Tadesse et al., 1999). Hence, this study presents the local petrological and geochemical characteristics of metavolcanic, metasediment, and intrusive bodies and the geochemical relationship of Mai Kinetal metavolcanic, metasediment, and intrusive bodies with other adjacent metavolcanics and metasediments in the region. These will serve for the larger discussion on the petrogenetic evolution and tectonic setting of Mai Kinetal area.

1.4. Objectives

1.4.1. General objectives

The main objective of this study is to examine the petrological and geochemical characteristics of the rock assemblages, their original protoliths and to understand the tectonic and petrogenetic evolution of these rocks.

1.4.2. Specific objectives

The specific objectives of the proposed research are as follow:-

- To relate the different metamorphic mineral assemblages with environments of metamorphism and geologic setting ;
- To recognize, describe and map the various geological structures;
- To reconstruct the stratigraphy and geologic history of an area;
- To produce detail geological map of Mai Kinetal area at the scale of 1:25,000;
- To explore the implication of geochemical and petrological data to understand the tectonic setting of metamorphic and intrusive rocks;

1.5. Basic research question

To address the objectives mentioned above; the following few research questions must be assessed:

- How can we relate the petrological and geochemical investigation in understanding the tectonic setting of the area?
- What is the contribution of petrological and geochemical investigation of Mai Kinetal area to understand the tectonic setting of the Arabian-Nubian Shield?
- What is the best geochemical interpretation techniques used to characterize and understand tectonic setting and petrogenetic characteristics of Neoproterozoic rock units?
- What are the geochemical criteria used for the identification of palaeotectonic setting and petrogenetic characteristics of Neoproterozoic rock units?

1.6. Methodology

Various activities are employed to achieve the stated objective successfully; the following methods and approaches have been followed.

1.6.1. Revision of previous work

A major activity conducted during the revision of previous works were collection of previous case studies, journals, extracting of relevant information from aerial photograph and satellite image, reviewing and compiling of literatures (published and unpublished reports) related to the study area.

1.6.2. Fieldwork

The main activity conducted during the field work were tracing of structural discontinuity, measuring and recording of geological structures, taking of representative and fresh rock samples for further laboratory analysis (petrographic and geochemical analysis). Furthermore, lithological variations, lithological contacts and the geological structures are transferred to a geological map of scale 1:25,000.

1.6.3. Petrographic analysis

Fresh and representative samples have been collected and the rock samples are cut perpendicular to foliations to prepare thin sections. Twenty (20) thin sections have been prepared at laboratory of Geological Survey of Ethiopia. Thin section samples are selected based on the variety of the lithologies, and their importance to construct the metamorphic and deformation history. Moreover, thin section samples have been examined under Leica petrographic microscope to determine the modal proportion of the identified mineral assemblages and rock fabrics (texture, microstructures).

1.6.4. Geo-chemical analysis

Sample preparation for geochemical analysis includes removal of the weathered part; break the sample into desirable sizes, crush the broken sample and the sample have been milled down to micron size particles. The sample preparation is done in Akaki Kaliti, Kebele 10/11 block 03 milling room. The samples are submitted to the Australian Laboratory Science (ALS) to determine the concentration of major and trace elements. Major elements (including loss on ignition) were analyzed by multi element Inductively Coupled Plasma06 (ME- ICP06). Besides, trace elements were analyzed by Multi Element Mass Sepectrometry81 (ME-MS81).

1.6.5. Structural data analysis

All the structural data that have been collected for different structural elements such as foliations, folds, and joints are plotted and analyzed using stereonet (version 8) and GeoRose. To get an overall orientation of the foliations, folds, and joint rose diagram have been used.

1.7. Significance of the research

The geotectonic setting of metamorphic terrane of northern Ethiopia has been studied before, often at smaller scale, the existing data seems to justify further work at a larger scale. This new result of petrological, geochemical and geological mapping may complement the existing structural and stratigraphical data of the area making a significant contribution to decipher the tectonic history of the area.

1.8. Review of previous works

The area has been receiving attention and geological investigation since the late 19th century during the Italian as well as British expeditions. It has been investigated by Blanford (1870), Danielli (1943), Mohr (1963), Levitte (1970), Arkin et al. (1971), Beyth (1971,1972), Kazmin (1971, 1975) and Garland (1972,1980).

Kazmin et al. (1978) reported on the stratigraphy and possible manner of evolution of Ethiopian Basement ; Asrat (1997) reported on geology and geochemistry of the Negash pluton and their metalogenic significance; Tadesse et al. (1997) studied on geochronology of the Mereb Granite; Alemu (1998) geochemistry of Neoproterozoic granitiods of the Axum area; Tadesse et al. (1999) studied the geochemistry of low grade metamorphic rocks from the Pan-African of the Axum area; Alene et al. (1999) reported on stable isotope composition (13C and 18O) of Neoproterozoic limestone and dolomites; Alene et al. (2000a) studied on the geochemistry and geotectonic setting of Neoproterozoic rocks; Alene et al. (2000b) studied on crystal chemistry of clinopyroxene in Neoproterozoic metavolcanic rocks of Tigray; Asrat et al. (2001) the review of Precambrian geology of Ethiopia; Asrat et al. (2003) studied on the Magma emplacement and mafic–felsic magma hybridization: structural evidence from the Pan-African Negash pluton ; Asrat et al. (2004) studied on the petrology and isotope geochemistry of the Pan-African Negash pluton ; Sifeta et al. (2005) studied on geochemistry, provenance, and tectonic setting of Neoproterozoic metavolcanic and metasedimentary units Werri area; Avigad et al. (2007) studied on the geochronology of Cryogenian Diamictite and Lower Paleozoic sandstone in Ethiopia (Tigrai); Sacchi et al. (2007) studied on the Paleozoic Tillie of the Adigrat Group; Miller et al. (2009) Cryogenian slate-carbonate sequences of the Tambien Group (Tigrai) and Swanson-Hysell et al. (2015) reported on stratigraphy and geochronology of the Tambien Group, Ethiopia.

CHAPTER TWO

2. REGIONAL GEOLOGY

2.1. TECTONIC EVOLUTION OF THE EAST AFRICAN OROGEN

East African Orogen has been formed due to the collision of East and West Gondwana (Fig.2.1) during the Neoproterozoic and it comprises two major segments namely Arabian–Nubian Shield (ANS) in the north and Mozambique Belt in the south (Stern, 1994; Kröner and Stern, 2005; Lulu Tsige and Abdelsalam, 2005).

Arabian–Nubian Shield (ANS) makes up the northern sector of East African orogen and extends from southern Israel to Ethiopia and Yemen. ANS is distinguished from the Mozambique Belt by its juvenile continental crust (mantle derived), relatively less deformed and less metamorphosed and abundance of ophiolites (Asfawossen Asrat et al.,2001; Kröner and Stern, 2005).

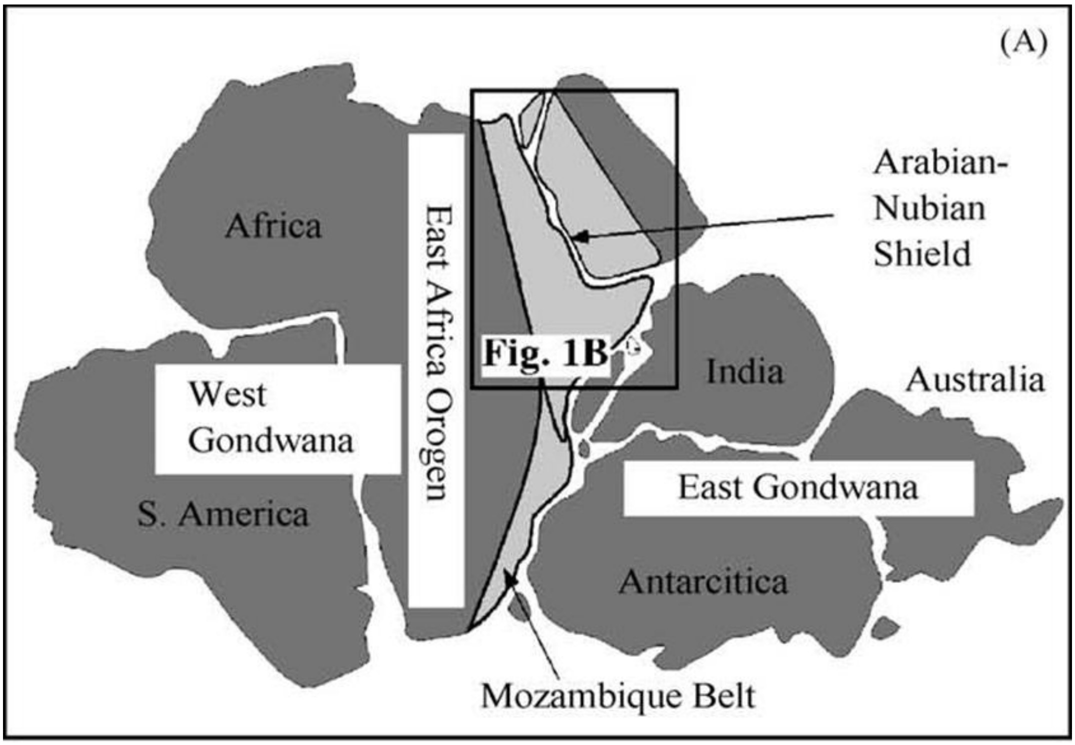

Fig.2.1: East African Orogen between East and West Gondwana (from Lulu Tsige and Abdelsalam, 2005).

The tectonic evolution of East African Orogen (EAO) involves (Fig.2.2) ; (1) rifting and breaking up of the supercontinent Rodinia into West and East Gondwana and initiation of Mozambique Ocean (~900 – 850 Ma) ; (2) sea-floor spreading, juvenile crust production, arcs and back-arc basin formation , terrane accretion and arc magmatism (870 - 690 Ma) ; (3) continental collision between West and East Gondwana forming the East African Orogen, closuring of the Mozambique Ocean, granitic magmatism and post-amalgamation volcano-sedimentary deposition (650-600 Ma) ; (4) crustal shortening, orogenic collapse and extension leading to the break-up of Gondwana (600 to 540 Ma) (Stern, 1994: Kröner and Stern, 2005).

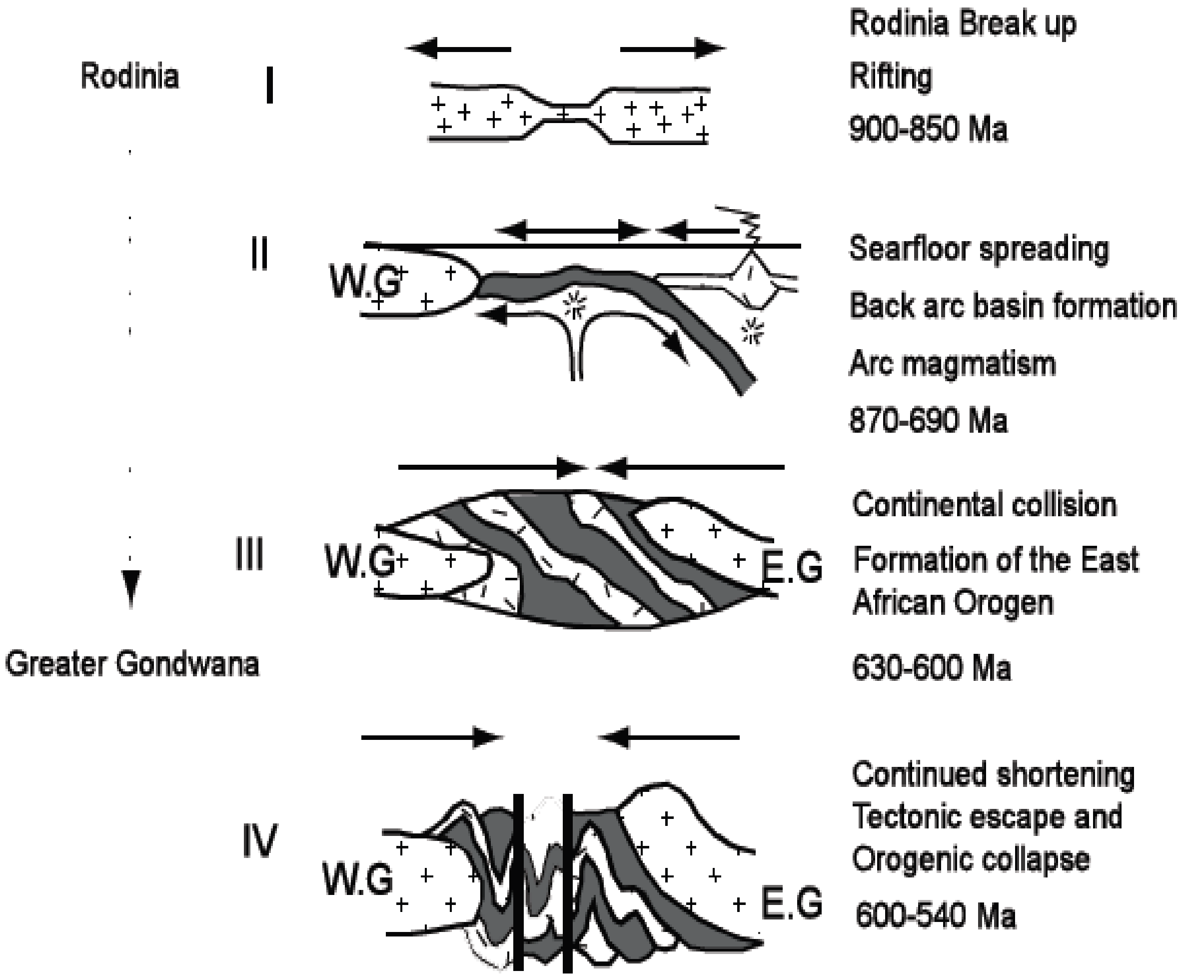

Fig.2.2: Tectonic evolution of the East African Orogen that resulted in the greater Gondwana Super continent (Stern et al., 2006). W.G=West Gondwana and E.G=East Gondwana.

2.2. Geology of the Arabian-Nubian Shield

The main units in the Arabian–Nubian Shield (ANS) consists of Neoproterozoic metasedimentary rocks, migmatites, metavolcanic suites, serpentinites, dismembered ophiolite complex, gabbro-diorite-tonalite complexes, unmetamorphosed volcanic and pyroclastic sequences that are extensively intruded by monzonite-granodiorite-granite complexes (Stern, 1994).

Abdelsalam and Stern (1996) have divided the deformation belts in the Arabian-Nubian Shield (ANS) into: arc-arc and arc-continent collisions and accretionary structures. Arc-arc deformation belts are characterized by the occurrence of N-S and E-W verging ophiolities and they are oriented east to northeast and north to north northeast in the northern and southern parts of the ANS respectively (800 -700 Ma). Arc-continent deformational belts are related to the collision of East and West Gondwana and define the eastern and western boundaries of the ANS (750-650 Ma). Post accretionary structures are formed from continuous shortening of the ANS (~650-550 Ma). These defromational belts are localized along north or northwest ternding pure or simple shear zones.

2.3. Geology of the Ethiopian Basement rocks

The basement rocks of Ethiopia are exposed in north, south, southwest, western, and eastern parts of the country which are grouped into three major groups by Kazmin et al. (1978) based on lithologic and structural mapping: Lower Complex (Archean), Middle Complex (Lower –Middle Proterozoic) and Upper Complex (Upper Proterozoic). In similar way, the Precambrian rocks of Ethiopian have been studied by various scholars [Beyth (1971, 1972); Kazmin (1971, 1975); Kazmin et al. (1978); Garland(1980); Seife Michael Berhe (1990); Mengesha Tefera et al.(1996); Beraki Weldhaimanot (1995);Tarekegn Tadesse (1996);Tarekegn Tadesse et al. (1997, 1999,2000); Asfawossen Asrat (1997); Tadesse Alemu (1998); Mulugeta Alene and Barker (1993,1997); Mulugeta Alene (1998) ; Mulugeta Alene et al. (2000a, 2000b, 2006) and Asfawossen Asrat et al. (2001, 2003, 2004)] to mention only few.

Recently, the three fold geosynclinal stratigraphy of Kazmin (1971, 1975) has been revised and rejected on the basis of geochronological, thermochronological, geochemical and lithotectonic data. The Ethiopian basement rocks are regrouped into two major blocks; (1) Volcanic-sedimentary terrain and (2) Gneisic–migmatitic terrain (Asfawossen Asrat et al., 2001). Asfawossen Asrat et al. (2001) identifies three periods of granitic magmatism from three complexes of Kazmin (1971) both in ANS and MB: 800-885Ma, 700-780Ma and 540-660Ma.

2.4. Geology of the Tigray Basement rocks

The northern Ethiopia Precambrian rocks are characterized by the occurrence of low-grade volcano-sedimentary rocks (Beyth, 1971; Kazmin, 1973; Tarekegn Tadesse et al., 1997; Tarekegn Tadesse et al., 1999; Mulugeta Alene et al., 2000). The basement rocks of central and eastern Tigray has been studied by different researcher [Levitte (1970), Beyth (1971, 1972); Garland (1980); Tadesse Alemu (1998); Tarekegn Tadesse (1996) ; Tarekegn Tadesse et al. (1997,1999); Mulugeta Alene (1998) ; Mulugeta Alene et al. (2000a, 2000b, 2006); Asfawossen Asrat et al. (1997, 2003, 2004); Kibret Sifeta et al. (2005) and Avigad et al.(2007)].

Tarekegn Tadesse et al. (1999) studied the geochemistry of metavolcanic rocks from Axum area; the geochemical result indicated that accreted intra-oceanic arc sequences with varied lithological characteristics. In similar way, the geochemistry of metavolcanic rocks from Mai Kenetal- Negash and Werii area display depleted magma source and volcanic arc setting (Mulugeta Alene et al., 2000; Kibret Sifeta et al., 2005).

Beyth (1972) divided the basement rocks of Northern Ethiopia into Tsaliet and Tembien Groups based on stratigraphic relationships. Tsaliet Group is mainly composed of metavolcanic/volcanoclastic, metagreywacke, metacarbonates, slate, calcareous siltstone, intermediate to acidic welded tuffs, and lapilli tuff (Beyth 1972; Beyth et al., 2003; Tarekegn Tadesse et al., 1999; Mulugeta Alene et al., 2006). Tambien Groups are mainly exposed in Mai Kenetal, Tsedia, Chehmit, and Negash synclinal inliers (Fig.2.3) surrounded by the Tsaliet Group rocks (Beyth, 1972; Mulugeta Alene et al., 2006;and Miller et al.(2009,2011). Furthermore, the lithostratigraphic sections of the Tambien Groups from the oldest to the youngest describe as follows; Werii Formation, Assem Formation, Tsedia Formation, Mai kenetal Formation, Amota Formation, Didikama Formation, Matheos Formation, Marian Bohkakho Formation, and Negash Diamictite (Mulugeta Alene et al., 2006; Swanson-Hysell et al., 2015).

Swanson-Hysell et al. (2015) have been reported that the Tambien Group consists of approximately 5-km thick mixed carbonate-siliciclastic succession. These sediments are accumulated above volcanics and volcaniclastics of the Tsaliet Group. In similar way, the Tambien Group consists of a number of inliers each containing 2-3 km thickness of interbedded carbonates and clastic sediments (Mulugeta Alene et al., 2006). The contact between the Tsaliet and Tambien Groups is transitional, and input of volcanic ash into the basin continued during the deposition of the Tambien Group (Mulugeta Alene et al., 2006; Swanson-Hysell et al., 2015).

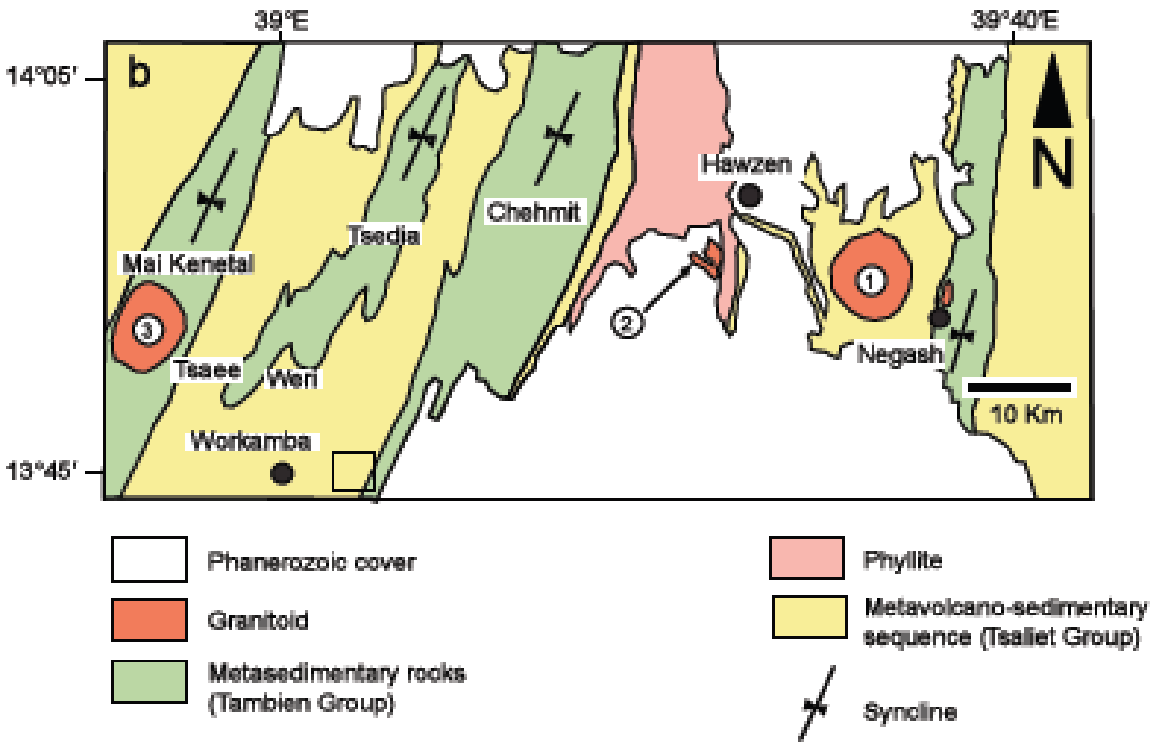

Fig.2.3: The distribution of Tambien Groups in four synclinal inliers (from Mulugeta Alene et al., 2003 after modified by Solomon Gebresilassie, 2009). The circles with number represent the location of dated granitoids in the region, which are both syn- and post-tectonic in origin.

CHAPTER THREE

3. GEOLOGY OF MAI KINETAL AREA

3.1. INTRODUCTION

The Mai Kinetal area is a part of low grade metamorphic terrain of northern Ethiopia that is dominated by Tsaliet and Tambien Groups (Fig.3.1). Tsaliet Group is represented by metavolcanics and metavolcanoclastics that are exposed in the northwestern and northeastern part of the study area, whereas the Tambien Group is represented by lower slate, lower limestone, upper slate and upper limestone that are exposed in the central part of the study area. Both Tsaliet and Tambien Groups are intruded by micrograntic intrusions (aplitic dykes). The study area has different types of rock units which are differentiated by their lithological and textural description, and degree of deformation.

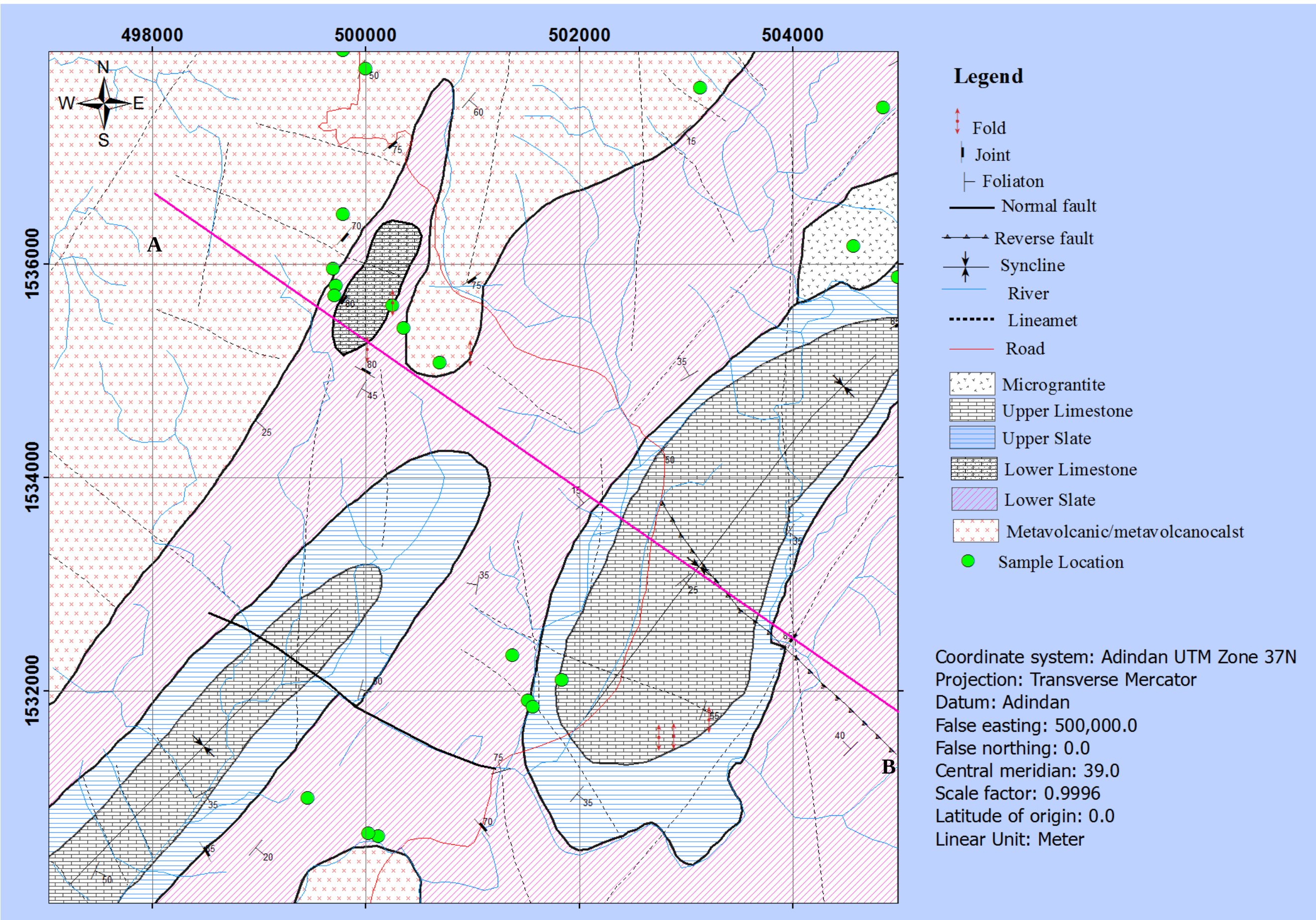

Fig.3.1: Geological map and sample location of the study area.

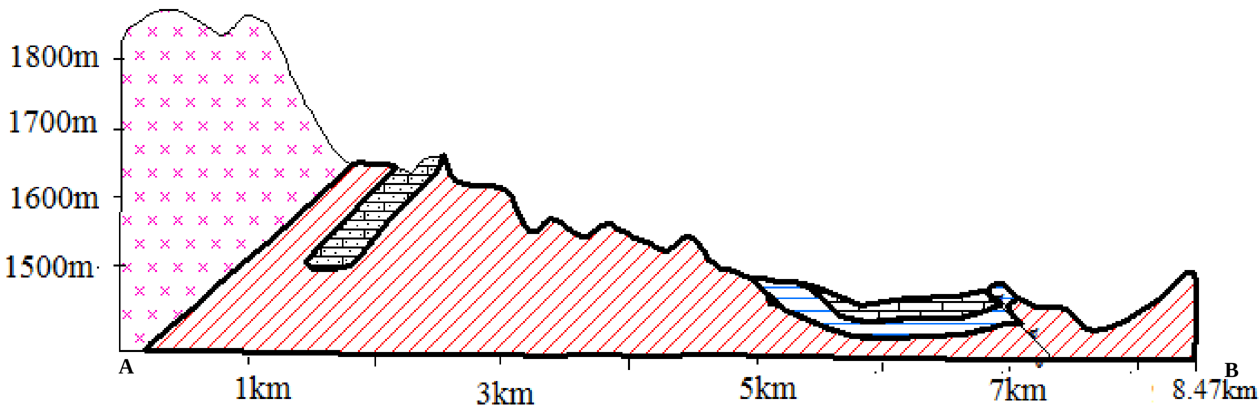

Fig.3.2: Geologic cross section of the study area

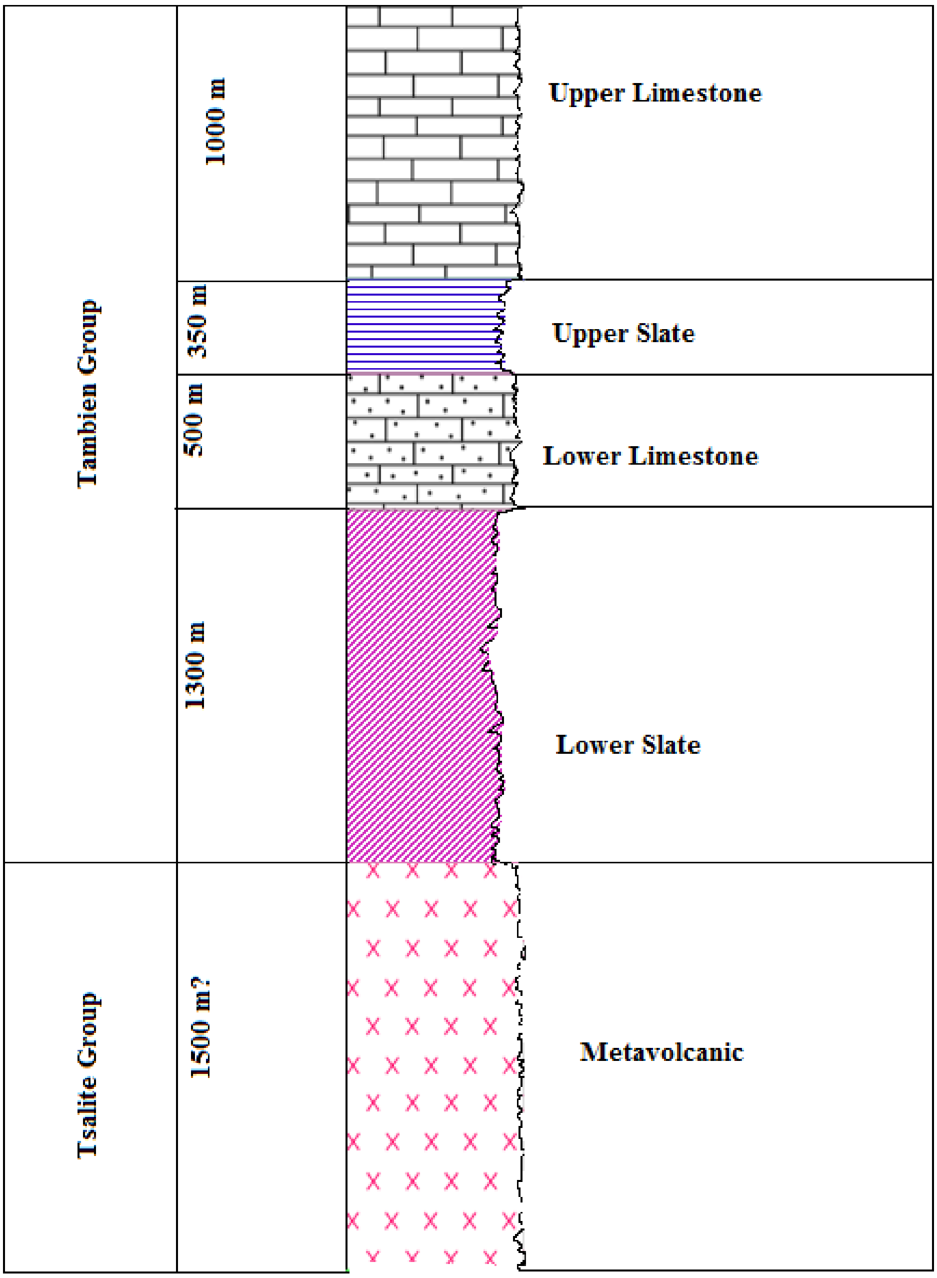

Fig.3.3: Lithostratigraphic section of the study area

3.2. Lithostratigraphic units of the study area

The common lithologies found in the study area are metavolcanic, metavolcanoclastic, lower slate, lower limestone, upper slate and upper limestone from oldest to youngest based on stratigraphic relationship (Fig.3.3).

3.2.1. Metavolcanics (MV)

This rock unit is exposed in north-western and north-eastern part of the study area. It is consisting of basic and acidic metavolcanics. Basic metavolcanics are weakly foliated, fine grained and contains some primary volcanic textures (porphyritic). Acidic metavolcanics are weakly foliated, medium grained, and show light gray to light yellow color. Both basic and acidic metavolcanics are characterized by ridge /steep topography and hillside exposure (Fig.3.4). The strike of the foliation varies from N20^0-30^0E and its dip from 40^0-70^0 NW. Petrographic examination of MV1 indicates that this rock is composed of 40% plagioclase, 20% k-feldspar, 15% quartz, 10% epidote, 5% calcite, 5% chlorite and 5% opaque, whereas MV9 is composed of 40% plagioclase, 20 % chlorite, 15% epidote, 10 % opaque, 10 % quartz, 3% sphene and 2 % garnet. Similarly, another thin section (MV12) shows 45 % plagioclase, 40 % opaque (hematite + other oxides), 5% chlorite and 5% epidote, and MV5 shows 50% epidote, 25 % quartz, 15% plagioclase and 10 % k-feldspar. Finally, sample MV1 is derived from acidic volcanic whereas the samples of MV5, MV9 and MV12 are from basic volcanic rocks.

Fig.3.4: Outcrop photo pictures of metavolcanic unit (0501980E: 1536850N).

3.2.2. Metavolcanoclastics (MVC)

This rock unit is exposed in north-western and north-eastern part of the study area. It consists of metagreywacke, welded tuff and metabreccia. Metavolcanoclastics show significant variation in size, shape and chemical composition of the clasts. The size of clasts varies from few mm scale to 5 cm and have angular, sub angular, elongated (elliptical), and sub rounded to round shapes. Furthermore, the composition of clasts (lithic and mineral fragment) ranges from mafic to felsic. The matrix of MVC consists of fine grained material that shows light gray to gray and light green to green color (Fig.3.5). It is characterized by steep topography and hillside exposure. This rock unit is slightly foliated and its strike varies from N20^0-40^0E and its dip amount from 40^0-75^0 NW. This unit is cut by zones of continuous and discontinuous quartz vein and joints with different orientations. Petrographic examination of this rock (MV2, MV4) shows 55- 60% plagioclase ,10- 15% quartz, 15% k-feldspars , 5% chlorite and 0- 5% opaque. The presence of rock fragments of plagioclase and k-feldspar implying that pyroclastic in origin. Another thin section MV8 contains 50% plagioclase, 20 % quartz, 10% epidote, 10% chlorite, 5% opaque and 5% pyroxene. The dominant plagioclase and quartz in samples of MV2, MV4 and MV9 indicates that felsic volcanic rocks are the protolith.

Fig.3.5: Field photo pictures of metavolcanoclastic unit. This rock unit consists of coarser angular rock fragments of quartz and feldspar in fine grained ground mass (0499800E: 1535666N).

3.2.3. Lower Slate

This rock unit is mainly exposed in the central part of the study area (Fig.3.6) and it has an estimated thickness of ~1300 m. It shows tectonic contact with the underlying unit in the northeastern part, whereas in the central part it has a gradational contact with the overlying unit. Thin graphite bed and some primary sedimentary structures (e.g. thin lamination and cross-bedding) are found as lens in some parts. These primary sedimentary structures are locally preserved in less deformed pods. This unit is highly variegated from light brown to brownish, light gray to gray and reddish color. Petrographic study of siliciclastic sediment (MS3) shows 40% plagioclase, 25% quartz, 15% calcite, 15% k-feldspar and 5% opaque, whereas MS4 contain 50% plagioclase, 25% quartz, 15% k-feldspar, 5% chlorite and 5% opaque. Petrographic study of the graphite bed (MS9) shows 60% graphite, 15% quartz, 15% plagioclase and 10% sericite. The strike orientation of the foliation varies from N20^0-60^0E and its dip amount from 20^0-70^0 NW. However, the exposures in the southern part of the study area are relatively less foliated. In general, the petrographic examination of this unit shows variable mineralogy: ~25-55% muscovite/ sericite, ~10-15% quartz, ~5-15% K feldspar, ~10- 50 % plagioclase, 5-25% opaque and 0-20% calcite (MS13, MS17, MS19, and MS20). The original (protolith) of this unit is acidic metavolcanic rocks.

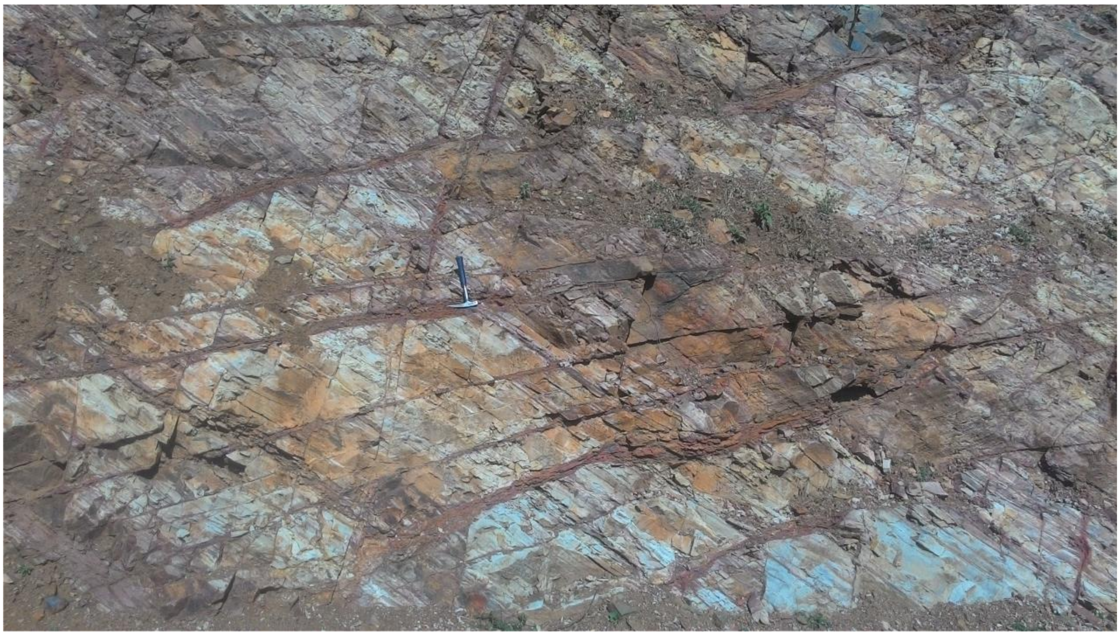

Fig.3.6: Field photo pictures of lower slate unit (0505000E:1535439N).

3.2.4. Lower Limestone

This rock unit is overlaying the lower slate and underlying the upper slate. In some places also found as lens in metavolcanic rock units. It is characterized by stromatolithic lamination, breccia imbedded within the bedding, and ridge forming topography (Fig.3.7). The stromatolithic laminations are dissected by quartz veins. This unit is highly variegated from brownish to light brown and light gray to dark gray color. It has an estimated thickness of ~500 m. Petrographic examination of this unit (ML4) show that this rock is mainly composed of micrite 90% and 10 % sparite.

Fig.3.7: Field photo pictures of lower limestone unit (0500250E: 1535608N). This unit contains stromatolithic lamination and this structure is important to reconstruct and determine the stratigraphic way up (younging directions).

3.2.5. Upper Slate

This rock unit is exposed in the core of the Mai Kinetal syncline. Besides, it is highly variegated from light gray to dark gray and light brown to brownish color. It has an estimated thickness of ~350 m. It shows composite fabric .i.e. the presence of parallel to subparallel primary and secondary foliations. The primary foliations are recognized by variation of thickness, composition and grain size of the layers (Fig.3.8). The upper slate shows gradational contact with the upper limestone in the central part of the study area. It is also intercalated with limestone in some places. The strike of slaty cleavage is N15^0-

60^{0}E and its dip varies from 20^0-70^0 NW. Petrographic examination of this unit indicates that this rock is mainly composd of 65% epidote, 15% quartz, 15% feldspar and 5% opaque. The abundance of epidote indicates that basic volcanic rocks are the parent materials.

Fig.3.8: Field photo pictures of upper slate (0498833E: 1530415N). This unit show composite fabric i.e. the presence of parallel to subparallel primary bedding and secondary foliations.

3.2.6. Upper Limestone

This rock unit is mainly exposed in the core of the Mai Kinetal syncline. The color of this unit varies from light gray to dark gray and black color. It has an estimated thickness of about ~1000 m. This unit shows composite fabric i.e. the presence of parallel to subparallel primary bedding and the secondary foliations. Small scale micro-folds are observed on this unit. The micro folds on limestone and slate unit have N-S plunging direction with sub horizontal to horizontal fold axes. It is fine-grained and contains abundant calcite veins

3.2.7. Micrograntic intrusion

The micrograntic intrusion is exposed in all part of the study area .They have a wide spread distribution within the metavolcanic, lower slate and upper slate. They are massive, forming small linear ridges in some places and most of them are vertical to sub vertical. The width and length of aplitic dikes is variable, but in some area occur as small linear ridges around 200 m wide and 350 m long which roughly strikes NE–SW. It is dissected by various joints and fractures producing sub rounded massive blocks (Fig.3.9).

Petrographic study of this unit (PR2 and PR3) shows 30-35 % plagioclase, 20-25 % K-feldspar, 20% quartz, 10 % epidote, 5% opaque and 5% chlorite. This unit shows weak foliation which are defined by chlorite and epidote.

Fig.3.9: Field photo pictures of micrograntic intrusion (0503585E: 1535094N). This unit shows sub rounded and massive blocks. Massive and sub rounded blocks are formed perhaps due to jointing, fracturing and weathering effect.

3.2.8. Quartz vein

Quartz veins have wide distribution throughout the study area. Most of the quartz veins are associated with joints as well as fractures and crosscut the regional trend of the foliations. A quartz vein occurs as a small vein ridges, thin and stringers and having a size range from 1-2m thickness and 5-10m length (Fig.3.10). Moreover, petrographic analysis indicates that the generations of quartz veins are postdated than D1 and pre to post to D2.

Fig.3.10: Field photo pictures of quartz vein. The photo pictures are taken north facing (050200E:1536800N).

CHAPTER FOUR

4. PETROGRAPHY AND METAMORPHISM

4.1. PETROGRAPHY

To further characterize the deformation and metamorphism history of an area, thin sections from representative rock samples have been prepared and examined. The thin section was analyzed to supplement microstructural analysis using both plane-polarized light (PPL) and cross polarized light (XPL). The analyzed samples show relic texture of the protolith and new minerals that have been developed due to metamorphic processes.

4.1.1. Metavolcanic rocks

Petrographic analysis of the representative samples (Fig.4.1A-D) from metavolcanic rocks indicates that these rocks are largely composed of quartz, k-feldspar, plagioclase, epidote, chlorites and opaque minerals.

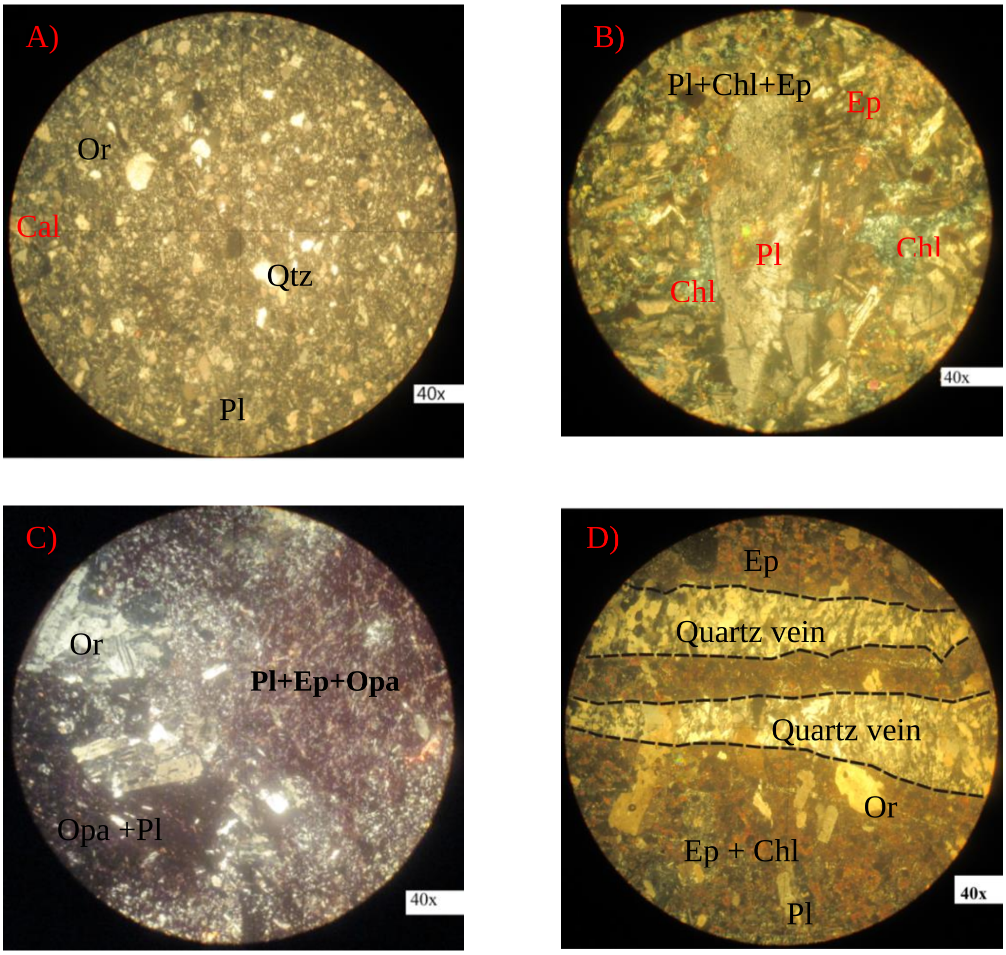

Fig.4.1A-D: Microscopic photo-pictures of metavolcanic rock unit. **(A)** Sample # MV1 in XPL, 40 X magnifications, location (0503137 E: 1537646 N). Mineral content: 40% plagioclase, 20% k-feldspar, 15% quartz, 10% epidote, 5% calcite, 5% chlorite and 5% opaque. This rock unit exhibit porphyritic texture i.e. relatively larger grains of k-feldspar and plagioclase are set in a fine grained matrix of k-feldspar, plagioclase and quartz. The faint foliations are defined by the plagioclase feldspar. The relicts of pyroxene are altered into chlorite and epidote elsewhere in the thin section. Besides, the quartz grains are recrystallized and deformed. Quartz grains have angular to sub angular shape and exhibiting undulose extinction. The abundance of plagioclase and k-feldspar and porphyritic textures indicates that acidic volcanic rocks are the protolith materials (Asfawossen Asrat, 1997). **(B)** Sample # MV9 in XPL, 40 X magnifications, location (0499998 E: 1537827 N). Mineral content: 35 % plagioclase, 25 % epidote, 15% chlorite, 10 % opaque, 10 % quartz, 3% sphene and 2% garnet. The protolith mineral remnants of pyroxene are altered into epidote and chlorite elsewhere in the thin section. Besides, the lager crystal of plagioclase feldspar consists of enormous amount of inclusions. Most of the minerals do not show any preferred orientation; however, faint foliations are defined by chlorite and plagioclase feldspar. The presence of garnet may indicate that slightly higher grade (upper green schist facies). The presence of dominant epidote and chlorite minerals indicates that they are derived from basic volcanic rocks (Asfawossen Asrat, 1997). **(C)** Sample # MV12 in XPL, 40 X magnifications, location (0499788 E: 1537999 N). Mineral content: 50 % plagioclase, 45 % opaque (other oxides +hematite), 5% chlorite and 5% epidote. Most of the plagioclase and opaque minerals have diffused pattern. This sample does not have preferred alignment of minerals. The larger crystals of plagioclase feldspar are set in a fine grained plagioclase and opaque minerals. Furthermore, the pyroxenes are altered in some extent to chlorite and epidote. The mineral assemblages i.e. the presence of chlorite, epidote and the dominant of hematite indicates that basic volcanic rocks are the parent materials. **(D)** Sample # MV5 in XPL, 40 X magnifications, location (0499800 E: 1535666 N). Mineral content: 50% epidote, 25 % quartz, 15 % plagioclase and 10 % k-feldspar. Most of the minerals have random orientation. The quartz crystals within the quartz vein have elongated shape and irregular grain boundaries. This elongated shape and irregular grain boundaries of quartz crystals are formed probably due to intracrystalline deformation and dynamic recrystallization. Furthermore, the development of the fiber is also visible in the quartz vein. The presence of the abundance of epidote indicates that basic volcanic rocks are the parent materials.

4.1.2. Metavolcanoclastic rocks

A thin section (Fig.4.2A-C) from representative metavolcanoclastic rocks has been prepared, analyzed, presented and interpreted as follows. Compositionally, these rock units are composed of chlorite, epidote, quartz, opaque, k-feldspar and plagioclase.

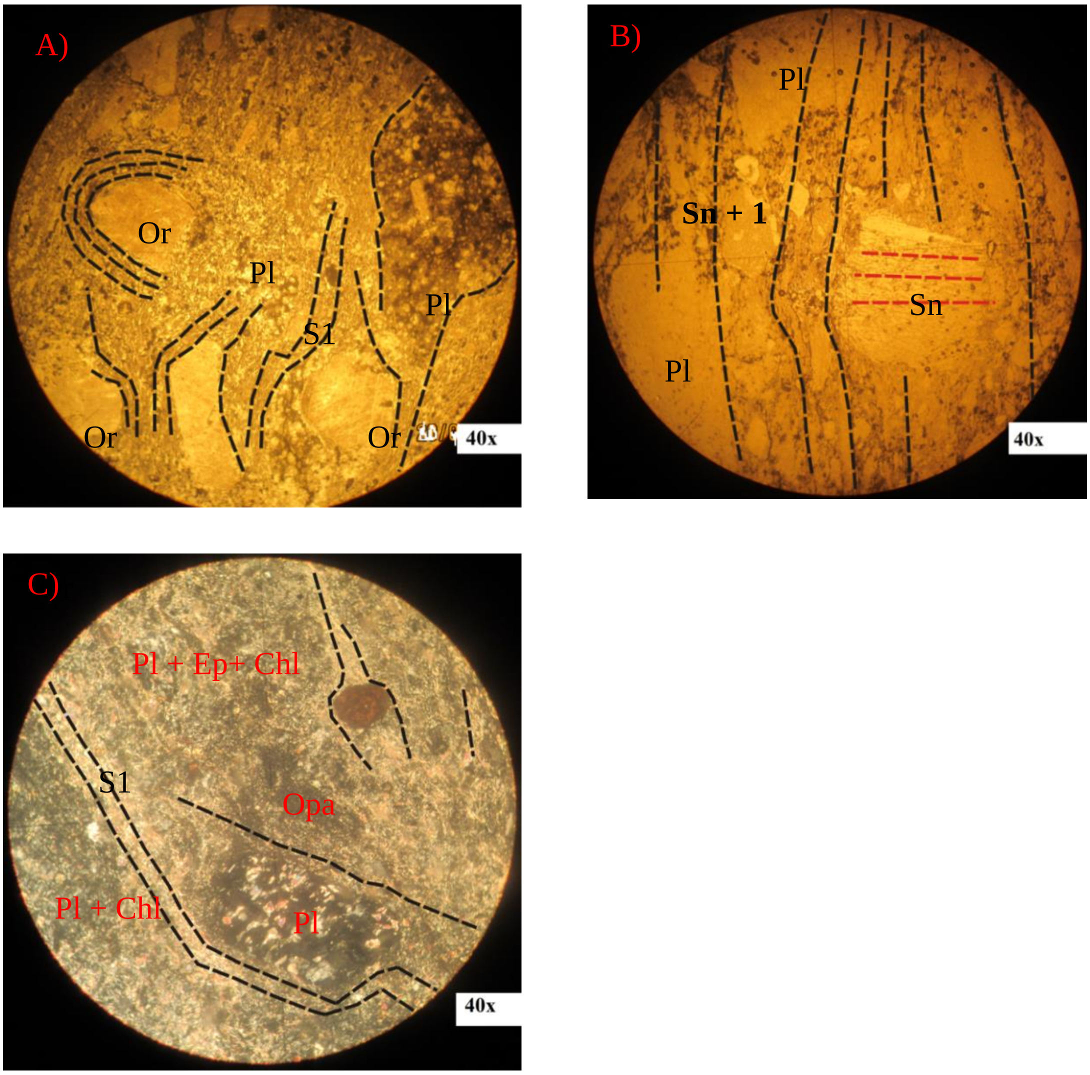

Fig.4.2A-C: Microscopic photo-pictures of metavolcanoclastic rock unit. **(A)** Sample # MV2 in XPL, 40 X magnifications, location (0500690 E: 1535074 N). Mineral content: 55% plagioclase, 20% k-feldspar, 15% opaque and 10% quartz. S1 foliations are deflected around the porphyroclasts of k-feldspar. The porphyorclasts are pre tectonic relative to the external foliations because the matrix foliations are deflected around the porphyroclast. S1 foliations are mainly defined by preferred alignment of plagioclase feldspar. The porphyroclasts of plagioclase and k – feldspar are set in a fine grained matrix of plagioclase and quartz. This rock exhibits relict porphyritic textures. Hence, the presence of rock fragments of plagioclase and k-feldspar implying that pyroclastic in origin. **(B)** Sample # MV4 in XPL, 40 X magnifications, location (0500354 E: 1535400m N). Mineral content: 60% plagioclase, 20% k-feldspar, 15% quartz and 5% opaque. The porphyroclasts of plagioclase and k-feldspar are set in a fine grained matrix of quartz and feldspar. Moreover, the plagioclase feldspar in some part of the thin section show coarse grained aggregates with preferred orientation and in other partly of the thin section coarse grained aggregates of plagioclase displays random orientation. The preferred orientations (Sn) of

coarse grained aggregates of plagioclase are probably developed due to either the flow band or the deformation effect. The external foliation (Sn+1) are wrapping around the clusters of plagioclase and k- feldspar. Sn+1 foliation are mainly defined by plagioclase feldspars. This unit exhibit at least two phase of deformation under this observation. The presence of fragments of plagioclase and k feldspar indicates that pyroclastic in origin (Asfawossen Asrat, 1997). **(C)** Sample # MV8 in XPL, 40 X magnifications, location (0499788 E: 1536463 N). Mineral content: 50 % plagioclase, 20 % quartz, 10 % chlorite, 10 % epidote, 5% opaque and 5% pyroxene. The spaced foliations (S1) are defined by epidote and plagioclase feldspar. This spaced foliation is wrapped around the subhedral to euhedral plagioclase. The porphyroclasts of plagioclase are set in a fine grained matrix of plagioclase and quartz. In addition, clusters of plagioclase and quartz fragment are visible in some part of the thin section. This rock show relict porphyritic texture with plagioclase phenocrysts. The dominant plagioclase and quartz indicates that felsic volcanic rocks are the protolith, whereas the presence of chlorite and epidote are resulted from alteration of relicts of pyroxene.

4.1.3. Slates

Petrographic analysis of the slate unit (Fig.4.3 A-J) indicates that these rocks are mainly composed of muscovite, sericite, chlorite, graphite, quartz, feldspar and calcite. The presence of mafic metamorphic minerals such as sericite, chlorite and epidote shows that the slate unit has a volcanic or volcanoclastic origin at the present scale of observation.

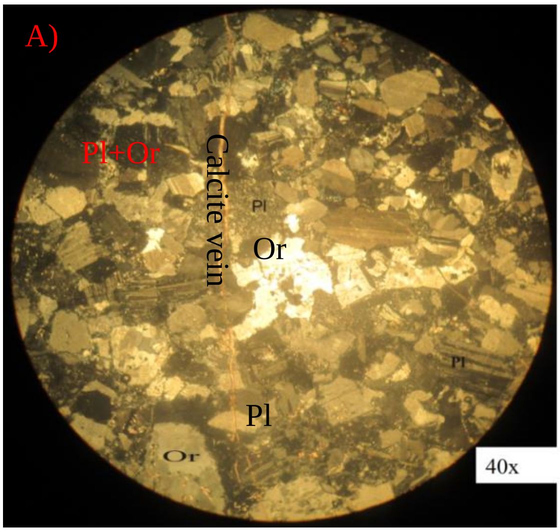

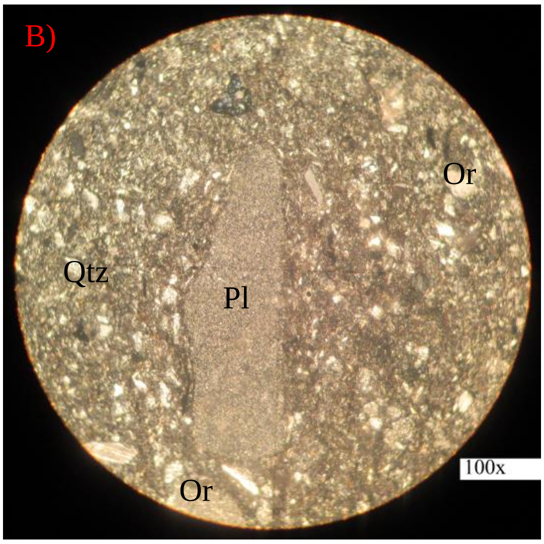

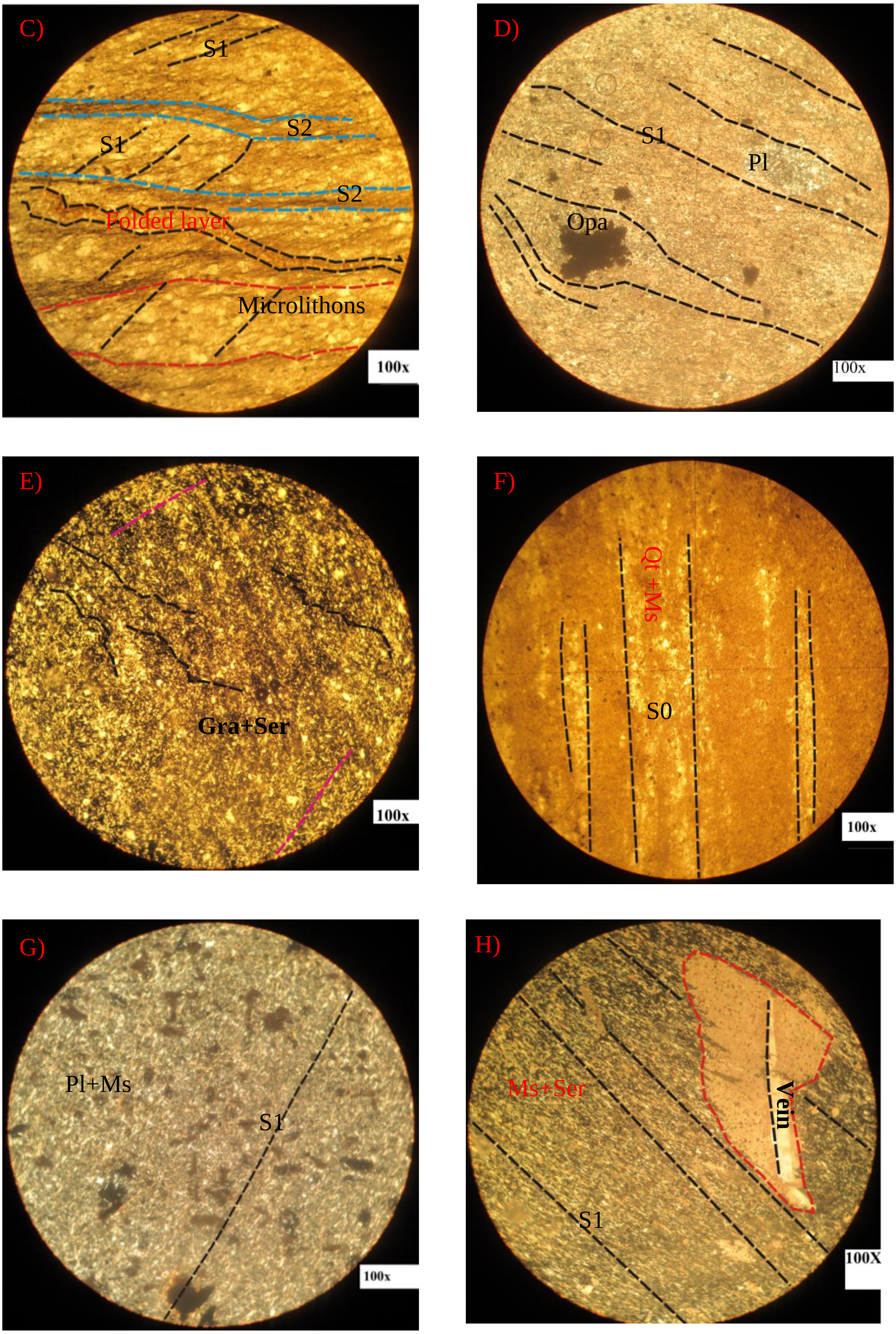
C)
S1
S2
S1
S2
Folded layer
Microlithons
100x
D)
S1
Pl
Opa
100x
E)
Gra+Ser
100x
F)
Qt +Ms
S0
100x
G)
Pl+Ms
S1
100x
H)
Ms+Ser
Vein
S1
100X

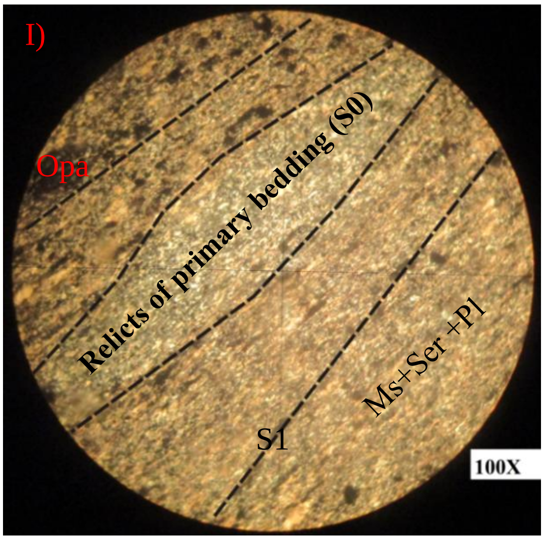

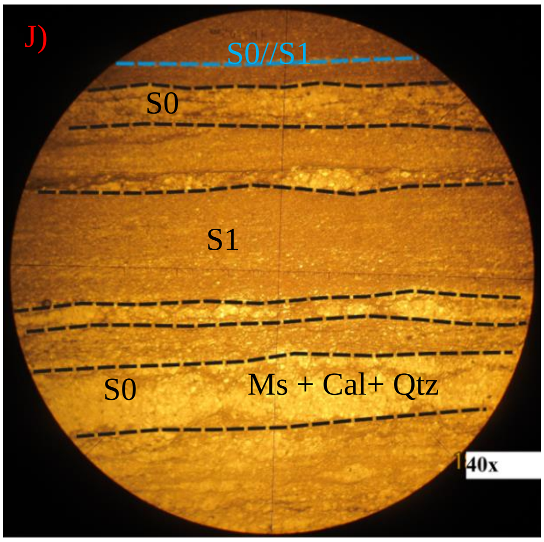

Fig.4.3A-J: Microscopic photo-pictures of the various types slate unit from different locations. **(A)** Sample # MS3 in XPL, 100 X magnifications, location (0500022 E: 1530665 N). Mineral content: 40% plagioclase, 25% quartz, 15% calcite, 15% k-feldspar and 5% opaque. Most of the minerals have random orientation. The quartz grain shows undulatory extinction and irregular grain boundary. The elongated and irregular grain boundaries of quartz are formed probably due to intracrystalline deformation and grain boundary migration recrystallizations. K-feldspar and plagioclase shows euhedral to subhedral grain shape, whereas the quartz grains have anhedral shape. Calcite vein are also visible. In adition, the sample show weak foliations defined by plagioclase feldspar. The dominace of plagioclase, quartz, and k-feldspar indicates that this rock unit has an acidic volcanic rock in origin. **(B)** Sample # MS4 in XPL, 100 X magnifications, location XPL (0500022 E: 1530665 N). Mineral content: 50% plagioclase, 25% quartz, 15 % k-feldspar , 5% chlorite and 5% opaque . The faint/weak foliations are defined by muscovite and plagioclase; however k-feldspar and quartz show random orientation.

This sample show relicts of porphyritic i.e. larger phenocrysts of quartz and plagioclase are set in a fine grained matrix of feldspar and quartz. The grain size of plagioclase feldspars approximately is up to 0.1 mm. Quartz vein are also visible and the quartz crystals within the vein shows some sort of undulatory extinctions. The overall texture and mineral assemblage indicates that pyroclastic in origin. **(C)** Sample # MS7 in PPL, 100 X magnifications, location (0498823 E: 1530415 N). Mineral content: 40% muscovite/ sericite, 25% plagioclase, 20% quartz, 10 % chlorite and 5% opaque. S1 foliations are defined by preferred alignment of muscovite and feldspar and formed as result of D1 event. S1 foliation has been crenulated by D2, as the result crenulation cleavage (S2) is formed. The crenulation cleavages (S2) are defined by cleavage domains (flanks of microfolds) and microlithons (fold hinge). This crenulation cleavage has been formed due to the migration of minerals or solution transfer in response to stress gradient during the formation of microfolds (Mulugeta Alene, 1993). S2 is more pronounced due to the compositional variation. The micaceous layers has been folded and boudinaged and are parallel to the crenulation cleavage (S2). The sequence of such events can be explained as follows: formation of first foliation (S1), later deformation caused S1 to produce crenulation cleavage (S2), formation of folded muscovite layer, and micaceous layer is boudinaged elsewhere on the thin section. **(D)** Sample # MS8 in PPL, 100 X magnifications, location (0501520 E: 1531907 N). Mineral content: 40 % muscovite, 20 % plagioclase, 15% opaque, 10% chlorite, 10% sericite and 5% quartz. S1 foliations are defined by preferred alignment of muscovite/ sericite. S1 are deflected around the opaque minerals and k-feldspar. The presence of pressure shadows in the direction of the main foliation around the opaque minerals shows that D1 must have post-dated than the opaque and plagioclase. **(E)** Sample # MS9 in PPL, 100 X magnifications, location (0501569 E: 1531852 N). Mineral content: 60% graphite, 15 % plagioclase, 15% quartz and 10 % sericite. This sample consists of fine grained quartz and alkali feldspar. S1 foliations are mainly defined by preferred alignment of plagioclase, graphite and sericites. Besides, the development of weak crenulation cleavage (S2) is visible due to the micro folding/crenulation of S1. S2 foliation is defined by graphite and sericites. **(F)** Sample # MS11 in PPL, 100 X magnifications, location (0501834 E: 1532101N). Mineral content: 65% epidote, 15% feldspar, 15% quartz and 5% opaque. The sub vertical compositional layering can be interpreted as bedding (S0) because of its thickness and compositional variations. S1 foliations are mainly defined by muscovite, quartz and feldspar that run parallel to the bedding (S0). This rock unit show composite fabric .i.e. the presence of parallel to sub parallel primary and secondary foliations. The presence of dominant epidote minerals indicates that basic volcanic rocks are probably the protolith materials. **(G)** Sample # MS13 in XPL, 100 X magnifications, location (0501377 E: 1532334 N). Mineral content: 50% plagioclase, 25% muscovite /sericite, 15 % opaque and 10% quartz. The continuous cleavages (S1) are mainly defined by preferred orientation of fine-grained feldspar and mica. This continuous foliation is consisting of non-layered homogeneous distribution of platy minerals (muscovite) and feldspar with a preferred orientation. The isotropic minerals are overprinted and overgrown on the slaty cleavage (S1). The growths of isotropic minerals are postdated than D1 since the minerals are overprinted and overgrown on the continuous foliations. **(H)** Sample # MS17 in XPL, 100 X magnifications, location (0504847 E: 1537460 N). Mineral content: 55% mica/ sericite, 25 % opaque, 10 % calcite and 10 % plagioclase. The continuous foliations (S1) are mainly defined by the preferred orientation of fine mica. Crystals of calcite are overprinted and overgrown on the slaty cleavage implying that calcite crystals are post-tectonic with respect to slaty cleavage. Moreover, the calcite veins are boudinaged into smaller fragments elsewhere in the thin section. The sequence of events can be explained as follows: formation of first foliation (S1), formation of calcite crystals, formation of calcite vein, and boudinaged the calcite veins into smaller fragments. **(I)** Sample # MS19 in XPL, 100 X magnifications, location (0505849 E: 1535875 N). Mineral content: 50 % muscovite/sericite, 20% opaque, 10% quartz, % 10 plagioclase and 10 % calcite. The trace of the bedding (S0) is defined by the variation in the composition and thickness of the layers. The continuous foliations (S1) are defined by preferred alignment of mica, calcite and feldspar. S1 foliations are parallel/sub parallel to the bedding; hence this unit show composite fabric. The crystals of calcite are overgrown on the continuous foliations (S1) indicating that calcite is post tectonic with respect to the continuous foliations.**(J)** Sample # MS20 in PPL, 40 X magnifications, location (0499831 E: 1535746 N). Mineral content: 50 % mica/ sericite, 20 % calcite, 15% quartz, 10% feldspar and 5 % opaque. This sample consists of very fine grained plagioclase and quartz and exhibiting primary bedding (S0) and secondary foliations i.e. well developed continuous foliations (S1). The bedding is boudinaged into small sections and parallel to the S1 foliation. S1 foliations are defined by muscovite/ sericite, calcite and feldspar. S1 foliations are parallel to the primary foliations; hence this rock show composite fabric. Besides, the S_1S_0 composite fabric also observed in the microlithons.

4.1.4. Limestone

Petrographic study of this unit indicates that the rocks are composed of micrite/carbonate mud and sparite.

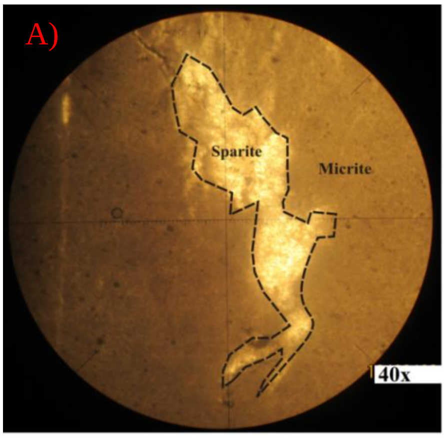

Fig.4.4: Microscopic photo-pictures of limestone unit. **(A)** Sample # ML4 in PPL, 40 X magnifications, location (0500250 E: 1535606 N). Mineral content: 90% micrite and 10% sparite. This unit does not show any allochems (carbonate grain). Sparite is distinguished from micrite by their large grain size and clarity. Sparites are appearing clear or white when viewed in plane-polarized light and relatively larger grain size than the micrite. Moreover, the coarse grained calcite is formed probably due to the re-precipitated solution in pore spaces.

4.1.5. Micrograntic intrusions

Petrographic study of this unit indicates that (Fig.4.5A-B) the rocks are composed of biotite, muscovite, k-feldspar, quartz and plagioclase. The majority of minerals have more or less random orientation, occasionally the muscovite and biotite shows faint foliations.

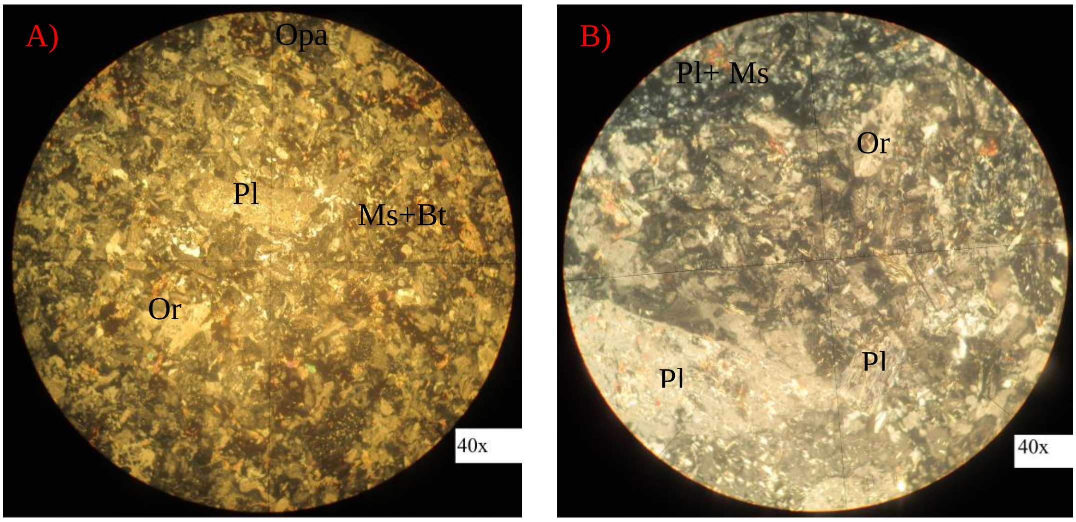

Fig.4.5A-B: Microscopic photo-pictures of micrograntic intrusions. (A) Sample # PR2 in XPL, 40 X magnifications, location (0499454 E: 1530995 N). Mineral content: 35% plagioclase, 20% K-feldspar, 20% quartz, 10 % opaque, 10% biotite and 5% muscovite. The presence of little undulatory extinction in the quartz crystals and the development of biotite and muscovite indicate that this unit is not post tectonic at least under this observation. The grain size of the plagioclase is up 0.05 mm. The plagioclase feldspar is twinned (polysynthetic twining). (B) Sample # PR3 in XPL, 40 X magnifications, location (0501569 E: 1531852 N). Mineral content: 30% plagioclase, 25% K-feldspar, 20% quartz, 15 % muscovite, 5% biotite and 5 % opaque. This sample show weak foliation is defined by biotite and muscovite; however, k feldspar, plagioclase and quartz do not have preferred alignment. The quartz crystals have little exhibits undulatory extinction. The grain size of the plagioclase and k-feldspars is approximately 0.05mm. The plagioclase feldspar shows elongated lath and lamellar texture.

4.2. Metamorphism

The presence of recrystallized quartz, relict minerals (plagioclase and pyroxene), altered pyroxene, preservation of compositional layering/primary bedding (S0), relict porphyritic texture, and secondary minerals such as sericite, chlorite, epidote, calcite, and graphite indicates that these rocks have been subjected to very low to low grade metamorphism. Critical mineral assemblages are used to determine the grade and metamorphic facies (Bucher and Grapes, 2011). Majority of the lithological units in the study area are generally metamorphosed; though the degree of metamorphism and deformation is variable from unit to unit.

The mineral assemblages of the various rock units are shown below and the critical mineral assemblage that indicates the grade of metamorphism are in **bold.**

Metavolcanic rocks

- ❖ Quartz + k-feldspar + plagioclase **(albite)** + **chlorite**+ **muscovite** + opaque ± sphene ± hematite

Metavolcanoclastics rocks

- ❖ Quartz + plagioclase **(albite)** + k-feldspars **+ muscovite + chlorite+ sericite** ± sphene **± epidote** ± garnet +opaque

Slate units

- ❖ Quartz + plagioclase+ k-feldspar + **muscovite** +**sericite+ graphite ± calcite+ chlorite ± epidote** ± opaque

Limestone units

- ❖ Calcite ± quartz ± opaque

Micrograntic intrusions

- ❖ Plagioclase **(albite)** +K-feldspar +quartz +**muscovite**+ **biotite**+ **chlorite ±** opaque

In conclusion, the critical mineral assemblages that are in bold demonstrate that the rocks experienced regional metamorphism in the lower green schist facies.

CHAPTER FIVE

5. DEFORMATION AND GEOLOGICAL STRUCTURES

5.1. INTRODUCTION

The basement rocks of northern Ethiopia experienced at least two major structural episodes. Early N–S compression produced E–W trending recumbent folds, tight minor folds and pervasive regional foliation , whereas the later episode of E–W compression produced upright and open parallel folds without producing a significant cleavage (Kibret Sifeta et al., 2005: Mulugeta Alene et al., 2006). Form field and microstructural data analysis the rocks of Mai Kinetal area have been subjected to polyphase deformation. This polyphase deformation is marked by the existence of different structural elements such as regional foliations, folds, faults, joints, dykes and quartz veins. Microstructural analysis revealed that the rocks of the study area have been experienced at least three (D1 to D3) phases of deformation.

5.2. First phase of deformation (D1) and associated structures

5.2.1. S1 Foliation

This structure is predominantly developed over the slate unit. S1 foliations are represented by slaty cleavage (Fig.5.1). However, weak S1 foliations are developed on metavolcanic and metavolcanoclastic units. Furthermore, microscopically S1 foliations are defined by the preferred alignment of muscovite, chlorite, epidote, sericite, plagioclase, quartz and opaque minerals (Fig.4.1A-C; 4.2A-C; 4.3C-J; 4.5A-B). Regionally these structural elements are correlated with first phase of deformation (D1) which was caused as a result of N-S compression (Mulugeta Alene et al., 2006).

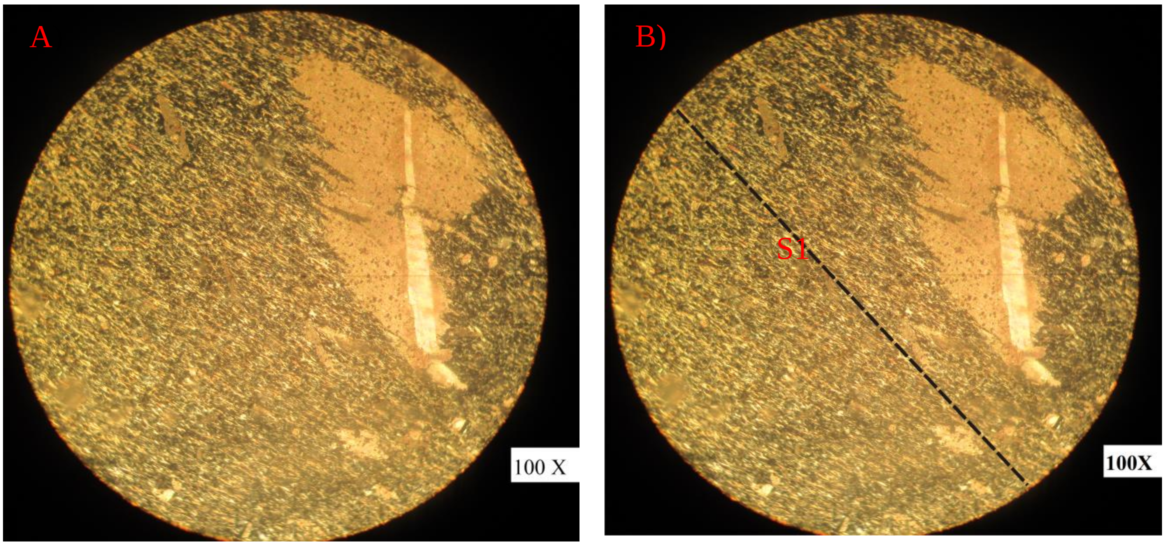

Fig.5.1A-B: Microscopic photo-pictures of slate unit that shows S1 foliation. Both A and B (Sample # MS17 in XPL, 100 X magnifications, location (0504847 E: 1537460 N) represent the fabric pattern before and after labeling S1. S1 foliations are mainly defined by preferred alignment of muscovite /sericite.

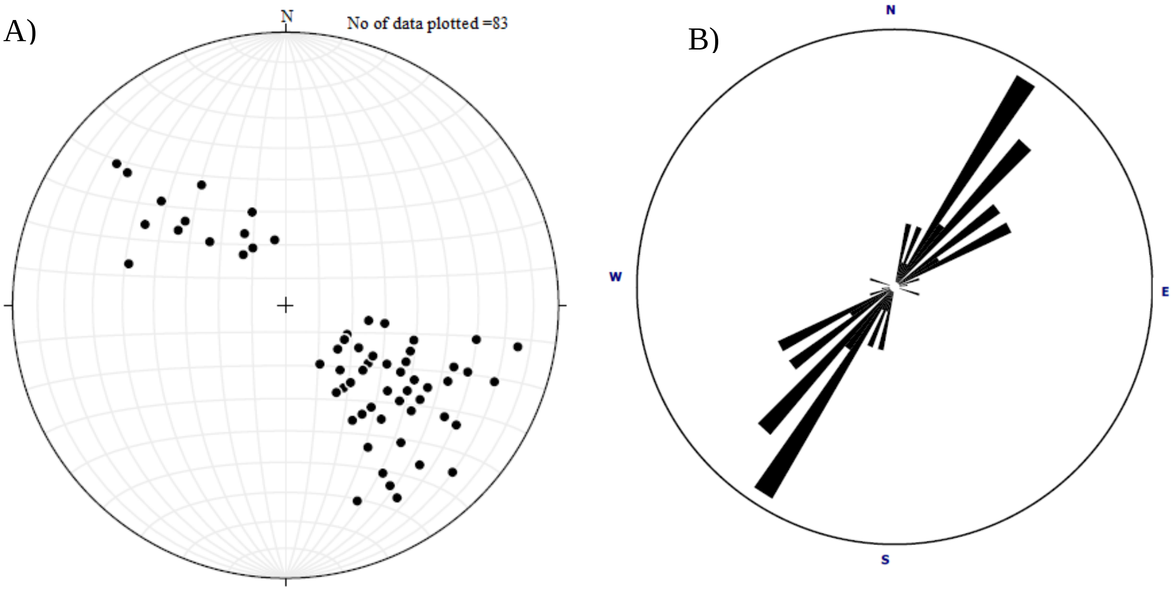

Fig.5.2: Stereo-plot of S1 foliations. (A) The poles to the foliations (S1) are clustered on the SE and NW quadrant of the stereonet; whereas the dominant poles are clustered on the SE indicates that the foliations are dipping towards the NW. (B) Rose diagram for the foliations: The longest wedge of the rose diagram represents N30^0 - 40^{0}E and this value indicates that the mean value of the strike direction of the foliations in the study area.

5.3. Second phase of deformation (D2) and associated structures

5.3.1. S2 Foliation

S2 foliations are mainly found in the slate rock unit .This foliation is difficult to identify and trace in the field, although it can be recognized through microscopic examination of the thin section (Fig.5.2). Furthermore, microscopic examination of the thin sections prepared from slate unit show the development of crenulation cleavage due to second phase of deformation (D2) (Fig.4.4C-E). The crenulation cleavages (S2) are defined by preferred alignment of chlorite, graphite, sericite and opaque minerals.

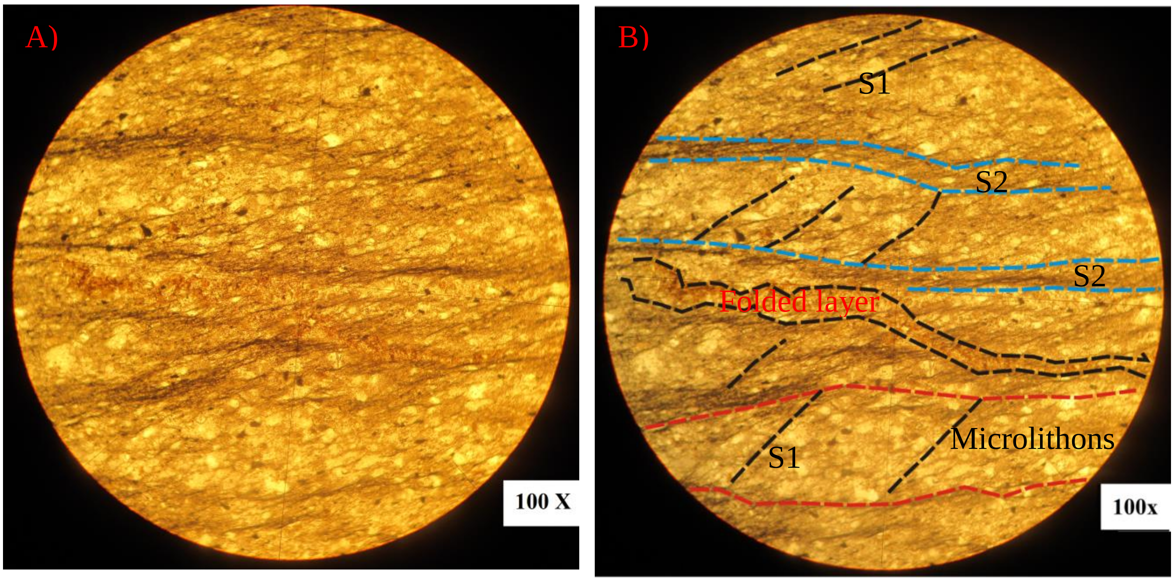

Fig.5.2A-B: Microscopic photo-pictures of slate unit that shows S1 and S2 foliation. Both A and B (Sample # MS7 in PPL, 100 X magnifications, location (0498823 E: 1530415 N) represent the fabric pattern before and after labeling S1 and S2. S1 foliations are mainly defined by preferred alignment of muscovite /sericite, whereas S2 are defined by preferred alignment chlorite and opaque minerals along the cleavage domains. The S1 foliations are clearly observed on the microlithon part. The microlithons are mainly composed of quartz and feldspar.

5.3.2. Fold

Small scale micro-folds are observed on upper limestone (Fig.5.3A) and slate unit in central and northwestern part of the study area. The micro folds on limestone and slate unit have N-S plunging direction with sub horizontal to horizontal fold axes. All folds plunging N-S directions are correlated to D2 that resulted from E-W shortening (Mulugeta Alene et al., 2006).

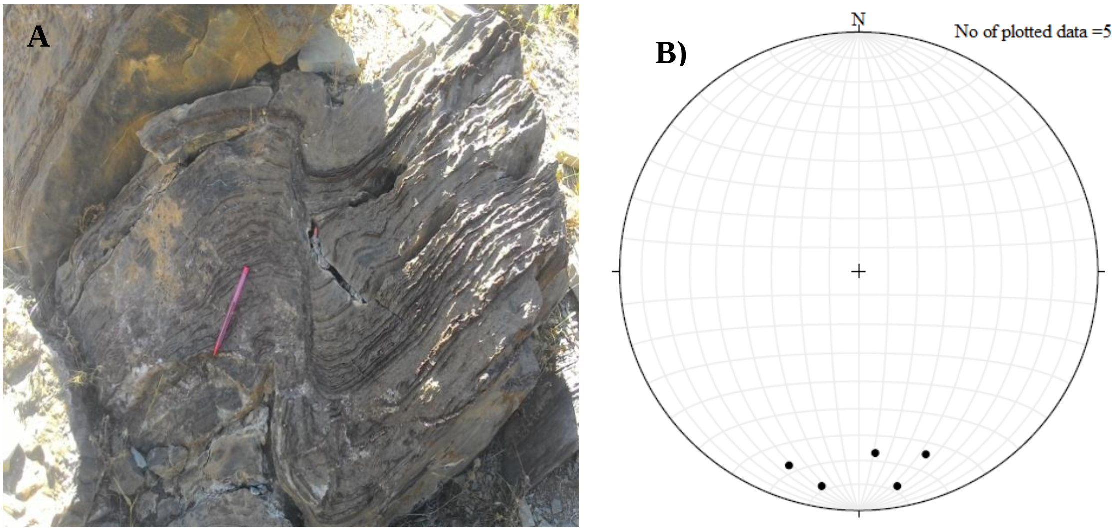

Fig.5.3A-B: Field photo pictures and stereo plot of folds. The fold axes are plunging with shallow degree towards the south (0500249E: 1535609N).

5.4. Third phase of deformation (D3) and associated structures

The rocks of the study area have been affected by the brittle structures (joints and faults) besides of the ductile structures (foliations and folds). Dykes and quartz veins are the associated brittle structures. These brittle structures are dissected the pervasive regional foliations.

5.4.1. Joint

This structure is commonly observed on metavolcanic, slate, limestone and microgranite units. It dissected the whole units in the study area. They are formed due to later deformation events and hence they are postdated than D1 and D2. Most of the joint set in metavolcanic, limestone and microgranite units have nonsystematic pattern; however systematic joint sets are found in slate units (Fig.5.4). The average joint spacing is up to few cm to 50cm.

Fig.5.4: Systematic joint sets in lower slate unit. This systematic joint has N-S trending (0505000E:1535439N).

A)

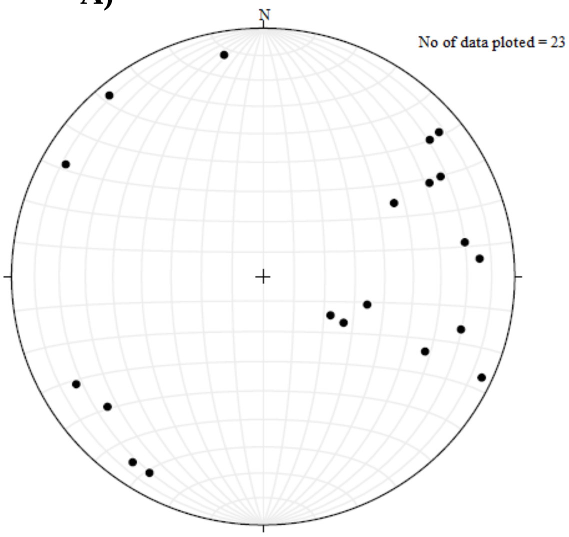

B)

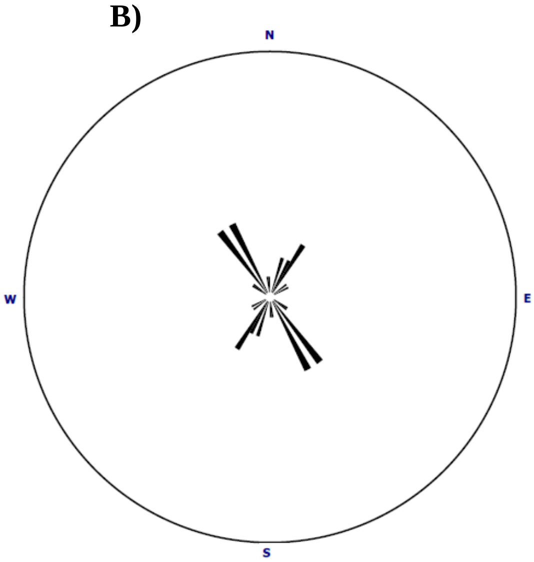

Fig.5.5: Stereo-plot of joints: (A) the poles of the joints show wide scatter as the result of the existence of different sets of joint across the regional foliation. (B) Rose diagram of the joints: The longest wedge of the rose diagram N50^0 - 40^{0}W represents one set of the joint system indicating that mean value of the strike direction of the joint sets ,whereas the second joint set have N25^0 - 30^{0}E, implying that mean value of the strike direction of the second joint sets.

5.4.2. Normal fault

Normal faults are found in north western and north eastern part of the study area (Fig.3.1). The fault system in the north eastern part of the study area are characterizes by linearly to curvilinearly alignment; whereas the north western parts of the faults have more or less linear geometry. Both of the NW and NE faults have dissected all the units in the study area. Lineaments are exposed but undifferentiated linear features traced on the surface of the Earth. Although, such structures are commonly occurred in basement complexes, mainly characterized by the development of series of NE- SW and NW-SE trending lineaments (Fig.3.1).These lineaments apparently follow the shear zones of the Neoproterozoic basement. The lineaments/major fractures systems of the Mai Kinetal areas are identified from the patterns of the drainage using satellite image and aerial photographs.

5.5. Time relationship between deformation and metamorphism

The time relationship between deformation and metamorphism events can be established from microstructural analysis. The relationship between internal fabric (Si) within the porphyroblasts and the matrix foliation (Se) outside the porphyroblasts are used to determine the relative timing of mineral growth, metamorphic conditions and deformation (Passchier and Trouw, 2005). The rocks of the study area show three planar structural elements such as S0, S1 and S2. S1 and S2 planar structures are developed during D1 and D2 event respectively. The strong S1 foliations are defined by preferred alignment of muscovite, sericite, chlorite, epidote, calcite, graphite, and some recrystallized quartz (Fig.4.2A-C and 4.3C-J), whereas weak S1 foliations are defined by preferred alignment of plagioclase, muscovite and biotite (Fig.4.1A-C, 4.3B and 4.5A-B). S1 foliations are deflected around the porphyroclasts of k-feldspar. The porphyorclasts are pre tectonic relative to the external foliations because the matrix foliations are deflected around the porphyroclasts (Fig.4.2A-B). The porphyroblasts of calcite minerals are overprinting and overgrown on S1 foliations, implying that the calcite minerals are post tectonic with respect to the S1 foliations (Fig.4.3H). Furthermore, the strong crenulation cleavages (S2) are defined by preferred alignment of chlorite, sericite and opaque minerals (Fig.4.3C-D) and weak S2 crenulation cleavages are defined by graphite and sericite (Fig.4.3E).

CHAPTER SIX

6. GEOCHEMISTRY

6.1. INTRODUCTION

A total of 12 fresh (7-metavolcanic, 3-metasedimentary and 2-plutonic rocks) samples were selected for whole-rock geo-chemical analyses from Mai Kinetal area. The samples were prepared in powder form in Akaki Kaliti, Kebele 10/11 block 03 milling room. About 200 mg of the powdered samples were sealed and packed into a plastic, and then the samples are submitted to the Australian Laboratory Science (ALS) for the purpose of geochemical analysis in order to determine the concentration of major and trace elements.

Major elements (including loss on ignition) were analyzed by multi element Inductively Coupled Plasma 06 (ME- ICP06) in Ireland by Australian Laboratory Science. Trace elements were determined by multi element Mass spectrometry 81 (ME-MS81), whereas multi element four acid digestion 81 were used for base metal determinations. More information on the procedure, precision, accuracy, and detection limits of ALS of ME-ICP06 and ME-MS81 analyses could be found at www.alsglobal.com. The sample locations are illustrated in Fig.3.1 and their assigned sample names and corresponding major element (wt %) and trace elements (ppm) values are listed in Table 6.1 and Table 6.2 respectively. All the major element values used in plots are recalculated on an anhydrous free. To use the analyzed geochemical data for the purpose of this research the data have been integrated through different software packages such as Microsoft excel 2010, excel 2007 (xlsx) sample worksheet, Petrograph version 2beta and GCDKit 3.00 version . Petrograph version 2beta and GCDKit 3.00 version software packages are used to produce different geochemical variation diagram. These variation diagrams are used to understand the petrogenetic evolution, tectonic setting and to determine provenance signatures as well as to determine the behavior of elements during metamorphism.

6.2. Metavolcanic rocks

Major element concentrations are recalculated to volatile free bases (Table 6.1). Major element data are used for rock classification purpose and they have limited application in understanding the petrogenesis evolution since they are sensitive to weathering, hydrothermal fluid activities and metamorphic processes (Tarekegn Tadesse et al., 1999; Mulugeta Alene et al., 2000; Rollinson, 1993). The analyzed metavolcanic rocks display wide compositional spectrum from basalt to rhyolite in their major-element composition, i.e. the SiO_2 content ranges from (48.4 – 71.1 wt %). The analyzed samples show a general trend of decreasing MgO, Fe_2O_3 , Al_2O_3, CaO, P_2O_5, and TiO_2 with increasing SiO_2 (Fig. 6.1). It shows normal differentiation of magma and it is consistent with the fractionation of olivine, pyroxene, magnetite, calcic plagioclase, ± apatite, ± ilmenite, and ± titanomagnetite. Primary magma is characterized by high MgO content (> 6%wt), Ni (250 -300 ppm) and Cr (500- 600 ppm) (Wilson, 1989). The low MgO content (<3.5 wt %), Cr (10-20 ppm), Ni (<1-13 ppm) and Co (3-31 ppm) and La_N/Yb_N ratio (with an average of 4.43) in all the samples including the basic/intermediate and acidic metavolcanic rocks indicates that they were derived from highly differentiated magma source. The scatter trends of Na_2O and K_2O with SiO_2 (Fig.6.1) can be linked to the mobility because these elements are highly mobile under hydrothermal fluid activities, metamorphic and alteration processes (Mulugeta Alene et al., 2000). The high content of CaO in samples (MV5 and MV9) and Na_2O in the samples (MV5 and MV9) in Table 6.1 are related to the presence of epidote and diffuse albitization of the plagioclase (Mulugeta Alene et al., 2000). The high iron content of MV12 sample indicates that the abundance of secondary opaque phase (hematite?). The analyzed samples show high-alumina Al_2O_3 content range from 13.15 wt % to 17 wt %, (average 15.31wt %) values similar to those of calc-alkaline series rocks (Lissan and Bakheit, 2010).

Trace elements are plotted against Zr to evaluate the behavior of elements in magmatic evolution and to establish their relative mobility of elements (Fig.6.2) because Zr is incompatible, immobile and alteration resistant element (Mulugeta Alene et al., 2000). Th, Y, and U show positive correlation with Zr for acidic metavolcanic and basic/ intermediate rocks; this indicates that they have not been affected by metamorphism and hydrothermal alterations. Rb and Sr show a broad scatter against zircon (Fig.6.2) perhaps due to the mobility during the metamorphic processes. Ni and Sc show negative correlation with Zr suggested that the fractionation of olivine, clinopyroxene and spinel in the early phase.

Primitive-mantle-normalized trace element plots of the basic/intermediate and acidic metavolcanics (Fig.6.3) display marked troughs at Ti and Nb which are possibly due to the fractionation of titanomagnetite, ilmenite, rutile and small subducted component in to the mantle source (Rollinson, 1993; Wilson, 1998, Mulugeta Alene et al., 2000; Best, 2003). Moreover, Nb anomalies are also characteristics of the continental crust and may be an indicator of crustal involvement in magma processes (Rollinson, 1993; Wilson, 1998, Mulugeta Alene et al., 2000). Similarly, the negative anomaly of P can be linked possibly due to the crystal fractionation of apatite during the magmatic evolution. The positive anomaly of Ba, Sr, U, Pb and negative anomaly of Rb, K, could be linked to the mobility because these elements are highly mobile under secondary processes (hydrothermal activities, alterations and metamorphic processes). Two basalt samples (MV9 and MV12) show cross cutting pattern on primitive-mantle-normalized trace element plots, implying that the presence of non-cogenetic magma. Over all, the analyzed metavolcanic samples are characterized by enrichment of large ion lithophile elements (Rb, Ba, Sr, Th, U and Pb) relative to high field strength elements (Nb, Y, Zr, Hf, Ti and Yb). Thus, this is probably due to their high mobility under the metamorphic conditions, alterations, weathering, erosion and hydrothermal activities.

Rare earth element (REE) concentrations are normalized to chondrite (Fig.6.4) according to Boynton (1984). The analyzed metavolcanic rock show slight enrichment of light rare earth element relative to heavy rare earth elements. Moreover, the degree of light REE fractionation is moderate with fairly steep slope pattern [(La_N/Yb_N) = 3.12- 6.15], while the heavy REE are very weakly fractionated with almost flat pattern [(Gd_N/Yb_N) = 0.32-1.63]. Eu/Eu* is a measure of europium anomaly and the value less than 1 indicates negative anomaly (Rollinson, 1993). The analyzed samples show negligible negative Europium anomaly (Eu/Eu*) ranges from (0.86 – 0.99), implying that small degree of plagioclase fractionation during magmatic evolution or partial melting of rock in which the feldspar is retained in the source (Wilson, 1989; Rollinson, 1993). However, MV1 and MV8 samples show pronounced negative Eu anomaly ranges from (0.60– 0.80).

Table 6.1: Major element content (Wt. %) of metavolcanic, metasedimentary and plutonic rocks from Mai Kinetal area. The geochemical data is normalized in volatile free base.

	Metavolcanic							Clastic metasedimentary			Plutonic	
Sample	MV1	MV2	MV4	MV5	MV8	MV9	MV12	MS4	MS17	MS20	PR2	PR3
SiO_2	67.9	71.1	62.2	61.3	65.8	48.7	54.6	59.8	61.3	60.2	66.6	67
TiO_2	0.64	0.56	1.09	0.66	0.34	1.46	1.46	1.0	1.03	0.76	0.44	0.48
Al_2O_3	13.15	13.7	15.15	17	15.8	16.3	16.1	18.55	15.55	14.05	15.1	15.7
Fe_2O_3	6.59	5.48	8.51	6.15	4.44	11.45	12.15	8.37	8.62	6.2	3.15	2.95
MnO	0.06	0.05	0.04	0.06	0.09	0.18	0.17	0.14	0.02	0.04	0.03	0.02
MgO	2.05	0.86	1.91	0.62	1.32	3.33	2.98	2.3	2.84	5.21	0.91	1.43
CaO	1.7	0.74	1.71	9.06	5.07	11.55	2.61	1.24	2.48	3.44	1.74	1.33
Na_2O	5.06	5.93	6.16	4.34	0.47	2.73	8	3.17	0.2	1.29	4.41	4.64
K_2O	0.13	0.82	0.05	0.3	3.08	0.18	0.4	2.89	2.48	2.15	4.19	3.09
P_2O_5	0.29	0.17	0.55	0.19	0.08	0.49	0.45	0.22	0.14	0.22	0.16	0.15
LOI	2.41	1.09	2.57	1.34	2.72	4.55	1.73	3.53	4.96	6.93	2.79	1.72
Total	99.98	100.5	99.94	101.02	96.49	96.37	98.92	101.21	99.62	100.49	99.52	98.51

Table 6.2: Trace element content (ppm) for Mai Kinetal metavolcanic, metasedimentary and plutonic rocks.

	Metavolcanic							Metasedimentary			Plutonic	
Sample	MV1	MV2	MV4	MV5	MV8	MV9	MV12	MS4	MS17	MS20	PR2	PR3
Sc	11	19	14	32	11	34	12	20	25	16	5	6
V	28	104	114	334	13	84	42	124	116	128	60	57
Cr	20	10	20	20	10	10	20	30	50	120	40	30
Co	6	20	3	31	3	29	16	16	14	17	6	7
Ni	<1	5	1	13	<1	9	7	12	13	55	13	21
Cu	29	4	139	8	11	291	40	57	25	49	37	53
Zn	72	64	94	23	72	110	111	94	75	107	50	60
Ga	11.6	14.4	15.3	24	18.5	22.2	19	22.2	18.4	17.7	21.6	21.2
Rb	9.1	1.3	4.7	3.2	68.8	3.4	4.1	73.6	79.6	61.2	114	69.3
Sr	252	195	4680	485	1055	251	345	324	48.9	120.5	234	493

Y	24.1	26.4	17.8	28.8	35.5	33.9	13.9	24.8	14.2	24.6	7.8	10.4
Zr	141	137	125	102	234	110	87	87	129	145	181	188
Nb	4.5	4.6	3.3	3.1	6.5	2.7	0.9	2.9	4.7	6.2	2.1	2.5
Cs	0.2	0.07	0.35	0.45	2.47	0.09	0.06	1.29	1.6	2.14	1.08	0.55
Ba	737	127.5	166.5	106.5	1200	270	151.5	2790	769	773	1835	1400
Hf	4.1	3.9	3.5	3	6.8	3.3	2.6	2.4	3.5	4.4	5	5.2
Ta	0.3	0.3	0.2	0.2	0.4	0.2	0.1	0.2	0.3	0.5	0.2	0.2
Pb	4	4	8	22	15	3	4	0.11	0.06	0.07	16	16
Th	3.4	3.51	3.36	1.32	5.02	1.4	1.64	2.16	3.4	4.17	10.8	10.8
U	1.32	1	0.97	0.56	1.82	0.42	0.83	1.11	0.41	1.62	3.21	3.62
La	19.8	17.1	12.4	15.8	29.4	14.9	13.5	30.3	12	21.8	29.1	29.5
Ce	38.2	37.8	25.1	33.4	55.2	33.4	26.9	54	26.3	42.6	52.6	55.4
Pr	4.58	5.04	3.26	4.68	6.76	4.88	3.41	6.99	3.24	5.33	5.77	6.33
Nd	20	24.1	15.1	22.6	29.5	24.2	15.7	28	14	23.3	22.3	25
Sm	4.03	5.39	3.04	5.69	6.04	6.17	3.16	5.11	3.06	4.73	3.42	4
Eu	1.05	1.59	0.98	1.8	1.14	1.78	0.92	1.25	0.88	1.16	0.88	1.03
Gd	4.03	5.39	3.03	5.43	5.6	6.49	2.96	4.62	2.63	4.71	2.38	2.94
Tb	0.65	0.84	0.53	0.9	0.96	1.04	0.44	0.75	0.47	0.72	0.28	0.4
Dy	4.4	5.29	3.08	5.81	6.24	6.39	2.54	4.47	3.02	4.71	1.5	2.12
Ho	0.86	1.05	0.63	1.13	1.37	1.3	0.53	0.83	0.58	0.93	0.29	0.39
Er	2.5	2.77	1.88	3.24	3.91	3.74	1.39	2.46	1.7	2.73	0.73	1.06
Tm	0.39	0.41	0.28	0.4	0.56	0.52	0.19	0.28	0.27	0.37	0.1	0.13
Yb	2.67	2.65	2.18	2.92	4.01	3.22	1.48	1.9	1.75	2.68	0.69	0.84
Lu	0.38	0.38	0.31	0.41	0.61	0.49	0.17	0.24	0.24	0.42	0.1	0.11
$\sum REE$	103.5	109.8	71.8	104.2	151.3	108.5	73.3	141.2	70.14	116.19	120.4	129.3
La_N/Yb_N	5.00	4.35	3.83	3.65	4.94	3.12	6.15	10.8	4.62	5.48	28.4	23.7
Gd_N/Yb_N	0.32	0.43	1.12	1.50	0.29	1.63	0.42	1.96	1.21	1.42	2.78	3.44
Eu/Eu*	0.80	0.90	0.99	0.99	0.60	0.86	0.92	0.79	0.95	0.75	0.94	0.92

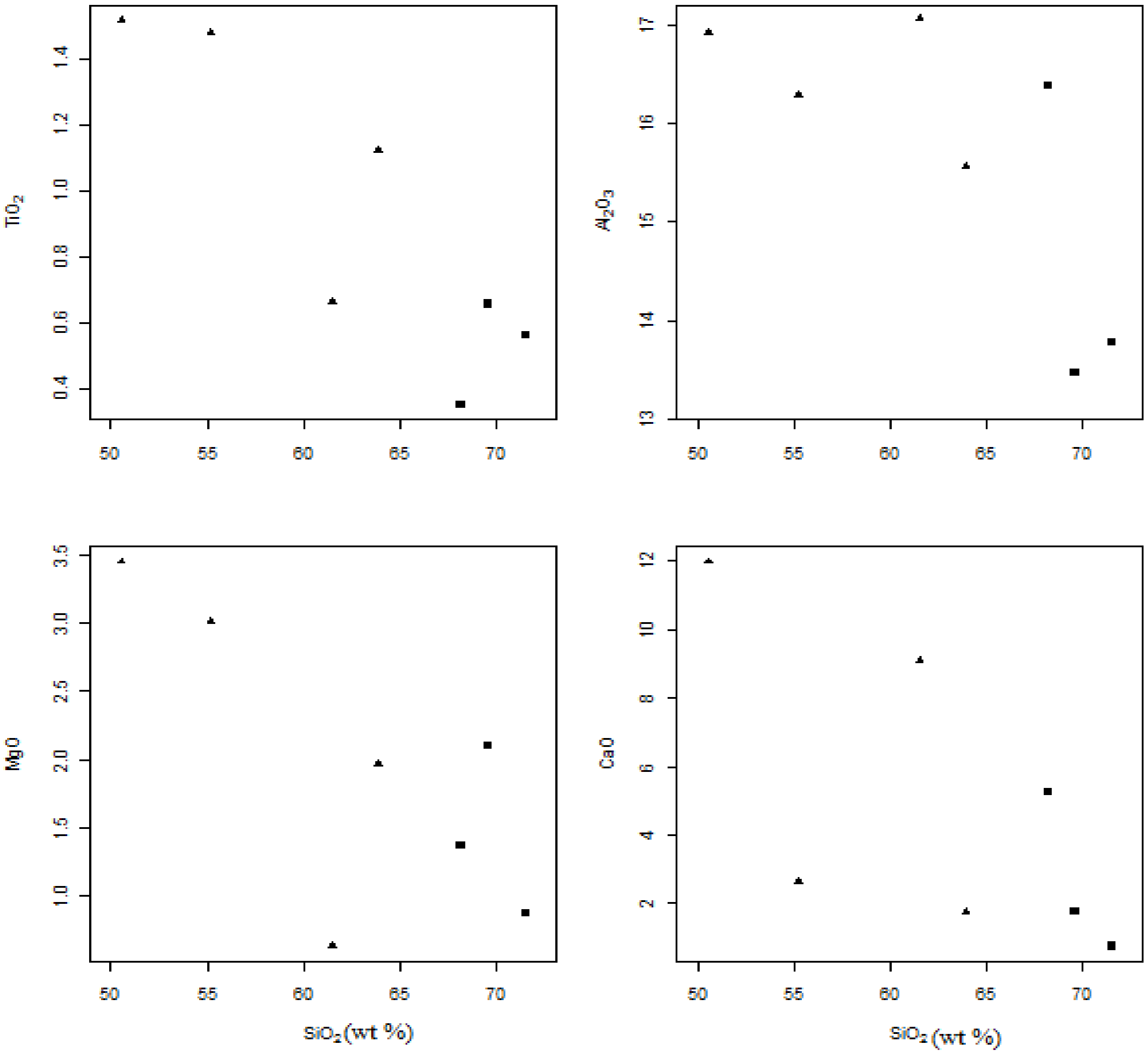
TiO2
Al2O3
MgO
CaO
SiO2(wt %)
SiO2 (wt %)

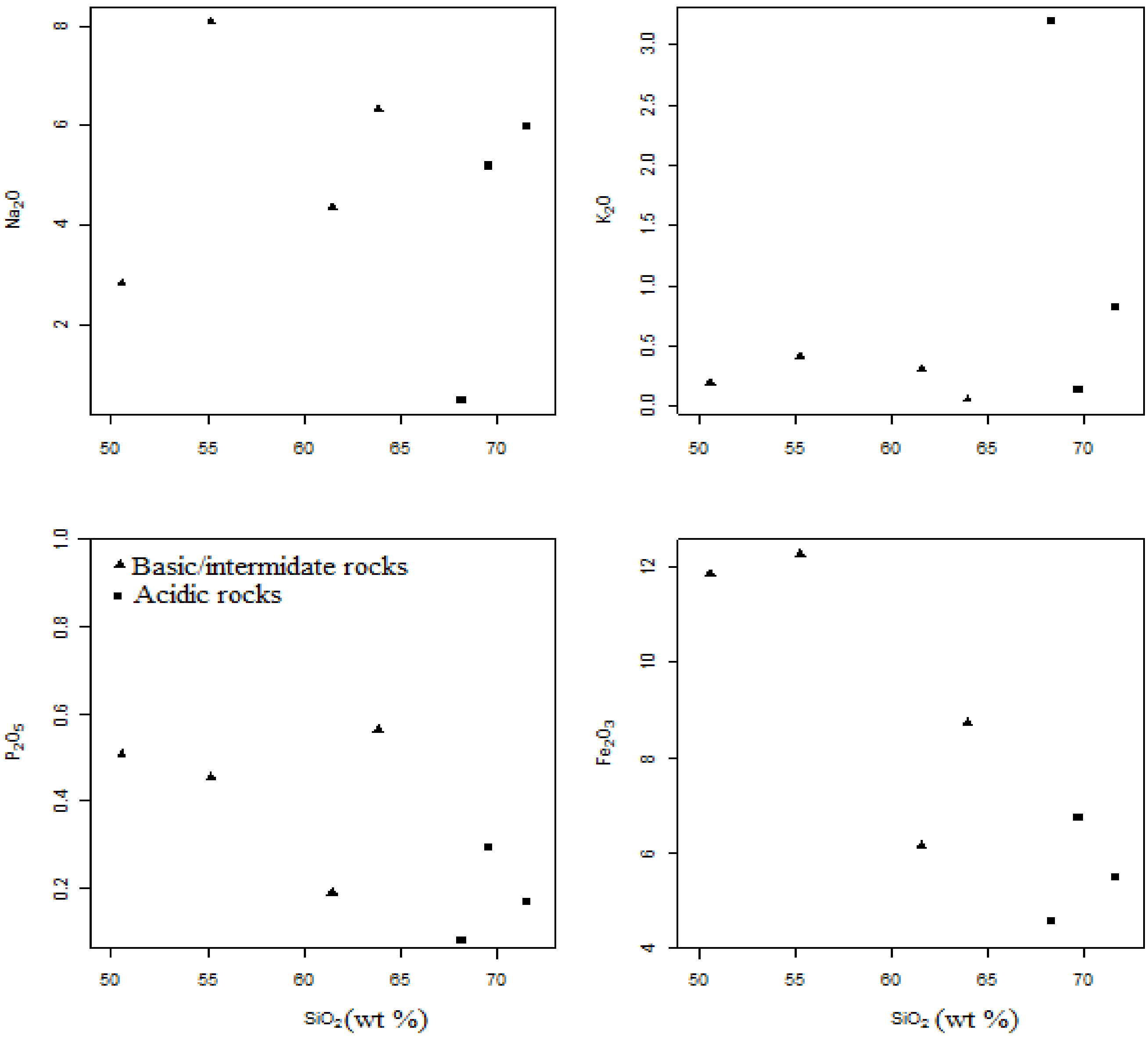

Fig.6.1: Harker variation diagrams for the metavolcanic rocks of the study area. The major element concentrations are volatile free base and expressed by wt. %.

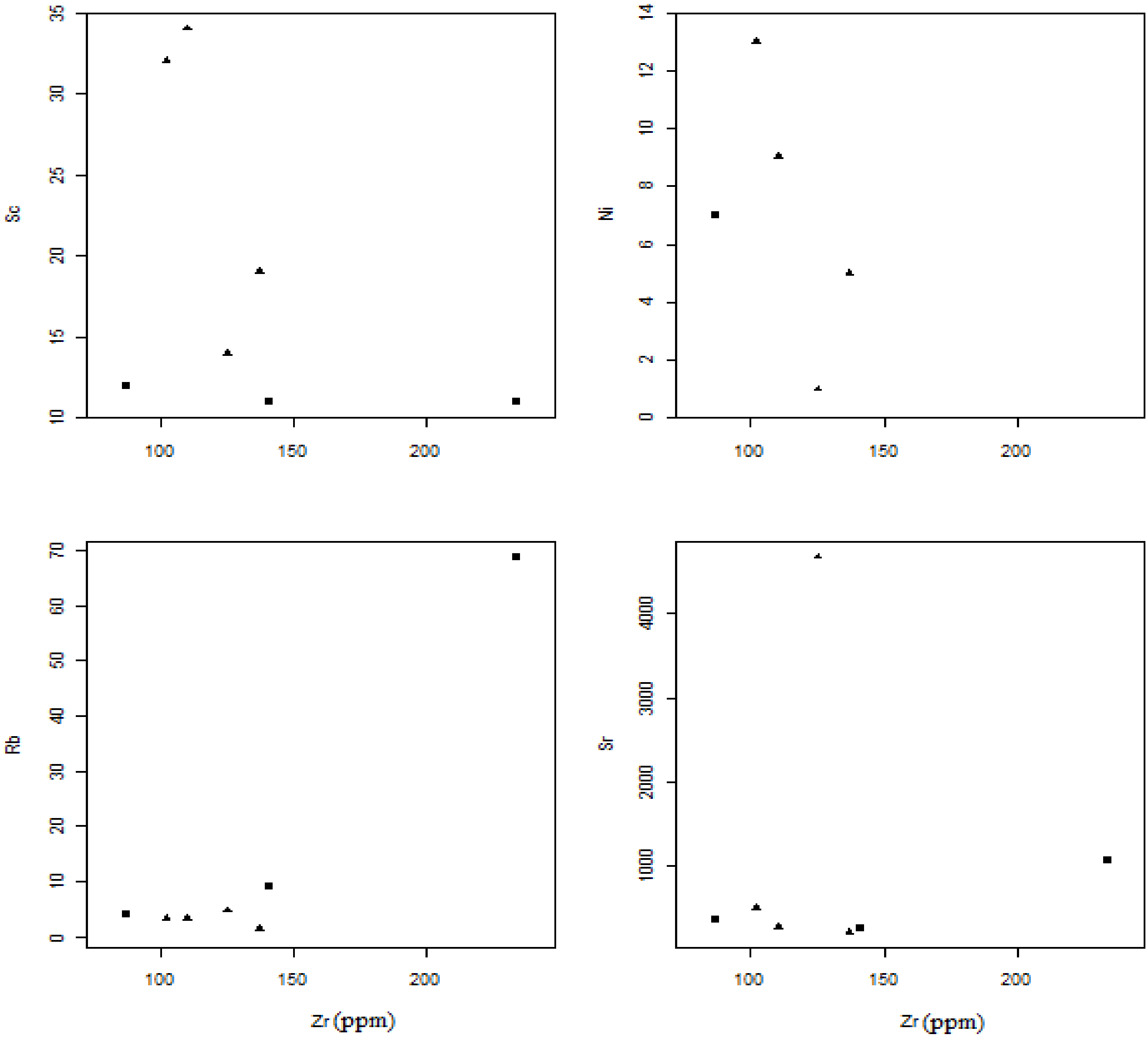
Sc
35
30
25
20
15
10
100
150
200
Ni
14
12
10
8
6
4
2
0
100
150
200
Rb
70
60
50
40
30
20
10
0
100
150
200
Zr (ppm)
Sr
4000
3000
2000
1000
100
150
200
Zr (ppm)

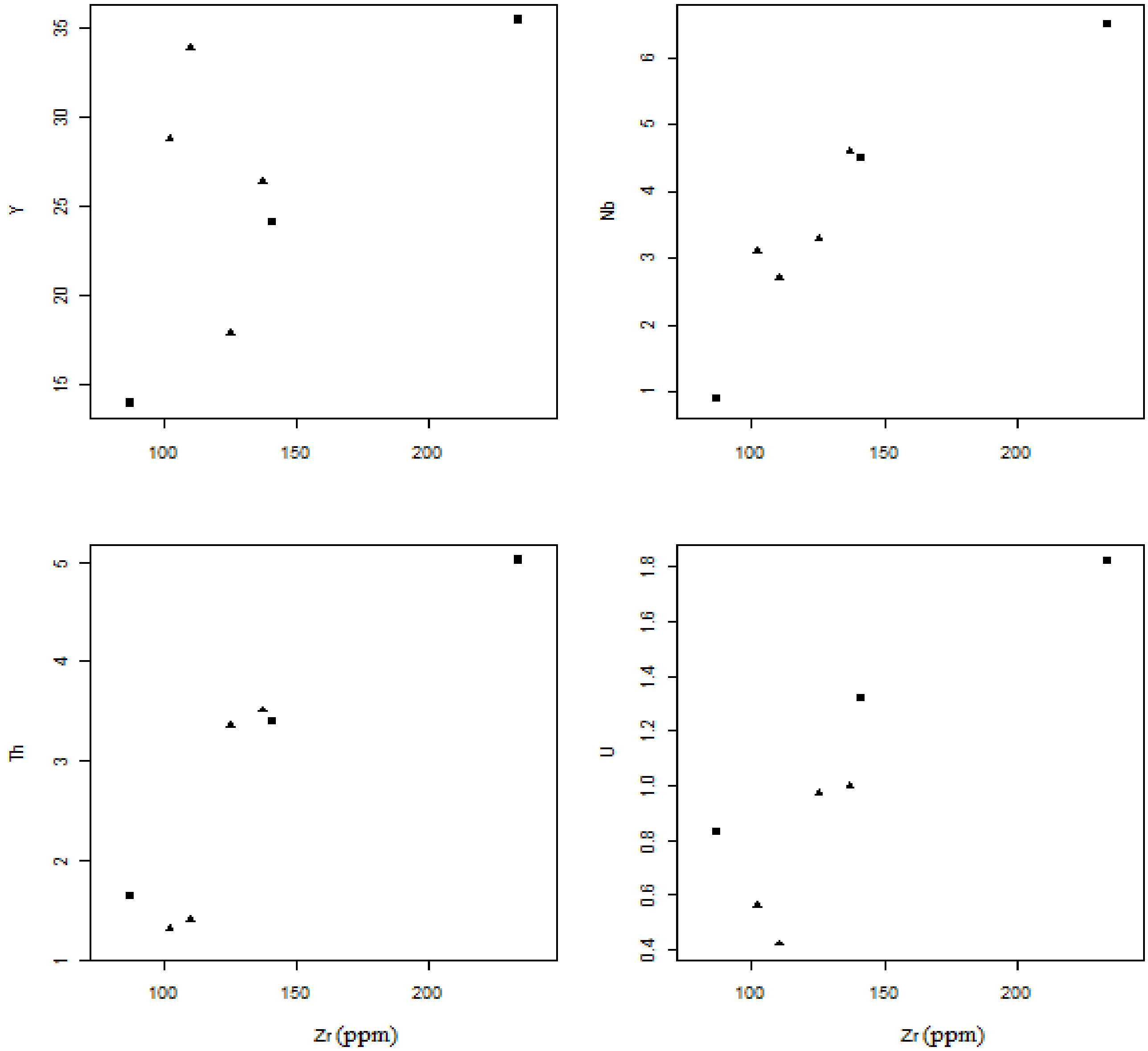

Fig.6.2: Zr variation diagram for various trace elements of the Mai Kinetal metavolcanic rocks (symbols as in Fig.6.1).

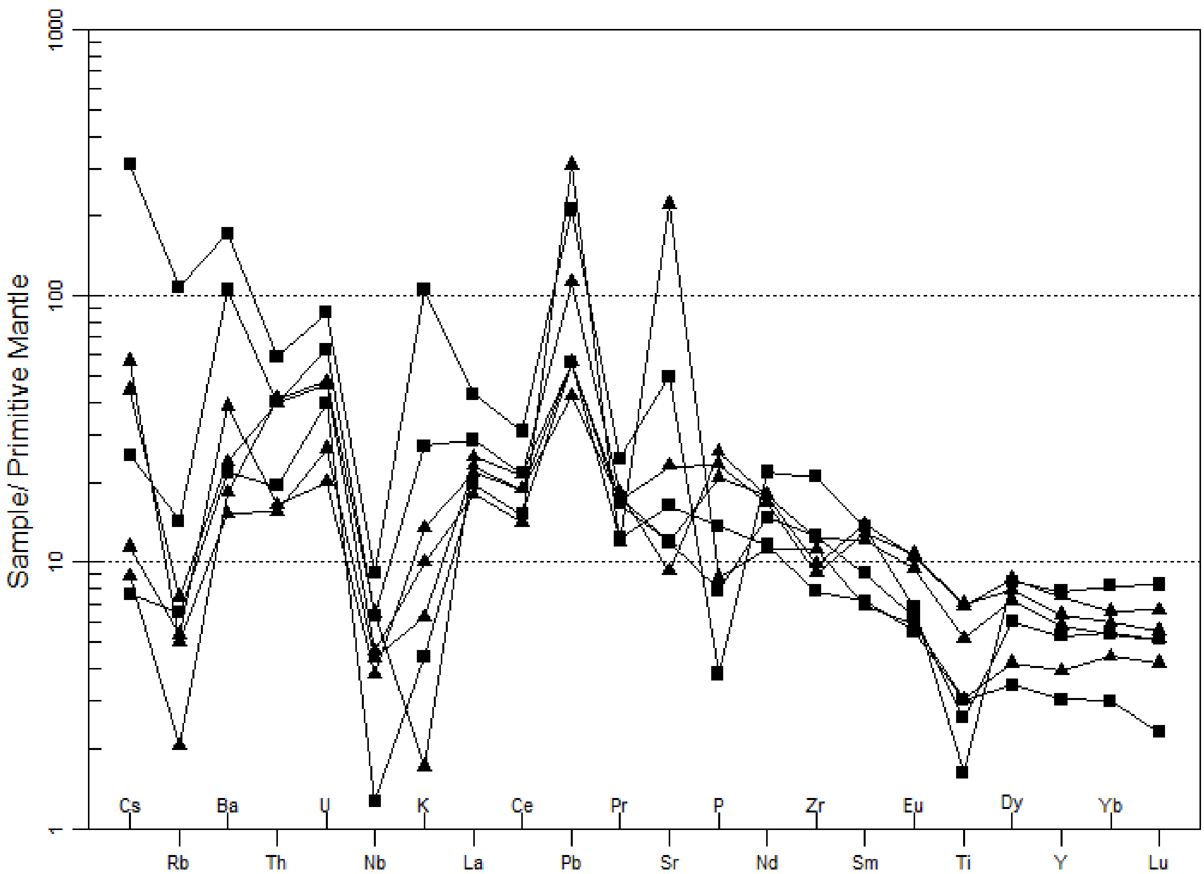

Fig.6.3: Primitive mantle normalized mult-element varation diagram for Mai Kinetal metavolcanic rocks. The samples are normalized to primordial mantle of value determined by (Sun and McDonough, 1989), (symbols as in Fig.6.1).

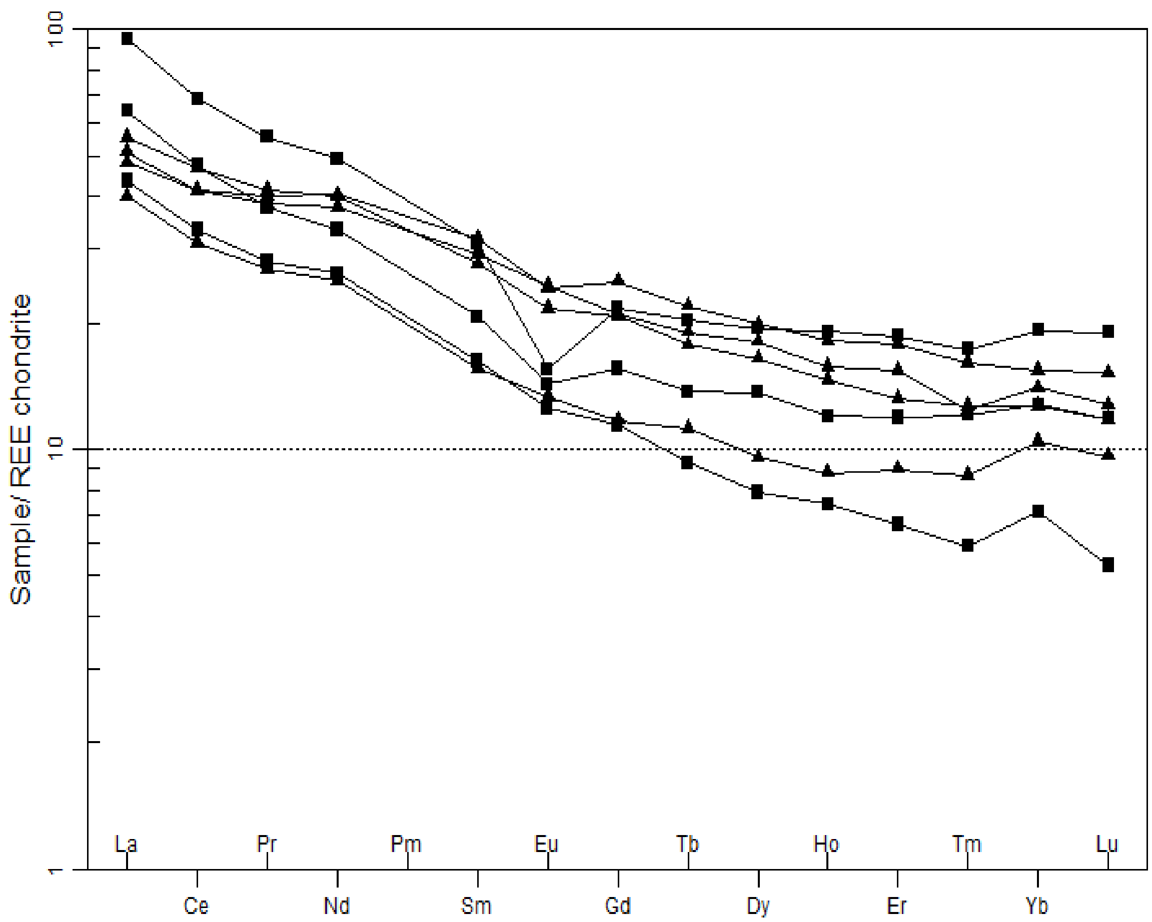

Fig.6.4: Chondrite normalized REE pattern for Mai Kinetal metavolcanic rocks. The concentration value of the rock samples are normalized to chondrite value determined by Boynton (1984) (symbols as in Fig.6.1).

6.2.1. Tectonic setting of the Mai Kinetal metavolcanics

The study area has been affected by very low to low grade of metamorphism. This affects the distribution and mobility of large ion lithophile elements. The discrimination diagrams of Wood (1980) have been used for identifying the tectonic setting of the metavolcanic rocks. The elements used in this discriminant diagram (Th, Hf and Ta) are generally immobile under low to medium grade of metamorphism and hydrothermal activities. Moreover, this diagram also separates tholeiitic and calcalkaline magma series. As a result the tholeiitic and calcalkaline magma series are defined by line of Hf/Th = 3 (Wood, 1980). The bulk of the metavolcanic samples (Fig.6.5) are plotted in the field of destructive plate margin i.e. falls inside the volcanic arc basalt field below the line of Hf/Th = 3, indicating that the metavolcanic rocks have been erupted in volcanic arc setting and have calcalkaline magma affinity.

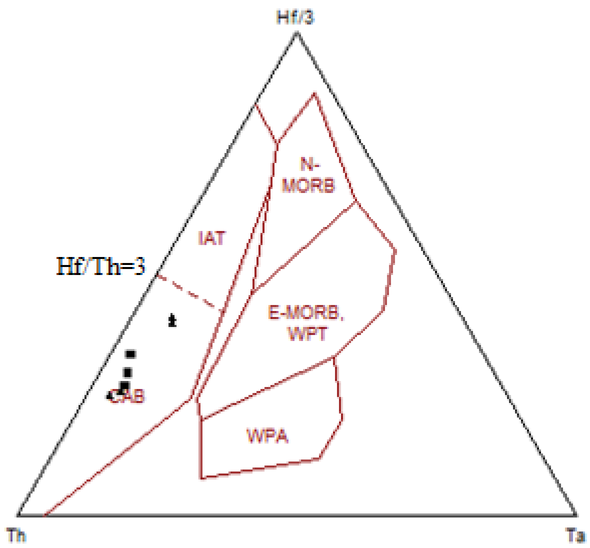

Fig.6.5: Th-Hf-Ta ternary diagram for Mai Kinetal metavolcanic rocks (Wood, 1980). Note N-MORB= Normal mid oceanic ridge basalt, E-MORB= Enriched mid oceanic ridge basalt, WPA= within plate tholeiites, IAT= Island arc tholeiites CAB= Calc alkaline basalts (symbols as in Fig.6.1).

Precise determination of the tectonic setting and petrogenetic evolution of metavolcanics in this study is difficult because the numbers of analyzed geochemical samples are small. However, the suites elsewhere studied in the region compared together with the limited present geochemical data and the results are almost consistent with Mulugeta Alene et al. (2000) and Kibret Sifeta et al. (2005).

6.3. Plutonic rocks (microgranitic intrusions)

The raw analytical data of the two samples (PR2 and PR3) from microgranitic intrusions are recalculated to volatile free bases. SiO_2 content of the analyzed microgranitic intrusions ranges from 66.6%wt to 67%wt. On the SiO_2-Feot/MgO binary plot (Miyashiro, 1974) both of the samples fall in the calc-alkaline series field (Fig.6.6) and similar observation has also confirmed in SiO_2-K_2O plot (Peccerillo and Taylor, 1976) both of the samples also occupy on the high-K calc alkaline series (Fig.6.7). In conclusion, the binary plot of Miyashiro (1974), and Peccerillo and Taylor (1976), indicates that the microgranitic intrusions have calc-alkaline affinity. The granitoids are studied elsewhere in the region compared together with very limited present geochemical data and the results are almost consistent with Asfawossen Asrat (1997),Tadesse Alemu(1998), Mulugeta Alene et al .(2000) and Tarekegn Tadesse et al.(2000).

Crustal derived granitoids are calcalkaline and peraluminous, mixed-origin granitoids are calc-alkaline and metaluminous, whereas mantle derived granitoids are alkaline or peralkaline (Barbarian, 1990). Crustal granitoids are produced by melting of crustal materials due to tectonic thickening of the continental crust in an orogenic belt (Barbarian, 1990).

On the primitive-mantle-normalized multi-element variation diagram (Sun and McDonough, 1989), (Fig.6.8), both of the samples display marked troughs at Nb, P, Ti and peaks at Ba, U, K and Pb respectively. The depletion of high field strength elements such as Y, Zr, and Yb relative to large ion lithophile elements (Rb, Ba, Sr and Pb) could be explained by fractionation of zircon and monazite during the evolution of magma (Mulugeta Alene et al., 2000). The negative anomaly of Nb, Ti and P can be linked to the fractionation of Ti apatite bearing phase (Wilson, 1989; Best, 2003). The slightly enrichment of incompatible trace elements such as Ba, U, K and Pb is probably due to the strong fractionation processes. Y/Nb ratios greater than 1.2 are the characteristics of the source magma interaction with crustal rocks or involvement of crustal material in their evolution (Eby, 1990, as cited in Asfawossen Asrat et al., 2003). The Y/Nb ratio of micrograntic intrusions ranges from 3.7 to 4.2 (with an average of 3.4), implying that the rocks are derived from crustal protolith or involvement of crustal materials.

Chonderite normalized Rare Earth Elements (REE) diagram (Boynton, 1984), (Fig. 6.9) shows strong negative slope with [(La_N/Yb_N) =23.68- 28.43] and [(Gd_N/Yb_N) =2.78-3.44]. Over all, the REE pattern indicates that strong fractionation of LREE and little fractionation in HREE. The depletion of HREE could be due to the presence of garnet in the melts. Furthermore, the analyzed samples show negligible negative Europium anomaly (Eu/Eu*) ranges from 0.90- 0.92, implying that small degree of plagioclase fractionation during magmatic evolution (Rollinson, 1993). Granitoids have > 1 wt % of K_2O, < 0.8 Fe_2O_3/ (Fe_2O_3+MgO) ratio and <1.1 Al_2O_3/ (CaO+Na_2O+K_2O) ratio indicate that they were probably arc environment of emplacement (Maniar and Piccoli, 1989 as cited in Mulugeta Alene et al., 2000). The analyzed samples have K_2O content ranges from 3.09 to 4.19 (average 3.64), Fe_2O_3/ (Fe_2O_3+MgO) ratio ranges from 0.34 to 0.47 and Al_2O_3/ (CaO+Na_2O+K_2O) ratio ranges from 1.01 to 1.17 (with an average 1.09). These values indicate that the micrograntic intrusions have arc environment of emplacement (Maniar and Piccoli, 1989). The ratio of Al_2O_3/ (CaO+Na_2O+K_2O) of the analyzed samples ranges from 1.01 to 1.17 (with an average 1.09) is the distinctive chemical property of the I-type peraluminous intrusive granitoids (Chappell and White, 1974).

6.3.1. Tectonic setting of the plutonic (micrigranitic intrusions) rocks

Granites are classified into oceanic ridge granite (ORG), within plate granite (WPG), volcanic arc granite (VAG) and collisional granite (COLG) based on their tectonic setting (Pearce et al., 1984). The elements of Rb, Nb, Y, Ta, and Yb are the most effective discriminate variables between granites derived from different tectonic setting (Pearce et al., 1984). On Nb -Y binary plot of (Fig.6.10) Pearce et al (1984) both of the samples are plotted on the volcanic arc granite field together with syn-collisional granite. However, volcanic arc granite (VAG) and syn-collisional granite (syn-COLG) can be separated by Ta-Yb, Rb- (Y+Nb) and Rb- (Yb+Ta) diagrams of Pearce et al. (1984). In similar way, on Rb- (Y+Nb) and Rb - (Yb+Ta) diagrams of (Fig.6.10) Pearce et al. (1984) both of the samples are plotted on the volcanic arc granite fields. In conclusion, on the Ta -Yb, Rb – Yb + Ta, and Rb-Y + Nb discrimination diagrams of Pearce et al.(1984), both of the samples are plotted within the VAG field, indicating that the micorgranitic intrusions were erupted in volcanic arc setting.

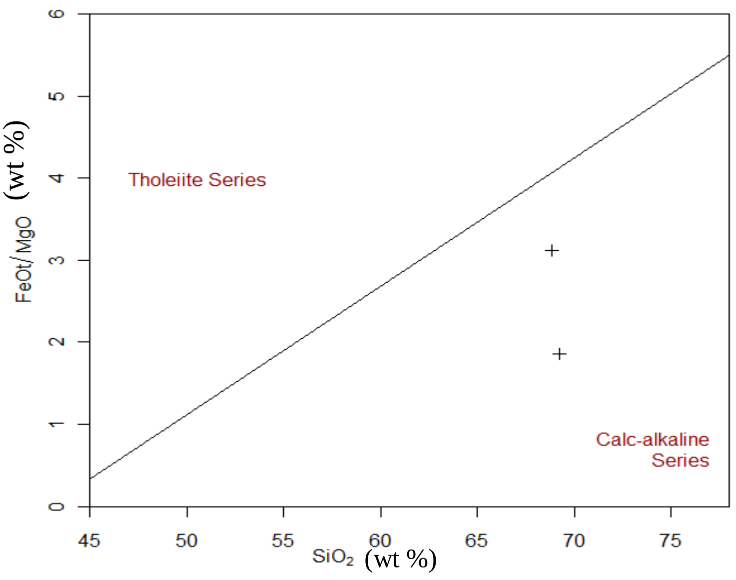

Fig. 6.6: SiO2 - FeOt/MgO binary plot of the microgranitic intrusions (Miyashiro, 1974). The symbol + (plus) represents microgranitc rock.

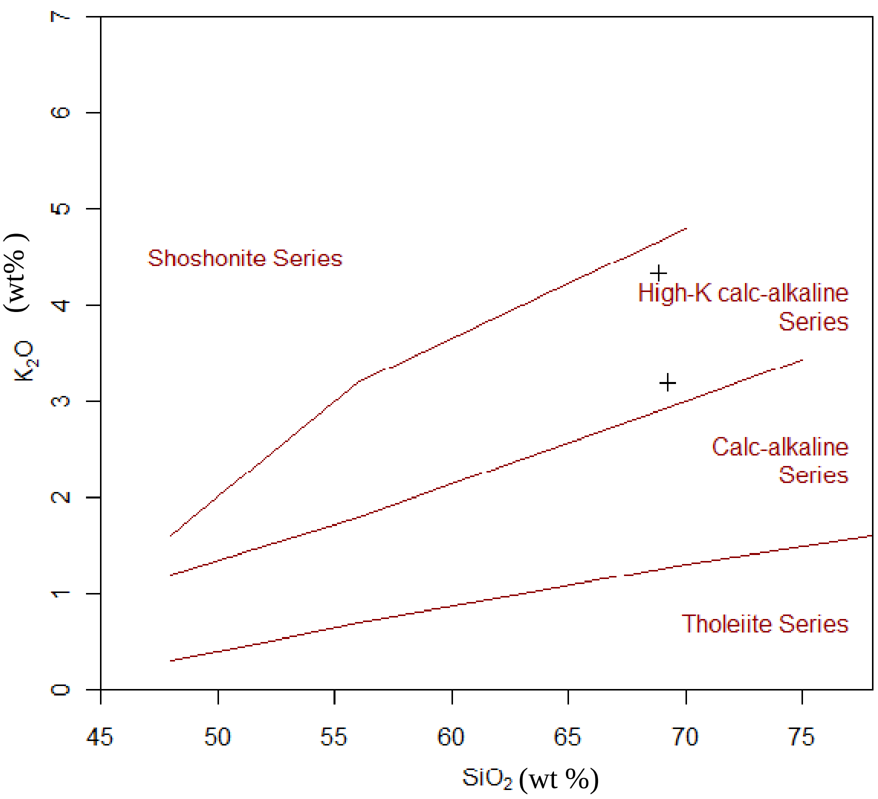

Fig.6.7: K2O - SiO2 binary plot of the microgranitic intrusions (Peccerillo and Taylor, 1976) (symbols same as Fig.6.6).

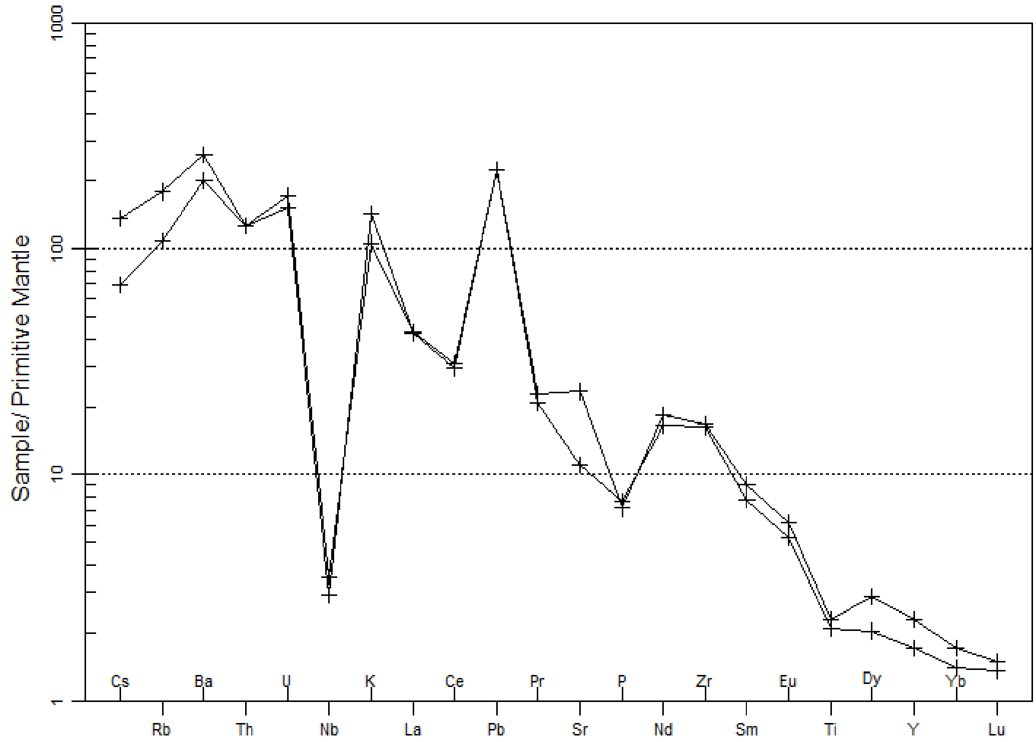

Fig.6.8: Primitive Mantle normalized multi-element varation diagram for microgranitic intrusions (Sun and McDonough, 1989), (symbols as in Fig.6.6).

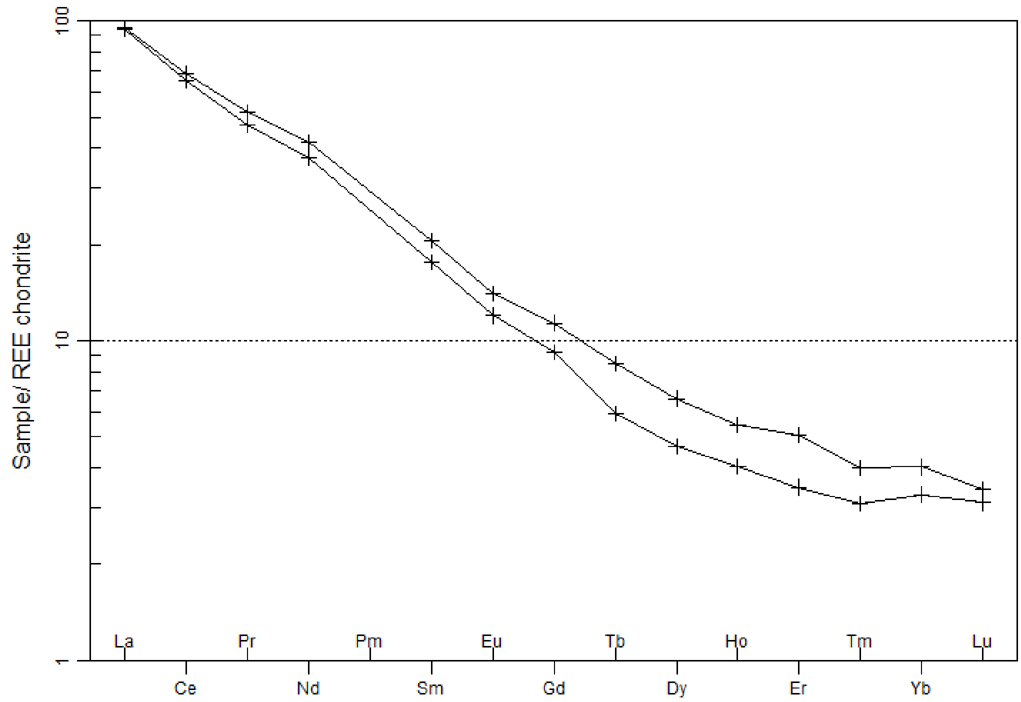

Fig.6.9: Chonderite-normalized REE pattern for microgranitic intrusions (Boynton, 1984), (Symbols same as Fig. 6.6).

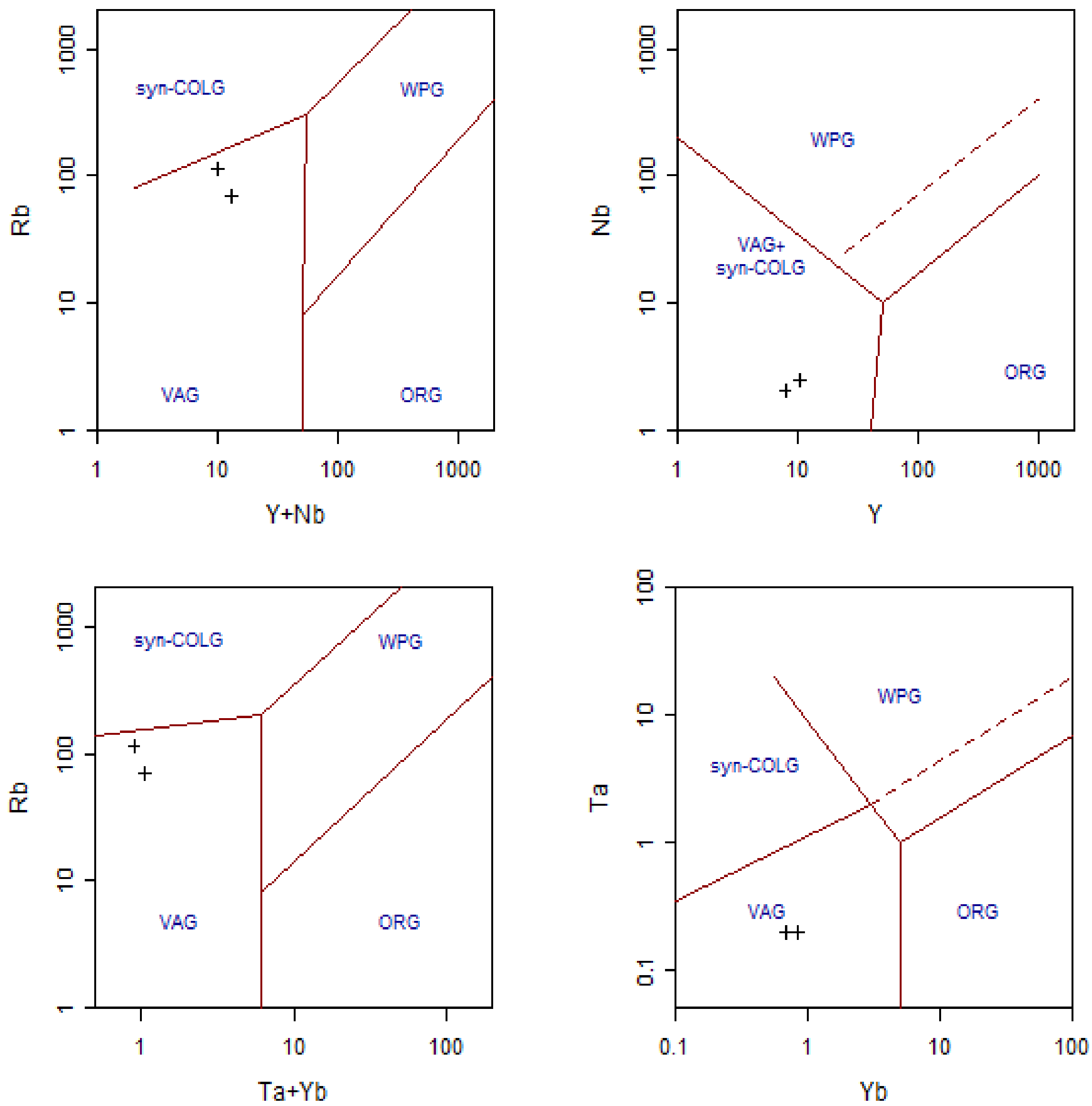

Fig.6.10: Nb-Y, Ta- Yb, Rb- Yb+ Ta and Rb-Y+Nb discrimination diagrams for microgranitic intrusions (Pearce et al., 1984). Note syn-COLG= Syn-collision granites, VAG =Volcanic arc granite, WPG = Within-plate granites and ORG= Ocean ridge granites. Both of the samples are plotted within the VAG field (symbols same as Fig. 6.6).

6.4. Metasedimentary units

The samples of clastic metasedimentary rocks are recalculated to volatile free bases and presented in Table 6.1. The analyzed samples display andesitic composition in their major-element composition, i.e. the SiO_2 content ranges from (59.8 – 61.3wt %) (Cox et al., 1979). Major oxides are plotted against Al_2O_3 (Fig.6.11). Thus, CaO and K_2O show good correlations with Al_2O_3, whereas Na_2O shows scatter trend. The depletion of CaO and scattered trend of Na_2O are probably related to the destruction of plagioclase during chemical weathering, whereas the content of K_2O increase with increasing Al_2O_3 this may be linked to the K- metasomatism or the presence of K hosted minerals in the source (Nesbitt and Young, 1982; Fedo et al., 1995). Moreover, CaO, K_2O and Na_2O are mobile under weathering, digenesis, hydrothermal activities and metamorphic processes. However, other major oxides (not shown here) are poorly correlated with Al_2O_3. The depletion of CaO, Na_2O, and Sr in metasedimentary rocks compared to the metavolcanic rocks is probably due to intensive chemical weathering.

Trace elements of Zr, Hf, Cs, Nb, and Ba have good correlation with Al_2O_3 (Fig.6.11), though, other trace elements (not shown here) are poorly correlated with Al_2O_3. The concentrations of Zr, Hf and Nb decrease with increasing the Al_2O_3 content. This is probably due to the fractionation of heavy minerals such as zircon and sphene during the early phase of crystallization of the source rocks (Bhatia and crook, 1986; McLennan and Taylor, 1991; Nyakairu and Koeberl, 2001). Likewise, the negative correlation of Cs and Ba with Al_2O_3 content is probably due to the alterations and progressive destruction of K-feldspar in the source area. In addition to this, the fractionation of K-feldspar from the melt during crystallization of the source rock also contributes to reduce the concentrations of Cs and Ba (Nesbitt and Young, 1982; Fedo et al., 1995; Nyakairu and Koeberl, 2001). The relative enrichment of Cr and Ni in the metasedimentary rocks relative to the metavolcanics is perhaps due to adsorption of these elements onto sediment particles during weathering and deposition (Kibret Sifeta et al., 2005). Europium anomaly (Eu/Eu*) of the samples range from 0.75 - 0.95 (with an average of 0.83) indicates that the fractionation of plagioclase feldspar during the early phase of the source rock or the progressive destruction of plagioclase feldspars during chemical weathering (McLennan and Taylor, 1991; Nyakairu and Koeberl, 2001).

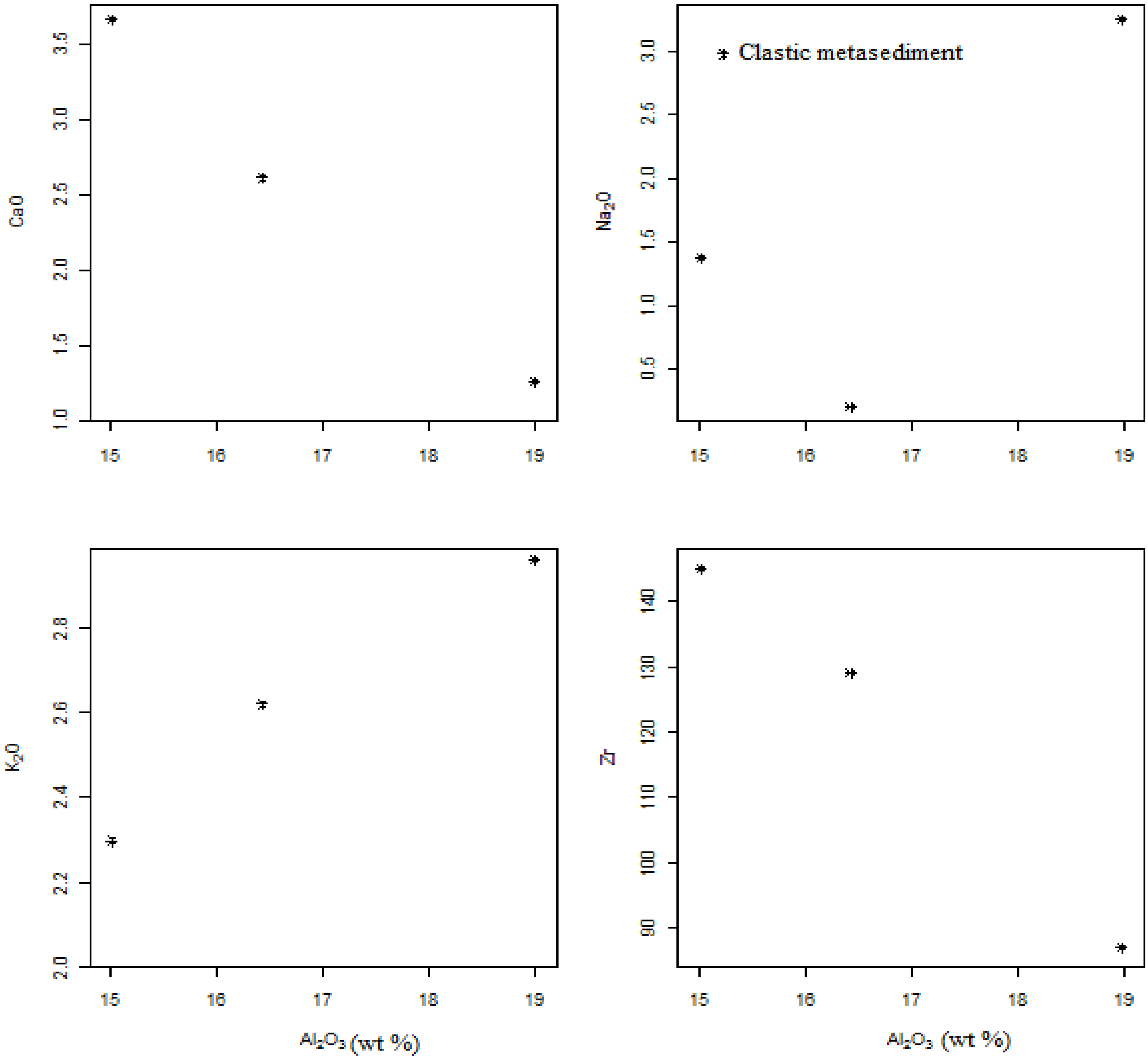
CaO
Na$_2$O
Clastic metasediment
K$_2$O
Zr
Al$_2$O$_3$ (wt %)
Al$_2$O$_3$ (wt %)

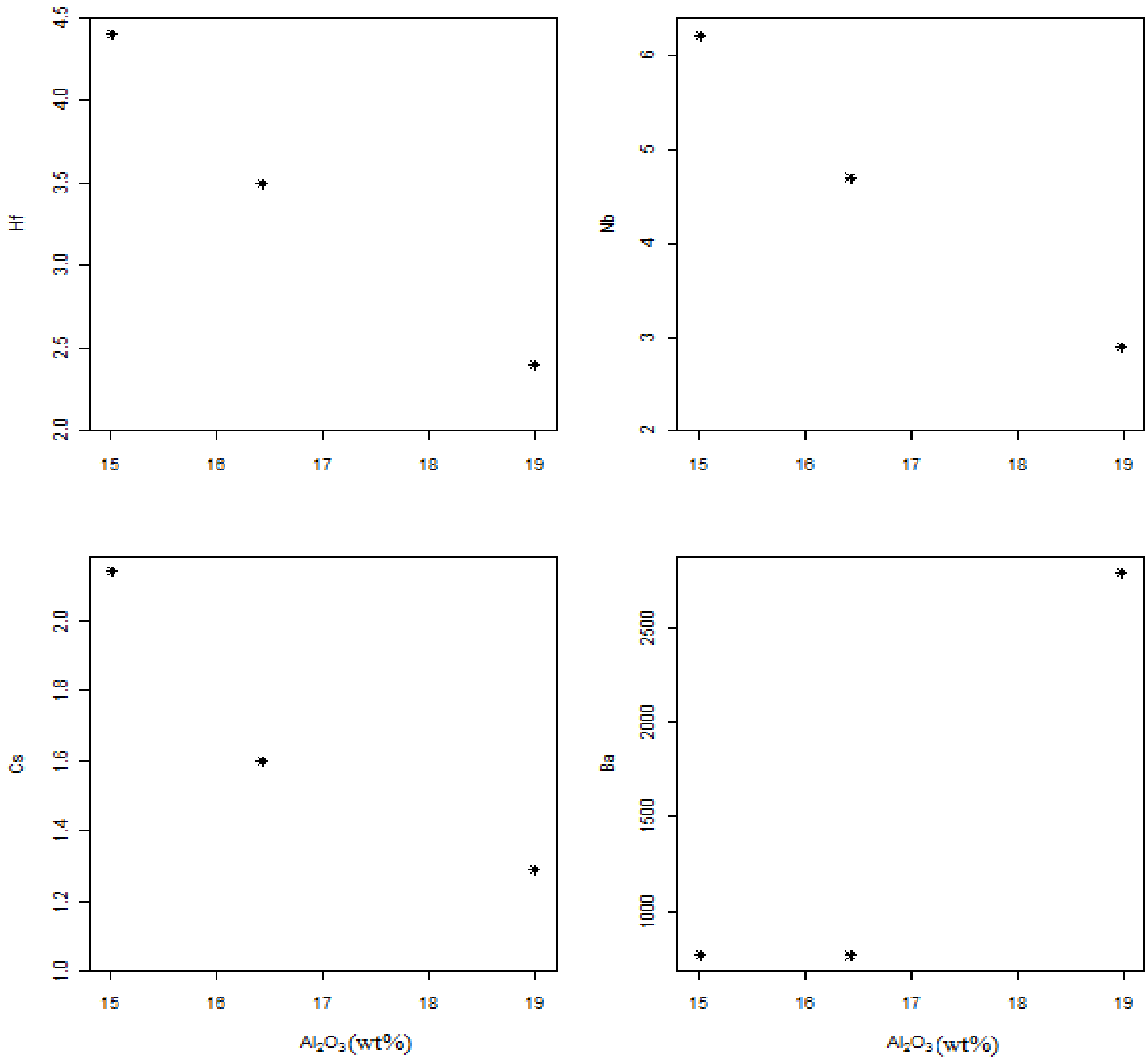

Fig.6.11: Some selected major element and trace element against Al_2O_3 for Mai Kinetal metasedimentary rocks. The major oxides are plotted on an anhydrous basis.

6.4.1. Weathering and weathering indices of metasedimentary rocks

Weathering processes decompose and breakdown the mineral grains from the parent rocks and thus it enhances the mobility of ions. The large cation elements such as Cs, Rb, and Ba are remaining fixed in the weathered profile by preferential exchange and adsorption processes, whereas the smaller cations (Na, Ca, and K) are leaching by degradation processes (Nesbitt et al., 1980: Rollinson, 1993). Furthermore, the abundance of Ca, Na and K elements with respect to the resistant elements (Al, Ti) can be used to measure the degree of chemical weathering (Nesbitt and Young, 1982).

Weathering indices are used to measure the extent of depletion of mobile elements relative to immobile elements during chemical weathering (Harnois, 1988).

Various types of weathering indices (CIA, CIW and PIA) are proposed by different scholars such as (Nesbitt and Young, 1982; Harnois, 1988 and Fedo et al., 1995).

Nesbitt and Young (1982) proposed chemical index of alteration to evaluate the alteration of plagioclase and potassium feldspar to clay minerals or to measure the relative enrichment of Al relative to Ca, Na, and K during chemical weathering.

The chemical index of alteration is defined as:

$CIA = [A1_2O_3 / (Al_2O_3 + CaO^{*}\cdot + Na_2O + K_2O)]\ x100$

Where, the oxides are expressed in molecular proportions and CaO* represents the amount of CaO present in silicate minerals only. The correction also made for carbonate and apatite content [$CaO^{*} = (\text{mole } CaO - \text{mole } P_2O_5 \times 10/3)$].

The higher values of CIA indicates that the removal of mobile elements such as Ca, Na, K relative to Al during chemical weathering, whereas low values of CIA indicates near absence of chemical weathering (Nesbitt and Young ,1982 ; Fedo et al.,1995 and Kibret Sifeta et al .,2005) . Likewise, Fedo et al. (1995) classified the CIA and PIA values into low (50%–60 %), intermediate (60%–80%) and extreme high (80%-100%) chemical weathering. Thus, the CIA values of the analyzed samples (Table 6.3) range from 57.99 % to 68.39 % (average 63.73%), indicating that the sediments show intermediate degree of chemical weathering in the source area. Furthermore, the analyzed samples have higher $A1_2O_3$ content and $CaO + Na_2O + K_2O$ are generally low, implying that significant chemical weathering in the source area.

Harnois (1988) developed chemical index of weathering to measure and evaluate the extent of conversion of feldspar to clay minerals. Furthermore, this index removes the effects of remobilization and redistribution of K during diagenesis and metamorphic processes.

The chemical index of weathering defined as:

$CIW = [Al_2O_3 / (Al_2O_3+CaO^{*}+Na_2O) *100]$

The chemical index of weathering values of the analyzed samples (Table 6.3) range from 64.16% to 77.55% (average 71.49%), implying that the sediments show moderate degree of chemical weathering in the source area.

Fedo et al. (1995) proposed plagioclase index of alteration to evaluate the degree of chemical weathering of plagioclase feldspar and to measure the conversion of plagioclase feldspar to clays.

The plagioclase index of alteration is defined as:

$$PIA = [(Al_2O_3\text{-}K_2O)/ (Al_2O_3 + CaO^* + Na_2O\text{-}K_2O)] \times 100$$

The analyzed samples have PIA value (Table 6.3) range from 59.89 % to 74.07% (average 67.64%). Thus, this value suggested that moderate degree of plagioclase weathering in source area.

Cox et al. (1995) of K_2O/Al_2O_3 ratio also used to determine the extent of the alkali feldspar and plagioclase feldspar altered to clay minerals during chemical weathering and the ratio for clay minerals range from 0.1 to 0.3. The ratio of K_2O/Al_2O_3 of the analyzed sample ranges from 0.15 to 0.16 (average 0.15) this value indicates that the plagioclase and k- feldspar are converted to clay minerals during chemical weathering.

Th/U ratios greater than 4 is an indicator of chemical weathering in the source rock (McLennan and Taylor, 1991). Furthermore, weathering processes tends to result in oxidation of insoluble U^{+4} to soluble U^{+6} and its ratio of Th/U increase with increasing weathering intensity. The ratio of Th/U for Mai Kinetal sediments range from 1.95 to 8.29 (average 4.27), implying there is chemical weathering in the source rock.

Table 6.3: Calculated values of chemical index of alteration, chemical index of weathering and plagioclase index alteration.

Sample	Al_2O_3	CaO	Na_2O	K_2O	P_2O_5	CaO*	CIA %	CIW%	PIA%
MS4	0.186	0.023	0.052	0.031	0.002	0.017	64.808	72.759	68.949
MS17	0.161	0.047	0.003	0.028	0.001	0.043	68.390	77.546	74.075
MS20	0.147	0.066	0.022	0.024	0.002	0.060	57.993	64.156	59.894

A-CN-K (Al_2O_3- (CaO^*+ Na_2O)-K_2O) diagram

A–CN–K ternary plot are also used to evaluate weathering trends in the source rock, to estimate K-metasomatism and to infer the average composition of the source (Nesbitt and Young (1982, 1984) and Fedo et al., 1995). The ideal weathering lines are parallel to A-CN boundary because the removal rates of Na and Ca from plagioclase are greater than the removal rate of K from k-feldspars (Nesbitt and Young, 1984).

On the A–CN–K ternary plot (Fig.6.12) the analyzed samples are plotted more or less close to the ideal weathering lines implying that the removal of CaO and Na_2O under moderate degree of chemical weathering.

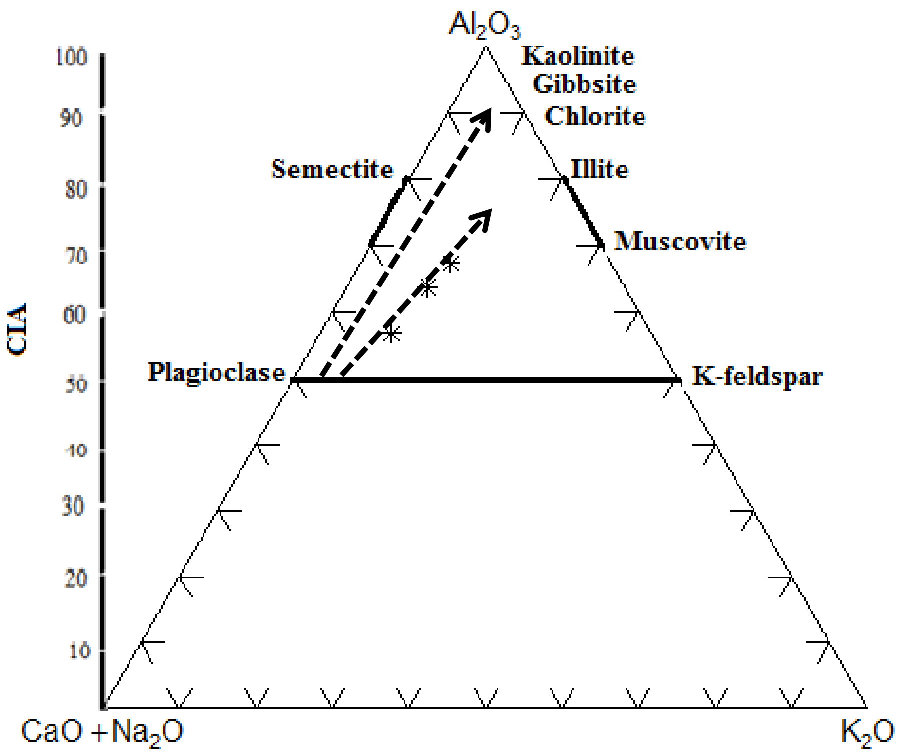

Fig. 6.12: A-CN-K (Al2O3-(CaO+Na2O)-K2O) ternary diagram for metasedimentary rocks (Fedo et al., 1995). The short arrow in the diagram indicates that weathering trend of the analyzed rocks. The longer arrow parallel to A-CN-boundary represents ideal weathering lines.

In conclusion, the various chemical indices such as CIA, CIW, PIA, K_2O/Al_2O_3 and Th/U and ACNK diagram suggest that the sediments have been subjected to intermediate degree of chemical weathering.

6.4.2. Provenance of the Mai Kinetal clastic metasedimentary rocks

The chemical composition of sediments can be used to determine the source rock composition. K, Na, Ca and Mg are less importance to estimate the source rock composition, whereas the immobile elements of such as Ti, Al and Zr are importance to estimate the source rock composition because they are more resistant, less mobile and less fractionated relative to other cations during sedimentary and metamorphic processes (Nesbitt and Young, 1982; McLennan et al., 1991). The ratio of Al_2O_3/TiO_2 of the analyzed samples range from 15.097 to 18.55 (average 17.38) with its SiO_2 content ranges from 61.2 - 64.8, indicating that these sediments are most likely derived from intermediate source rock.

REE, Th and Sc are used to identify the sedimentary provenance because these elements are little-fractionated by sedimentary and metamorphic processes (McLennan and Taylor, 1991; Rollinson, 1993; Nyakairu and Koeberl, 2001). The abundances of REE and Th are higher in felsic igneous rocks, whereas the abundance of Co, Sc, Ni, and Cr are higher in mafic igneous rocks. The ratios of incompatible-compatible elements (Th/Sc, Co/Th, Cr/Th, La/Sc and Zr/Sc) are used for discriminating between felsic and mafic source components (Cullers and Graf, 1983; McLennan et al., 1993; McLennan and Taylor, 1991; Rollinson, 1993; Nyakairu and Koeberl, 2001).

On the binary plot of Th/Sc against Zr/Sc of McLennan et al. (1993) the analyzed sediments (Fig.6.13) are distributed in between the basaltic and felsic end members of metavolcanic and they are also clustered around the intermediate composition. Hence, this indicates that the analyzed sediments were probably derived from intermediate composition source.

Table 6.4: Comparison of Th/Sc and Zr/Sc ratio for metavolcanic and metasedimentary units

Sample	MV1	MV2	MV3	MV5	MV8	MV9	MV12	MS4	MS17	MS20
Th/Sc	0.14	0.31	0.18	0.24	0.46	0.04	0.04	0.11	0.14	0.26
Zr/Sc	7.25	12.82	7.21	8.93	21.27	3.19	3.24	4.35	5.16	9.06

The absences of recycling effect in sediments are characterized by Zr/Sc ratio less than 10 (McLennan et al., 1993; Nyakairu and Koeberl, 2001). The analyzed samples have Zr/Sc ratio ranges from 4.35 to 9.06 (average 6.19). Accordingly, the data obtained in this study suggest that the samples do not show any sign of recycling effect.

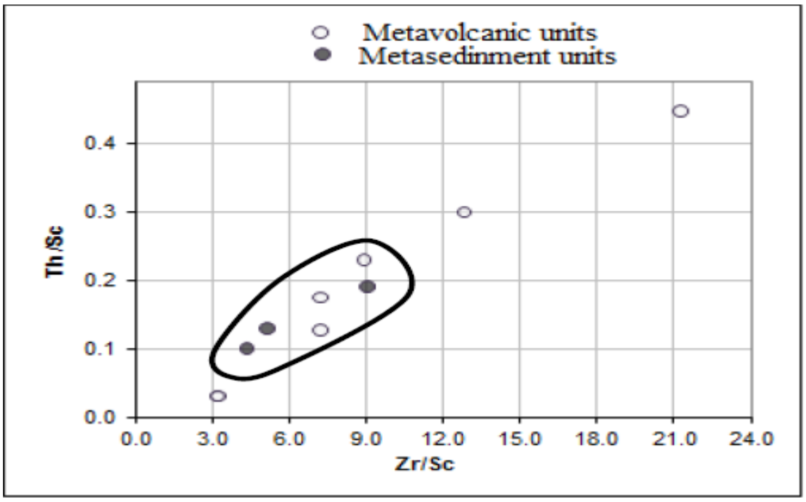

Fig.6.13: Th/Sc–Zr/Sc binary plot of Mai Kinetal metasedimentary units compared to the Mai Kinetal metavolcanic rocks (McLennan et al., 1993).

The chondrite normalized REE pattern (Fig.6.14) for Mai Kinetal metasediments are similar to PAAS, NASC, ES, and UCC. However, the analyzed samples display relatively lower REE content relative to PAAS, NASC, ES and UCC. The abundances of immobile elements such as Zr, Hf and Nb and LREE tend to be lower than the average upper continental crust, whereas compatible elements (Co, Cr and Ni) tend to be greater than UCC, implying that the sediments were not derived from upper continental crust related composition (Kibret Sifeta et al., 2005). The ratio of La_N/Yb_N of the sediments range from 4.62 to 10.75 (average 6.95), implying that moderate degree of LREE fractionation. The La_N concentrations of the analyzed samples range from 10 x chondrite to 100x chondrite. This feature suggests that the metasedimentary rocks are first cycle-sediments lacking appreciable recycling and mixing (McLennan, 1989 as cited in Kibret Sifeta et al., 2005).

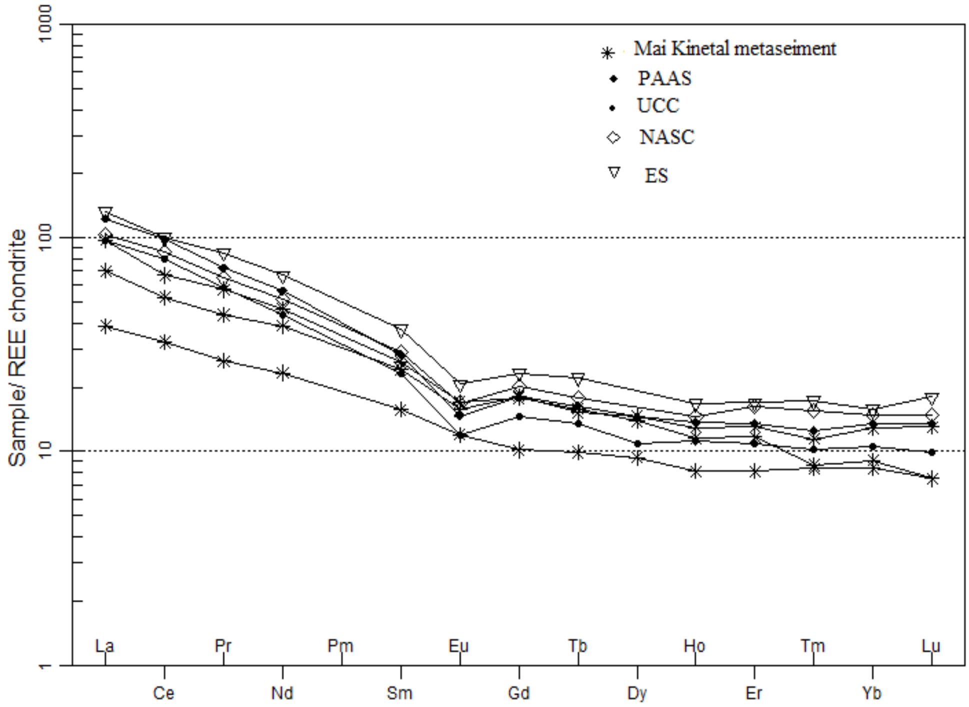

Fig.6.14: Chondrite-normalized REE patterns for Mai Kinetal metasedimentary units. The samples are normalized to Chondrite according to Boynton (1984). Post-Archean Australian Sedimentary rocks (PAAS) data is taken from McLennan (1989): North American shale composite (NASC) from Haskin and Haskin (1966); Average European Shale (ES) from Haskin and Haskin (1966): Average Upper Continental Crust (UCC) from Taylor and McLennan (1981).

6.4.3. Tectonic setting of the depositional basin of metasedimentary units

Major oxide data have limited application to determine the tectonic setting of the depositional basin of the sedimentary rocks because these elements are redistributed and remobilized by weathering, erosion, diagnesis, hydrothermal activities and low-grade metamorphic processes (Kibret Sifeta et al., 2005).

Immobile trace elements such as La, Nd, Th, Zr, Nb, Y, Sc and Co are used to characterize the geological setting of the depositional basin of the sedimentary rocks because these elements are insensitive to secondary processes (weathering, diagnesis metamorphism and hydrothermal activities).

On Co - Th - Zr/10 ternary diagram (Fig.6.15) of Bhatia and Cook (1986) discriminates the depositional environment of sediments into oceanic island arc, continental island arc, active continental margin and passive continental margin. The analyzed samples are plotted on oceanic island arc field and the sediments were deposited in oceanic island arc tectonic setting. The data obtained in this study is consistent with Kibret Sifeta et al. (2005). The concentration of Zr ranges from 87 ppm to 145 ppm (with an average 120.3); Co ranges from 14 ppm to 17 ppm (average 12.3) Sc ranges from 16 ppm to 25 ppm (average 20.3) and Th/Sc ranges 0.11 to 0.26 from (average 0.17). This could be reflecting the provenance from an oceanic island arc setting (Bhatia and Crook, 1986).

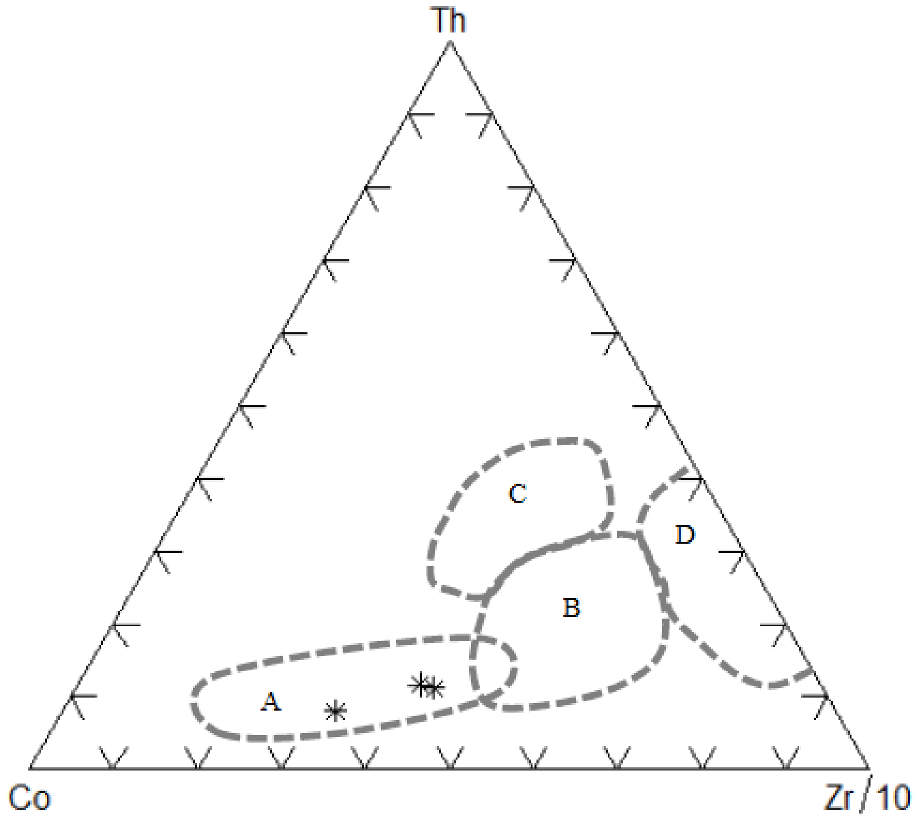

Fig .6.15: Th - Co - Zr/10 tectonic discrimination plot for Mai Kinetal metasedimentary rocks. (Bhatia and Cook, 1986): A = oceanic island arc; B = continental island arc; C = active continental margin; D = passive continental margin.

CHAPTER SEVEN

7. CONCLUSION AND RECOMMENDATION

7.1. CONCLUSION

From the field observations, petrographic and geochemical data obtained in the present work allows to draw the following conclusion:

1. The presences of relict igneous texture (porphyritic), preserved primary structure (bedding and cross bedding) and certain mineral assemblages such as chlorite, epidote ,muscovite, sericite and albite indicates that the rocks in the study area experienced very low to low grade of metamorphism that belong to green schist facies.
2. The rock units of the study area have been affected by at least three phases of deformation episodes: The earlier deformation (D1) produced pervasive regional foliation and tight minor folds: second phase of deformation (D2) produced crenulation cleavage: the latter phase of deformation was responsible for the formation of faults, joints and lineaments.
3. The overall geochemical characteristics of the Mai Kinetal metavolcanic rocks display calcalkaline affinity. The discrimination diagram of Wood (1980) suggested that the metavolcanics were developed in volcanic arc tectonic setting.
4. The micrograntic intrusions display high potassium calcalkaline and peraluminous affinity. The discrimination diagrams of Ta -Yb, Rb – Yb + Ta, and Rb – Y + Nb of Pearce et al. (1984) suggested that the micrograntic intrusions were developed in volcanic arc environment. This is consistent with tectonic environment of metavolcanic rocks.
5. Petrographic study of the clastic metasediment units show the presence of mafic metamorphic minerals such as sericite, chlorite, and epidote and indicate that these units have a volcanic or volcanoclastic in origin.
6. The various chemical indices such as CIA, CIW, PIA, K_2O/Al_2O_3, Th/U, and ACNK diagram suggest that the analyzed metasediments have been subjected to intermediate degree of chemical weathering.
7. The analyzed metasediments are most likely derived from intermediate source rock and the discrimination diagram of Th - Co - Zr/10 suggested that the sediments were deposited in the oceanic island arc tectonic setting.

8. The overall petrological and geochemical characteristics of metavolcanic and micro granitic intrusion indicates that they were developed in volcanic arc environment and this is consistent with the arc accretion models postulated in Sudan, Egypt and Saudi Arabia for the Neoproterozoic evolution of the Arabian-Nubian Shield.

7.2. Recommendation

- Geochemical data with more sample and isotopic analysis is required in order to have a better understanding of the petrogenic evolution and tectonic setting of an area. Hence, isotope geochemistry is suggested for further verification of the source and petrogenesis of the metavolcanic and metasedimentary rocks.

REFERENCE

Abdelsalam, M.G. and Stern, R.J. (1996). Sutures and shear zones in the Arabian–Nubian Shield. *Journal of African Earth Science,* **23**: 289–310.

Arkin, Y., Beyth, M., Dow, D. B., Levitte, D., Temesgen Haile and Tsegaye Hailu (1971). Geological Map of Mekelle Sheet (ND37-11), E.I.G.S, Addis Ababa, Ethiopia.

Asfawossen Asrat (1997). Geology and geochemistry of the Negash pluton and their metalogenic significance, central Tigray, Unpublished, MSc Thesis, Addis Ababa University, Ethiopia, 167 pp.

Asfawossen Asrat, Barbey, P. and Gleizes, G. (2001).The Precambrian geology of Ethiopia: a review. *Africa Geoscience Review,* **8(3):** 271-288.

Asfawossen Asrat and Barbeya, P. (2003). Petrology, geochronology and Sr–Nd isotopic geochemistry of the Konso pluton, south-western Ethiopia: implications for transition from convergence to extension in the Mozambique Belt. *Int. J. Earth Sci (Geol Rundsch),* **92:**873–890.

Asfawossen Asrat, Barbey, P., Ludden, J., Reisberg, L., Gleizes, G. and Dereje Ayalew (2004). Petrology and isotope geochemistry of the Pan-African Negash pluton, Northern Ethiopia: Mafic-felsic magma interactions during construction of shallow-level calc-alkaline plutons. *Journal of Petrology,* **45(6):** 1147-1179.

Avigad, D., Stern, R.J., Beyth, M., Miller, N. and McWilliams, M.O. (2007). Detrital zircon U–Pb geochronology of Cryogenian Diamictite and lower Paleozoic sandstone in Ethiopia (Tigrai): age constraints on Neoproterozoic glaciation and crustal evolution of the southern Arabian–Nubian Shield. *Precambrian Research,* **154:** 88–106.

Barbarian, B. (1990).Granitoids: main petrogenic class in relation to origin and tectonic setting. *Geological journal,* **25:** 227-238.

Beraki Woldehaimanot and Behrmann, J.H. (1995). A study of metabasite and metagranite chemistry in the Adola region (south Ethiopia): implications for the evolution of the East African orogeny. *Journal of Africa Earth Science*, **21:**459-476.

Best, M. G. (2003). Igneous and Metamorphic Petrology, 2nd Edition, Blackwell, 758pp.

Beyth, M. (1971) .The geology of central and western Tigre, Unpublished, Report, Ministry of Mines, Addis Ababa.

Beyth, M. (1972). The geology of central and western Tigre, Ethiopia, Unpublished PhD dissertation, University of Bonn, Germany, 155 pp.

Beyth, M., Avigad, D., Wetzel, H.U., Mattews, A. and Seife Michael Berhe (2003). Crustal exhumation and indications for Snowball Earth in the East African Orogen: north Ethiopia and east Eritrea. *Precambrian Research,* **123:** 187-201.

Bhatia, M.R. and Crook, K.A.W. (1986). Trace element characteristics of graywackes and tectonic setting discrimination of sedimentary basins. *Contributions to Mineralogy and Petrology***, 92:**181–193.

Blanford, W.T. (1870) .Observations on the Geology and Zoology of Abyssinia. MacMillan and Co., London

Boynton, W.V. (1984). Geochemistry of Rare Earth Elements: Meteoritic Studies, Elsevier, Amsterdam, 63-114pp.

Bucher, K. and Grapes, R. (2011). Petrogenesis of Metamorphic Rocks, 8th edition Springer-Verlag, Berlin, 441pp.

Chappell, B.W. and White, A.J.R. (1974). Two contrasting granite types, Pacific Geol., 8**:** 173-174pp.

Cox, K.G., Bell, J.D. and Pankhurst, R.J. (1979).The interpretation of igneous rocks, Allen and Unwin, London, 450pp

Cox, R., Lowe, D.R., and Cullers, R.L. (1995). The influence of sediment recycling and basement composition on evolution of mud rock chemistry in the southwestern United States. *Geochimica et Cosmochimica Acta, **59:*** 2919–2940.

Cullers, R. L. and Graf, J. (1983). Rare earth elements in igneous rocks of the continental crust: intermediate and silicic rocks, ore petrogenesis. *Rare-Earth Geochemistry Elsevier, Amsterdam. (Henderson, P., ed.)* , 275–312.

Cullers, R. L. (1994). The controls on the major-and trace-element variation of shales, siltstones and sandstones of Pennsylvanian-Permian age from uplifted continental blocks in Colorado to platform sediments in Kansas, USA. *Geochim. Cosmochim. Acta.,* **58**: 4955–4972.

Dainelli, G. (1943). Geologia dell'Africa Orientale. Reale Accade¬mia D'Italia, Rome.

Eby, G.N. (1990). The A-type granitoids: a review of their occurrence and chemical characteristics and speculations on their petrogenesis. *lithos.,* **26:**115- 134.

Fedo, C.M., Nesbitt, H.W. and Young, G.M. (1995). Unraveling the effects of potassium metasomatism in sedimentary rocks and paleosols, with implications for pale weathering conditions and provenance. *Geology*, **23:** 921–924.

Fritz, H., Abdelsalam, M., Ali, K.A., Bingen, B., Collins, A.S., Fowler, A.R., Ghebreab, W., Hauzenberger, C.A., Johnson, P.R., Kusky, T.M., Macey, P., Muhongo, S., Stern, R.J. and Viola, G. (2013). Orogen styles in the East African Orogen: A review of the Neoproterozoic to Cambrian tectonic evolution. *Journal of African Earth Sciences,* **86:** 65–106.

Garland, C.R. (1980). Geology of the Adigrat area, Min. Mines Memoir, No.1, Addis Ababa.

Harnois, L. (1988) .The CIW index: A new chemical index of weathering, sediment, *Geol.***, 55:** 319–322.

Haskin, M.A. and Haskin, L.A. (1966). Rare earths in European shales-A redetermination, Sci. **154:** 507-509.

Hayashi, K., Fujisawa, H., Holland, H.D. and Ohmoto, H. (1997). Geochemistry of ~1.9 Ga sedimentary rocks from northeastern Labrador, Canada. *Geochim. Cosmochim. Acta*, ***61****:*4115-4137.

http://en.climate-data.org/location/2108/ accessed on 01.04.2017.

Kazmin, V. (1971). Precambrian of Ethiopia. *Nature*, **230**: 176-177.

Kazmin, V. (1973). The Geological map of Ethiopia, 1:2,000,000, Inst. Geol. Surv. Ethiopia, Addis Ababa.

Kazmin, V. (1975). The Precambrian of Ethiopia and some aspects of the geology of the Mozambique Belt, Bull. *Geophysics, Obs., Addis Ababa,* **15:** 27-45.

Kazmin, V., Alemu Shiferaw and Tilahun Balcha (1978). The Ethiopian Basement: Stratigraphy and possible manner of evolution. *Geologische Rundschau*, **67:**531-546.

Kennedy, W.Q. (1964). The structural differentiation of Africa in the Pan-African (500 Ma) tectonic episode, Leeds Univ. Res. *Inst. Afr. Geol. Annu. Rep.*, **8:** 48-49.

Kibret Sifeta, K., Roser, B. P. and Kimura, J. I. (2005).Geochemistry, provenance, and tectonic setting of Neoproterozoic metavolcanic and metasedimentary units, Werri area, Northern Ethiopia .*Journal of African Earth Sciences,* **41:**212–234.

Kröner, A. (1984). Late Precambrian plate tectonics and orogeny: a need to redefine the term Pan-African. *In African Geology, ed. J Klcrkx, J Miehot, pp. Tcrvuren: Mus6e. R. l'Afriquc Centrale*, 23-28.

Kröner, A. and Stern, R .J. (2005). Pan-African Orogeny, Encyclopedia of Geology**,** Elsevier, Amsterdam, **1:** 1-12.

Levitte, D. (1970). The geology of Mekelle report on the geology of the central part of sheet ND 37-11, Geological Survey of Ethiopia, Addis Ababa, 66 pp.

Lissan, H.N and Bakheit, K.A. (2010). The Geology and Geochemistry of Metavolcanic Rocks from Artoli Area, Berber Province, Northern Sudan: An Implication for Petrogenetic and Tectonic Setting. *Journal of American Science,* **6(8):** 1-13.

Lulu Tsige and Abdelsalam, M.G. (2005). Neoproterozoic-Early Paleozoic gravitational tectonic collapse in the southern part of the Arabian-Nubian Shield: The Bulbul Belt of southern Ethiopia. *Precambrian Research,* **138:** 297-318.

Maniar, P.D. and Piccoli, P.M. (1989). Tectonic discrimination of granitoids. *Geol. SOCA. mer. Bull.*, **101**: 635-643pp.

McLennan, S.M. (1989). Rare earth elements in sedimentary rocks: Influence of provenance and sedimentary processes. In: Lipin B.R, McKay, G.A. (Eds.), Geochemistry and Mineralogy of Rare Earth Elements. *Mineralogical Society of America, Reviews in Mineralogy,* **21:** 169–200pp.

McLennan, S.M., Taylor, S.R., McCulloch, M.T. and Maynard, J.B. (1990). Geochemical and Nd–Sr isotopic composition of deep-sea turbidites: Crustal evolution and plate tectonic associations. *Geochim. et Cosmochim. Acta.,* **54:** 2015–2050.

McLennan, S. M. and Taylor, S. R. (1991). Sedimentary rocks and crustal evolution: tectonic setting and secular trends. *J. Geol.*, 99: 1–21.

McLennan, S. M., Hemming, S., McDaniel, D. K. and Hanson, G. N. (1993). Geochemical approaches to sedimentation, provenance, and tectonics. Processes controlling the composition of clastic sediments (Johnson, M. J. and Basu, A., eds.). *Geological Society of America, Special Paper,* **284:** 21–40.

Mengesha Tefera, Tadiwos Chernet and Workineh Haro (1996). Explanation of the Geological map of Ethiopia, Ethiopian Institute of Geological Survey.

Miller, N.R., Mulegeta Alene, Sacchi, R., Stern, R.J., Conti, A., Kroner, A. and Zuppi, G. (2003). Significance of the Tambien Group (Tigrai, N. Ethiopia) for Snowball Earth events in the Arabian-Nubian Shield. *Precambrian Research,* **121**: 263-283.

Miller, N.R., Stern, R.J., Avigad, D., Beyth, M. and Schilman, B. (2009). Cryogenian slate carbonate sequences of the Tambien Group, northern Ethiopia (I): Pre-"Sturtian" chemostratigraphy and regional correlations. *Precambrian Research,* **170:** 129–156.

Miller, N.R., Avigad, D., Stern, R.J. and Beyth, M. (2011).The Tambien Group, Northern Ethiopia (Tigre). *Geological Society, London, Memoirs,* **36:** 263–276.

Miyashiro, A. (1974). Volcanic rock series in island arcs and active continental margins. *Amer. J. Sci.* **274:** 321-355 pp.

Maniar, P.D. and Piccoli, P.M. (1989). Tectonic discrimination of granitoids. *Geol. SOCA. mer. Bull.*, **101:** 635-643.

Mohr, P. (1963). The Geology of Ethiopia, University college of Addis Ababa Press

Mulugeta Alene and Barker, A.J. (1993). Tectonometamorphic evolution of the Moyale region, southern Ethiopia .*Precambrian Research,* **62:** 271-283.

Mulugeta Alene and Barker, A.J. (1997). Geochemistry of meta-igneous rocks from southern Ethiopia: a new insight into Neoproterozoic tectonics of northeast. *Africa. J. Afr. Earth Sci.,* **24,** 351-370.

Mulugeta Alene (1998). Tectonomagnetic evolution of the Neoproterozoic rock of the Mai Kenetal-Negash area, Tigrai, Northern Ethiopia, Unpublished PhD Thesis, University of Turin, 260 pp.

Mulugeta Alene, Secco, L., Dal Negro, A. and Sacchi, R. (2000a). Crystal chemistry of clinopyroxene in Neoproterozoic metavolcanic rocks of Tigray, Northern Ethiopia. Bull. Soc. It., 119 pp.

Mulugeta Alene, Ruffini, R. and Sacchi .R. (2000b). Geochemistry and geotectonic setting of Neoproterozoic rocks from northern Ethiopia (Arabian-Nubian Shield). *Gondwana Res.*, ***3:*** 333-347.

Mulugeta Alene, Jenkin, G. R.T., Leng, M. J. and Darbyshire, F.D.P. (2006). The Tambien Group, Ethiopia: An early Cryogenian (ca. 800-735 Ma) Neoproterozoic sequence in the Arabian-Nubian Shield. *Precambrian Research,* **147**: 79-99.

Nesbitt, H. W., Markovics, G. and Price, R. C. (1980). Chemical processes affecting alkalies and alkaline earths during continental weathering. *Geochim. Cosmochim. Acta.* ***44:*** 1659–1666.

Nesbitt, H.W. and Young, G.M. (1982). Early Proterozoic climates and plate motions inferred from major element chemistry of lutites. *Nature,* **299:**715–717.

Nesbitt, H.W. and Young, G.M. (1984). Prediction of some weathering trends of plutonic and volcanic rocks based upon thermodynamic and kinetic considerations. *Geochemical et Cosmochimica, Acta.* **48:** 1523–1534.

Nyakairu, G.W. A. and Koeberl, C. (2001). Mineralogical and chemical composition and distribution of rare earth elements in clay-rich sediments from central Uganda. *Geochemical Journal*, 35:13 – 28pp.

Passchier, C.W. and Trouw, R.A.J. (1998). Microtectonics, Springer-Verlag, Berlin, 289pp.

Pearce, J.A., Harris, N.B.W. and Tindle, A.G. (1984). Trace element Discrimination Diagrams for the Tectonic Interpretation of Granitic Rocks. *Journal of petrology,* ***25**: 956-983pp.*

Peccerillo, A. and Taylor S .R. (1976). Geochemistry of Eocene calc-alkaline volcanic rocks from the Kastamonu area, Northern Turkey, Contrib Mineral Petrol. **58:** 63-81pp.

Rollinson, H. R. (1993). Using geochemical data: Evaluation, presentation, interpretation: Longman Group UK Ltd., 352 p.

Seife Michael Berhe (1990). Ophiolites in north east and east Africa, implication for Proterozoic crustal growth. *Journal of Geological Society, London,* **147**: 41-56.

Solomon Gebresilassie (2009). Nature and characteristics of metasedimentary rock hosted gold and base metal mineralization in the Workamba area, central Tigray, northern Ethiopia, PhD thesis, Ludwig Maximilians, Munich University, Germany, 148p.

Sugitani, K., Horiuchi, Y. and Adachi, M. (1996). Anomalously low Al2O3/TiO2 values for Archean crest from the Pilbara block, western Australia- possible evidence for extensive chemical weathering on the early earth. *Precambrian Res.,* ***80:*** *49-76.*

Stern, R.J. (1994). Arc assembly and continental collision in the Neoproterozoic East African Orogen: Implications for the consolidation of Gondwanaland. *Annual Reviews Earth Planetary Sciences,* **22:** 319-351.

Stern, R.J., Avigad, D., Miller, N.R. and Beyth, M. (2006). Evidence for the Snowball Earth hypothesis in the Arabian-Nubian Shield and the East African Orogen. *Journal of Africa Earth Science,* **44,** 1-20.

Sun, S., and McDonough, W.F. (1989). Chemical and isotopic systematics of oceanic basalts: implications for mantle composition and processes: In Sunders, A.D., and Norry, M.J. (eds), Magmatism in ocean basins. *Geological Society Special,* **42:** 313-345.

Swanson-Hysell, N.L., Maloof, A., Condon, D.J., Jenkin, G.R.T., Mulugeta Alene, Tremblay, M.M., Tadelle Tesema, Rooney, A.D. and Haileab, B. (2015). Stratigraphy and geochronology of the Tambien Group, Ethiopia: Evidence for globally synchronous carbon isotope change in the Neoproterozoic. *Geological society of America,* **43(4):** 1-5.

Tadesse Alemu (1998). Geochemistry of Neoproterozoic granitiods from the Axum area, northern Ethiopia. *Journal of African Earth Science,* **27**: 437- 460.

Tarekegn Tadesse (1996). Structure across a possible intra-oceanic suture zone in low-grade Pan-African rocks of northern Ethiopia. *Journal of African Earth Sciences,* **23:** 575-381.

Tarekegn Tadesse, Suzuki, K. and Hoshino, M. (1997). Chemical Th–U total Pb isochron age of zircon from the Mareb Granite in northern Ethiopia. *J. Earth Planet. Sci. Negoya Univ*. **44:** 21–27.

Tarekegn Tadesse, Hoshino, M., and Sawada, Y. (1999). Geochemistry of low-grade metavolcanic rocks from the Pan African of the Axum area, northern Ethiopia. *Precambrian Research***, 99:** 101-124.

Tarekegn Tadesse, Hoshino, M., Suzuki, K. and Iisumi, S. (2000). Sm-Nd, Rb-Sr, and Th-U-Pb zircon ages of syn and post-tectonic granitoids from the Axum area of northern Ethiopia. *Journal of African Earth Sciences,* **30:** 313-327.

Taylor .S.R. and McLennan.S.M. (1981). The composition and evolution of the continental crust: rare earth element evidence from sedimentary rocks. *Pkil.Trans.R.Soc,* A**301**: 381-399.

Wilson, M. (1989). Igneous Petrogenesis a global tectonic approach, Unwin Hyman, London, 480pp.

Wood, D.A. (1980). The application of a Th-Hf-Ta diagram to problems of tectonomagmatic classification and to establishing the nature of crustal contamination of basaltic lavas of the British Tertiary volcanic province. *Earth Planet. Sci. Lett.,* **50:** 11-30pp.

Appendix I

Structural data

№	structural element	Orientation			Location	Unit
	Foliations					
		Strike	Dip	Dip direction	Longitude: latitude	
1		190	75	NE	500293:1530539	Clastic sediment
2		60	40	NW	500022:1530539	Clastic sediment
3		25	20	NW	500335: 1530665	Clastic sediment
4		40	20	NW	499926: 1530356	Clastic sediment
5		25	55	NW	499267: 1530536	Lower slate
6		30	20	NW	499075; 1530536	Lower slate
7		55	30	NW	498744: 1530417	Lower slate
8		35	30	NW	498821: 1530233	Lower slate
9		30	30	NW	498828: 1530345	Lower slate
10		30	35	NW	498828: 1530345	Lower slate
11		10	30	NW	498833: 1530415	Lower slate
12		10	25	NW	498860: 1530419	Lower slate
13		60	50	NW	499097: 1530688	Lower slate
14		70	65	NW	499149: 1530730	Lower slate
15		60	70	NW	4991666:1530748	Lower slate
16		30	20	NW	499388: 1530959	Lower slate
17		50	65	NW	499454: 1530995	Lower slate
18		25	40	NW	499915: 1531229	Lower slate
19		35	60	NW	500876: 1531520	Lower slate
20		30	25	NW	500907: 1531518	Lower slate
21		15	50	SE	501943: 1531539	Lower slate
22		30	50	SE	502128: 1531472	Lower slate
23		15	40	NW	502884: 153552	Lower slate
24		60	40	NW	502988: 1531608	Lower slate
25		40	45	NW	503603: 1532172	Lower slate
26		40	50	NW	503625: 1533224	Lower slate
27		60	30	NW	503619: 1532541	Lower slate
28		30	40	NW	503617: 1532861	Lower slate

29		30	20	NW	503628: 1532546	Upper Limestone
30		30	40	NW	503608: 1532665	Upper Limestone
31		30	40	NW	503571: 1532670	Upper Limestone
32		10	75	NW	502060: 1531959	Upper Limestone
33		10	60	NW	502061: 1531972	Upper Limestone
34		35	65	NW	501999: 1532991	Lower slate
35		30	50	NW	501984: 1532094	Lower slate
36		20	55	NW	501985: 1532091	Lower slate
37		20	60	NW	501958: 1532071	Lower slate
38		25	40	NW	501919: 1532094	Lower slate
39		30	35	NW	501891: 1532071	Lower slate
40		30	45	NW	501873: 1532084	Lower slate
41		30	40	NW	501834: 1532101	Lower slate
42		40	45	NW	501458: 153267	Lower slate
43		55	40	NW	501371: 1532320	Lower slate
44		50	40	NW	501377: 1532334	Lower slate
45		50	55	NW	501364: 1532346	Lower slate
46		35	50	NW	501339: 1532326	Lower slate
47		40	45	NW	501312: 1532325	Lower slate
48		30	40	NW	501268: 1532347	Lower slate
49		30	45	NW	501237: 1532340	Lower slate
50		35	45	NW	501173: 1532356	Lower slate
51		40	45	NW	501129: 1532401	Lower slate
52		50	45	NW	501061: 1532407	Lower slate
53		45	75	NW	500807: 1532512	Lower slate
54		35	40	SE	500768: 1532478	Lower slate
55		55	45	SE	500737: 1532500	Lower slate
56		50	45	NW	500470: 1532491	Lower slate
57		30	40	NW	500364: 1532476	Lower slate
58		40	20	NW	499929: 1532729	Upper Limestone
59		20	70	NW	499868: 1532785	Upper Slate
60		20	55	NW	500236: 1533947	Upper Limestone
61		240	25	SE	500524:15334252	Upper Slate
62		260	20	SE	500512: 1534444	Lower slate
63		240	20	SE	500760: 1534695	Lower slate

64		230	20	SE	500986: 1534872	Lower slate
65		250	30	SE	501101: 1534986	Lower Slate
66		210	45	NW	502790: 1534506	Lower Slate
67		30	45	NW	502814: 1534532	Lower Slate
68		40	30	NW	502835: 1533432	Upper Limestone
69		40	45	NW	502856: 1534576	Lower Slate
70		40	65	SE	503401: 1534968	Lower Slate
71		40	40	SE	503445: 1535024	Upper Limestone
72		250	30	SE	503496: 1535042	Upper Limestone
73		220	70	SE	504072: 1535176	Upper Slate
74		220	50	SE	504264: 1535089	Upper Slate
75		220	30	SE	504362: 1535081	Upper Slate
76		230	25	NW	5045717:1535500	Upper Limestone
77		240	60	NW	504847: 1537460	Lower Slate
78		230	45	NW	504643: 1537620	Lower Slate
79		230	30	NW	503672: 1537714	Lower Slate
80		40	40	NW	501110: 1535196	Metavolcanic
81		20	40	NW	501072: 1535162	Metavolcanic
82		240	65	NE	499998: 1537827	Metavolcanic
83		240	20	NW	501095: 1530758	Metavolcanic
	Joint					
1		300	80	NE	500285:1530542	Clastic sediment
2		305	80	NE	500314: 1530536	Clastic sediment
3		30	80	SW	500335: 1530640	Clastic sediment
4		320	80	SW	500119: 1530324	Clastic sediment
5		25	60	NW	499210: 1531102	Lower Slate
6		15	35	NW	499622: 1531907	Lower Slate
7		30	25	NW	501520: 1531863	Lower Slate
8		320	80	SW	501562: 1531852	Lower Slate
9		320	75	SW	501569: 1531669	Lower Slate
10		50	85	SE	501855: 1531375	Lower Slate
11		25	85	NW	502203: 1531430	Lower Limestone
12		175	75	SW	502529: 1531547	Upper Slate
13		240	80	SE	502476: 1531506	Upper Slate
14		15	70	NW	502782: 1531477	Lower Limestone

15		350	70	SW	502817: 1531628	Upper Slate
16		330	65	SW	503253: 1532155	Upper Slate
17		330	50	SW	501717: 1535094	Lower Slate
18		330	75	NE	503595: 1535187	Lower Slate
19		320	70	NE	504057: 1535666	Lower Slate
20		330	70	SW	499800: 1537819	Metavolcanic
21		30	30	NW	499991: 1530534	Lower Slate
	Fold axis					
		Trend	Plunge			
1		160	20		500975: 1535138	Lower Limestone
2		175	25		502742: 1531536	Upper Slate
3		190	10		503216: 1531703	Upper limestone
4		200	15		502884: 1531552	Upper Slate
5		170	10		500250: 1535608	Lower limestone
6		160	20		500011: 1537171	Lower limestone

Appendix II

Geochemical data

The comparisons of REE content of the analyzed metasedimentary (MS4, MS17, and MS20) with standard sedimentary compositions (NASC, ES, PASS and UCC) used for normalizing the REE the concentrations (ppm) in sedimentary rock.

	Metasedimentary rock sample			Standard sedimentary compositions			
	MS4	MS17	MS20	NASC	ES	PAAS	UCC
La	30.3	12	21.8	32	41.1	38.2	30
Ce	54	26.3	42.6	70	81.3	79.6	64
Pr	6.99	3.24	5.33	7.9	10.4	8.83	7.1
Nd	28	14	23.3	31	40.1	33.9	26
Sm	5.11	3.06	4.73	5.7	7.3	5.55	4.5
Eu	1.25	0.88	1.16	1.24	1.52	1.08	0.88
Gd	4.62	2.63	4.71	5.21	6.03	4.66	3.8
Tb	0.75	0.47	0.72	0.85	1.05	0.774	0.64
Dy	4.47	3.02	4.71			4.68	3.5
Ho	0.83	0.58	0.93	1.04	1.2	0.991	0.8
Er	2.46	1.7	2.73	3.4	3.55	2.85	2.3
Tm	0.28	0.27	0.37	0.5	0.56	0.405	0.33
Yb	1.9	1.75	2.68	3.1	3.29	2.82	2.2
Lu	0.24	0.24	0.42	0.48	0.58	0.433	0.32

Appendix III

CIPW norm of the analyzed metavolcanic and plutonic rocks

Metavolcanic rocks								Plutonic rocks	
Sample	MV5	MV4	MV9	MV12	MV1	MV2	MV8	PR2	PR3
Quartz	18.99	21.79	8.97	0.00	32.89	31.27	40.08	20.96	24.41
Corundum	0.00	3.26	0.00	0.00	2.35	2.13	2.76	0.55	2.75
Orthoclase	1.78	0.30	1.10	2.39	0.79	4.88	18.85	25.60	18.87
Albile	36.84	53.53	23.97	68.43	43.88	50.48	4.12	38.58	40.57
Anorthtite	26.10	5.02	32.88	6.91	6.70	2.58	25.53	7.84	5.80
Diopside	3.34	0.00	14.56	0.00	0.00	0.00	0.00	0.00	0.00
Wollastonite	4.75	0.00	0.00	0.00	0.00	0.00	0.00	0.00	0.00
Hypersthene	0.00	4.89	1.86	2.29	5.23	2.16	3.40	2.34	3.68
Olivine	0.00	0.00	0.00	3.66	0.00	0.00	0.00	0.00	0.00
Ilmenite	0.13	0.09	0.40	0.37	0.13	0.11	0.20	0.07	0.04
Hematite	6.17	8.74	11.88	12.28	6.75	5.51	4.60	3.26	3.05
Sphene	1.46	0.00	3.20	2.26	0.00	0.00	0.00	0.00	0.00
Rutile	0.00	1.07	0.00	0.36	0.59	0.51	0.25	0.42	0.47
Apatite	0.45	1.34	1.20	1.08	0.70	0.41	0.20	0.39	0.37
Total	100	100	100	100	100	100	100	100	100